BSC	**Design Calculation or Analysis Cover Sheet** *Complete only applicable items.*	1. QA: N/A 2. Page 1 of 218

3. System	4. Document Identifier
Subsurface Facility	860-K0C-SSD0-00100-000-00B

5. Title

Shaft Liner Design

6. Group

Subsurface/Mining/Geotechnical

7. Document Status Designation

☐ Preliminary ☒ Committed ☐ Confirmed ☐ Cancelled/Superseded

8. Notes/Comments

1) Branko Damjanac (Itasca), and Zorica Radakovic-Guzina of Itasca provided technical support in numerical analyses presented in Section 6, Attachment A, and Attachment B.
2) This analysis supersedes the previous version 860-K0C-SSD0-00100-000-00A - Calculation revised due to new thermal and seismic parameters.
3) Extensive revision – all pages are affected.
4) This calculation is in COLOR.
5) Analysis of 8 m shaft diameter and 0.25 m shaft liner thickness and calculation for 5 m dimeter and 0.25 m liner thickness for one thermal mechanical unit are provided in this revision.

Attachments	Total Number of Pages
1. Derivation of Closed-Form Solution for Unlined Shaft	4
2. Results for T- and L-type intersection Analysis in TSw2_Nonlithophysal Unit	13
3. Derivation of Equivalent Material Properties for Mountain-Scale Model	3
4. List of CD Files	8
5. ATTACHMENT D	CD

RECORD OF REVISIONS

9. No.	10. Reason For Revision	11. Total # of Pgs.	12. Last Pg. #	13. Originator (Print/Sign/Date)	14. Checker (Print/Sign/Date)	15. EGS (Print/Sign/Date)	16. Approved/Accepted (Print/Sign/Date)
00A	Initial Issue	216	216	Marek Mrugala	Jay Cho	Fei Duan	Robert Saunders
00B	Revised input for seismic ground motion and thermal line load	218	218	Marek Mrugala 02/15/2008	Jay Cho 2/15/08	Fei Duan 2/15/08	Robert Boutin 2/15/08

DISCLAIMER

The calculations contained in this document were developed by Bechtel SAIC Company, LLC (BSC) and are intended solely for the use of BSC in its work for the Yucca Mountain Project.

CONTENTS

Page

1 PURPOSE 18
2 REFERENCES 20
2.1 PROCEDURES /DIRECTIVES 20
2.2 DESIGN INPUTS 20
2.3 DESIGN CONSTRAINTS 23
2.4 DESIGN OUTPUTS 23
3 ASSUMPTIONS 24
3.1 ASSUMPTIONS THAT REQUIRE VERIFICATION 24
3.1.1 Use of DTNs: MO0707THRB1E4A.000 for Seismic Velocities 24
3.2 ASSUMPTIONS THAT DO NOT REQUIRE VERIFICATION 24
3.2.1 Simultaneous Emplacement 24
3.2.2 Generic Shaft Collar Elevation and Depth of RHH 24
3.2.3 Horizontal-To-Vertical In Situ Stress Ratios 25
3.2.4 Ground Relaxation Prior to Installation of Shaft Liner 25
3.2.5 Dilation Angle 25
3.2.6 Duration of Thermal Load 26
3.2.7 Propagation of Seismic Waves 26
4 METHODOLOGY 27
4.1 QUALITY ASSURANCE 27
4.2 USE OF SOFTWARE 27
4.2.1 Specialized Level 1 Software Usage 27
4.2.2 Level 2 Software Usage 28
4.3 DESIGN METHODOLGY 28
4.3.1 Analysis 29
4.3.2 Loading Cases 43
5 LIST OF ATTACHMENTS 46
6 BODY OF CALCULATION 47
6.1 INTRODUCTION 47
6.2 YUCCA MOUNTAIN GEOLOGY 47
6.2.1 Generic Stratigraphy 50
6.3 REPOSITORY LAYOUT AND SHAFT CONFIGURATIONS 51
6.4 INPUT DATA AND PARAMETERS 57
6.4.1 Rock Properties 57
6.4.2 Shaft Diameters 57
6.4.3 Mechanical Properties of Ground Control Components 59
6.4.4 Field Stresses 59
6.4.5 Horizontal-to-Vertical Stress Ratio 59
6.4.6 Rock Thermal Properties Data and Field Temperature Characteristics 60
6.4.7 Repository Layout and Shaft Locations 60
6.4.8 Initial Ground Relaxation 61

6.4.9 Seismic Ground Motion Data 61
6.5 ANALYSIS 63
6.5.1 Solutions for Unlined Shaft – Baseline Case 63
6.5.2 Modeling of Lined Shaft 114
6.5.3 Shaft Performance 178
6.5.4 Implication of Current Design Analysis 182
6.6 UNCERTAINTY ANALYSIS 184
6.6.1 Uncertainty of Design Input 184
6.6.2 Variability of Rock Material Properties 185
6.6.3 Variations in Loading Conditions 185
6.6.4 Uncertainties in Calculations and Design Methodology 187
6.6.5 Remedial Measures 188
7 RESULTS AND CONCLUSIONS 189
7.1 SUMMARY OF RESULTS 189
7.2 CONCLUSIONS 190
ATTACHMENT A 191
ATTACHMENT B 195
ATTACHMENT C 208
ATTACHMENT D 211

FIGURES

Page

Figure 4-1 FLAC3D Model Used for Evaluating the Minimum Distance from the Advancing Shaft Bottom to the Fully Relaxed Shaft Wall 31
Figure 4-2 Two Typical Shaft/Drift Intersections, (a) T-type, and (b) L-type. 32
Figure 4-3 Refinement of the "Generic" L-type Intersection Used to Develop the Numerical Model 32
Figure 4-4 FLAC3D Model of the (a) T-type and (b) L-type Intersections 33
Figure 4-5 Detailed View of the FLAC3D Model for the "T-type" Intersection. 35
Figure 4-6 Detailed View of the FLAC3D Model for the "L-type" Intersection. 35
Figure 4-7 Model Geometry of the FLAC3D Model for Evaluating Effects of Seismic Load 37
Figure 4-8 Model Location Within Thermal Mechanical Units. 37
Figure 4-9 Detailed View of the FLAC3D Model for Evaluating Effects of Thermal Load in the Concrete Shaft Liner in Each Individual Rock Strata. 39
Figure 4-10 Geometry and Dimensions of the Repository Grid 40
Figure 6-1 General Stratigraphic Column for Yucca Mountain 49
Figure 6-2 Thermal Mechanical Units Used in Numerical Model to Represent the Rock Strata 50
Figure 6-3 Repository Footprint and Shaft Locations 52
Figure 6-4 Repository Ventilation System, Shaft Locations and Functions 53
Figure 6-5 Time Histories of Velocity Components of $1x10^{-4}$ Seismic Motion at Repository Horizon 62
Figure 6-6 Updated Time Histories of Velocity Components of $1x10^{-4}$ Seismic Motion at Repository Horizon 62
Figure 6-7 Ground Reaction Curve Obtained with an Analytical Solution for a Section of Shaft Excavated in PTn, Category 1 64
Figure 6-8 Extent of Failure Zone as a Function of Decreasing Internal Pressure as Obtained Analytically for a Section of Shaft Excavated in PTn, Category 1. 65
Figure 6-9 Profile of the Maximum Shaft Closure (Scaled to the Shaft Radius) Along the Shaft EX_3N Considering Category 1 Rock Mass in Each Unit 65
Figure 6-10 Profile of the Normalized Radius of the Plastic Zone along the Shaft EX_3N Considering Category 1 Rock Mass in Each Unit 66
Figure 6-11 FLAC3D Model of a Section of Shaft in Unit PTn, Category 1, Showing Magnitude of Displacement (m) After Excavation (i.e., internal pressure equal to zero) 68
Figure 6-12 FLAC3D Model of a Section of Shaft in Unit PTn, Category 1, Showing Zones in Failure State After Excavation - Internal Pressure Equal to Zero 69
Figure 6-13 FLAC3D Model of a Shaft Section in Unit TSw1, Category 1, Showing Zones in a Failure State After Excavation - Internal Pressure Equal to Zero. 70
Figure 6-14 Extent of Plastic Failure from the FLAC3D Model of the Advancing Shaft in

the PTn, Category 1. 73
Figure 6-15 Contours of Displacements (M) from the FLAC3D Model of the Advancing Shaft in the PTn, Category 1.....74
Figure 6-16 Distribution of Radial Displacements Behind the Front Obtained from the FLAC3D Models of the Advancing Shaft in the PTn, Category 1. (ur/R=0.178 %, Dist/R = 2.22) 75
Figure 6-17 Extent of Plastic Failure at T-type Intersection After Excavation Represented on a Vertical Plane Containing the Axis of the Drift.....77
Figure 6-18 Extent of Plastic Failure at T-type Intersection After Excavation Represented on a Vertical Plane Perpendicular to the Axis the Drift And Containing the Axis of the Shaft 78
Figure 6-19 Contours of Magnitude of Displacement (m) at T-type Intersection After Excavation Represented on a Vertical Plane Containing the Axis of the Drift.....79
Figure 6-20 Contours of Magnitude of Displacement (m) at T-type Intersection After Excavation Represented on a Vertical Plane Perpendicular to the Axis of the Drift and Containing the Axis of the Shaft 80
Figure 6-21 T-type Intersection - View 1 Showing Points, Where Velocities Induced by Seismic Excitation Have Been Calculated and Recorded During Simulations 81
Figure 6-22 T-type Intersection - View 2 Showing Points, Where Velocities Induced by Seismic Excitation Have Been Calculated and Recorded During Simulations 81
Figure 6-23 T-type Intersection - Record of Input Velocities (m/s) in the X-, Y- and Z-Directions at the Base of the Model.....82
Figure 6-24 T-type Intersection - Record of Velocities (m/s) at Point 1 in the “T-type” Intersection Induced by Application of Seismic Excitation. 82
Figure 6-25 T-type Intersection - Record of Velocities (m/s) at Point 4 in the “T-type” Intersection Induced by Application of Seismic Excitation 83
Figure 6-26 T-type Intersection - Record of Velocities (m/s) at Point 6 in the “T-type” Intersection Induced by Application of Seismic Excitation 83
Figure 6-27 T-type Intersection - Record of Input Velocities (m/s) in the X-, Y- and Z-Directions at the Base of the Model.....84
Figure 6-28 T-type Intersection - Record of Velocities (m/s) at Point 1 in the “T-type” Intersection Induced by Application of Seismic Excitation. 85
Figure 6-29 T-type Intersection - Record of Velocities (m/s) at Point 4 in the “T-type” Intersection Induced by Application of Seismic Excitation 86
Figure 6-30 T-type Intersection - Record of Velocities (m/s) at Point 6 in the “T-type” Intersection Induced by Application of Seismic Excitation 87
Figure 6-31 T-type Intersection - View of Extent of the Failure Zone After Application of the Seismic Load in the “T-type” Intersection (The vertical plane cutting the model contains the axis of the drift.) 88
Figure 6-32 T-type Intersection - View of Extent of the Failure Zone After Application of the Seismic Load in the “T-type” Intersection (The vertical plane cutting the model contains the axis of the drift.) 89

Figure 6-33 T-type Intersection - View of Extent of the Failure Zone After Application of the Seismic Load in the "T-type" Intersection (The vertical plane cutting the model contains the axis of the shaft and is perpendicular to the axis of the drift.) 90
Figure 6-34 T-type Intersection - View of Extent of the Failure Zone After Application of the Seismic Load in the "T-type" Intersection (The vertical plane cutting the model contains the axis of the shaft and is perpendicular to the axis of the drift.) 91
Figure 6-35 L-type Intersection - Extent of Plastic Failure After Excavation Represented on a Vertical Plane Containing the Axis of the Drift for the "L-type" Intersection....93
Figure 6-36 L-type Intersection - Extent of Plastic Failure After Excavation Represented on a Vertical Plane Parallel to the Axis of the Drift and Containing the Axis of the Shaft for the "L-type" Intersection 94
Figure 6-37 L-type Intersection - Extent of Plastic Failure After Excavation Represented on a Vertical Plane Containing the Axis of the Drift and the Connection Between Shaft and Drift....95
Figure 6-38 L-type Intersection - Extent of Plastic Failure After Excavation Represented on a Horizontal Plane Containing the Axis of the Drift and the Connection Between Shaft and Drift....96
Figure 6-39 L-type Intersection - Contours of the Vertical Normal Stress (MPa) After Excavation Represented on a Horizontal Plane Containing the Axis of the Drift and the Connection Between Shaft and Drift....97
Figure 6-40 L-type Intersection - Contours of Magnitude of Displacement (m) After Excavation Represented on a Vertical Plane Containing the Axis of the Drift for the "L-type" Intersection....98
Figure 6-41 L-type Intersection - Contours of Magnitude of Displacement (m) After Excavation Represented on a Vertical Plane Parallel to the Axis of the Drift and Containing the Axis of the Shaft for the "L-type" Intersection 99
Figure 6-42 L-type Intersection - Contours of Magnitude of Displacements (m) After Excavation Represented on a Vertical Plane Containing the Axis of the Drift and the Connection Between Shaft and Drift 100
Figure 6-43 L-type Intersection – View 1 Showing Points Where Velocities Induced by Seismic Excitation Have Been Calculated and Recorded During Simulations ...101
Figure 6-44 L-type Intersection – View 2 Showing Points Where Velocities Induced by Seismic Excitation Have Been Calculated and Recorded During Simulations ...101
Figure 6-45 L-type Intersection - Record of Input Velocities (m/s) in the X-, Y- and Z-Directions at the Base of the Model for the "L-type" Intersection (10-4 ground motion)....102
Figure 6-46 L-type Intersection - Record of Velocities (m/s) at Point 1 in the "L-type" Intersection Induced by Application of Seismic Excitation 102
Figure 6-47 L-type Intersection - Record of Velocities (m/s) at Point 4 in the "L-type" Intersection Induced by Application of Seismic Excitation. 103

Figure 6-48 L-type Intersection - Record of Velocities (m/s) at Point 6 in the "L-type" Intersection Induced by Application of Seismic Excitation. 103
Figure 6-49 L-type Intersection - Record of Input Velocities (m/s) in the X-, Y- and Z-Directions at the Base of the Model for the "L-type" Intersection (10-4 ground motion).....104
Figure 6-50 L-type Intersection - Record of Velocities (m/s) at Point 1 in the "L-type" Intersection Induced by Application of Seismic Excitation 105
Figure 6-51 L-type Intersection - Record of Velocities (m/s) at Point 4 in the "L-type" Intersection Induced by Application of Seismic Excitation. 106
Figure 6-52 L-type Intersection - Record of Velocities (m/s) at Point 6 in the "L-type" Intersection Induced by Application of Seismic Excitation. 107
Figure 6-53 L-type Intersection - View of Extent of the Failure Zone After Application of the Seismic Load in the "L-type" Intersection (The vertical plane cutting the model contains the axis of the drift). 108
Figure 6-54 L-type Intersection - View of Extent of the Failure Zone After Application of the Seismic Load in the "L-type" Intersection (The vertical plane cutting the model contains the axis of the drift). 109
Figure 6-55 L-type Intersection - View of Extent of the Failure Zone After Application of the Seismic Load in the "L-type" Intersection (The vertical axis cutting the model contains the axis of the shaft and is parallel to the axis of the drift).....110
Figure 6-56 L-type Intersection - View of Extent of the Failure Zone After Application of the Seismic Load in the "L-type" Intersection (The vertical axis cutting the model contains the axis of the shaft and is parallel to the axis of the drift).....111
Figure 6-57 L-type Intersection - View of Extent of the Failure Zone After Application of the Seismic Load in the "L-type" Intersection (The vertical axis cutting the model contains the axis of the drift and the connection between shaft and drift.) 112
Figure 6-58 L-type Intersection - View of Extent of the Failure Zone After Application of the Seismic Load in the "L-type" Intersection (The vertical axis cutting the model contains the axis of the drift and the connection between shaft and drift.) 113
Figure 6-59 Stress Change Profile Along Shaft IN_4 After 100 years of Heating (Rev A) ...116
Figure 6-60 Stress Change Profile Along Shaft IN_4 After 100 years of Heating (2.0 kW/m) 116
Figure 6-61 Stress Change Profile Along Shaft EX_4 After 100 years of Heating (Rev A) ..117
Figure 6-62 Stress Change Profile Along Shaft EX_4 After 100 years of Heating (2.0 kW/m) 117
Figure 6-63 Stress Change Profile Along Shaft IN_2 After 100 Years of Heating (Rev A) ..118
Figure 6-64 Stress Change Profile Along Shaft IN_2 After 100 Years of Heating (2.0 kW/m) 118
Figure 6-65 Stress Change Profile Along Shaft EX_3S After 100 Years of Heating (Rev A) 119
Figure 6-66 Stress Change Profile Along Shaft EX_3S After 100 Years of Heating (2.0

kW/m) 119
Figure 6-67 Displacement Profile Along Shaft IN_4 After 100 Years of Heating (Rev A) ...120
Figure 6-68 Displacement Profile Along Shaft IN_4 After 100 Years of Heating (2.0 kW/m) 120
Figure 6-69 Displacement Profile Along Shaft EX_4 After 100 Years of Heating (Rev A) ..121
Figure 6-70 Displacement Profile Along Shaft EX_4 After 100 Years of Heating (2.0 kW/m) 121
Figure 6-71 Displacement Profile Along Shaft IN_2 After 100 Years of Heating (Rev A) ...122
Figure 6-72 Displacement Profile Along Shaft IN_2 After 100 Years of Heating (2.0 kW/m) 122
Figure 6-73 Displacement Profile Along Shaft EX_3S After 100 Years of Heating (Rev A) 123
Figure 6-74 Displacement Profile Along Shaft EX_3S After 100 Years of Heating (2.0 kW/m) 123
Figure 6-75 View of Lined Shaft in the Contact of Units PTn and TSw1 (Location 1) - Showing the Three Different Levels....125
Figure 6-76 View of a Half-Section of Shaft - Showing the Location of the Points.....126
Figure 6-77 View of the Lined Shaft in TSw1_Lithophysal (Location 3)- Showing the Level on the Liner....127
Figure 6-78 A Typical View of the Lined Shaft at the Contact of Units PTn and TSw1 (Location 1) - Showing the Status of the Velocity Vector Field (m/s) During Dynamic Simulation 128
Figure 6-79 A Typical View in the Horizontal Cross-Section of the Lined Shaft at the Contact of PTn and TSw1 Units (Location 1) - Showing the Status of the Velocity Vector Field (m/s) During Dynamic Simulation....129
Figure 6-80 Histories of Forces Nx, Ny and Nxy (N/m) During Application of the Seismic Load at Point 1, Level 1, Location 1 (shaft in the contact of units PTn and TSw1)....132
Figure 6-81 Histories of Bending moments Mx, My and Mxy (Nm/m) During Application of the Seismic Load at Point 1, Level 1, Location 1 (Shaft in contact with units PTn and TSw1) 132
Figure 6-82 Histories of Shear Forces Qx and Qy (N/m) During Application of the Seismic Load at Point 1, Level 1,Location 1 (Shaft in contact with units PTn and TSw1)....133
Figure 6-83 Histories of Forces Nx, Ny and Nxy (N/m) During Application of the Seismic Load at Point 1, Level 1, and Location 1 (PTn and TSw1 Contact) – Case S1...138
Figure 6-84 Histories of Bending moments Mx, My and Mxy (Nm/m) During Application of the Seismic Load at Point 1, Level 1, Location 1 (PTn and TSw1 Contact) – Case S1....138
Figure 6-85 Histories of Shear Forces Qx and Qy (N/m) During Application of the Seismic Load at Point 1, Level 1, Location 1 (PTn and TSw1 Contact) – Case S1 139

Figure 6-86 Histories of Forces Nx, Ny and Nxy (N/m) During Application of the Seismic Load at Point 1, Level 1, and Location 1 (PTn and TSw1 Contact) – Case S2...144
Figure 6-87 Histories of Bending moments Mx, My and Mxy (Nm/m) During Application of the Seismic Load at Point 1, Level 1, Location 1 (PTn and TSw1 Contact) – Case S2.....145
Figure 6-88 Histories of Shear Forces Qx and Qy (N/m) During Application of the Seismic Load at Point 1, Level 1, Location 1 (PTn and TSw1 Contact) – Case S2 145
Figure 6-89 Histories of Forces Nx, Ny and Nxy (N/m) During Application of the Seismic Load at Point 1, Level 1, and Location 3 (TSw1_Lith) – Case S3 150
Figure 6-90 Histories of Bending moments Mx, My and Mxy (Nm/m) During Application of the Seismic Load at Point 1, Level 1, Location 3 (TSw1_Lith) – Case S3 151
Figure 6-91 Histories of Shear Forces Qx and Qy (N/m) During Application of the Seismic Load at Point 1, Level 1, Location 1 (TSw1_Lith) – Case S3 151
Figure 6-92 Axial Stress Profile Along the Liner of Shaft IN_4 After 100 Years of Heating (Rev A).....161
Figure 6-93 Axial Stress Profile Along the Liner of Shaft IN_4 After 100 Years of Heating (Case T1).....161
Figure 6-94 Shear Stress Profiles Along the Liner of Shaft IN_4 After 100 Years of Heating (Rev A).....162
Figure 6-95 Shear Stress Profiles Along the Liner of Shaft IN_4 After 100 Years of Heating (Case T1).....162
Figure 6-96 Axial Stress Profiles Along the Liner of Shaft EX_4 After 100 Years of Heating (Rev A).....163
Figure 6-97 Axial Stress Profiles Along the Liner of Shaft EX_4 After 100 Years of Heating (Case T1).....163
Figure 6-98 Shear Stress Profiles Along the Liner of Shaft EX_4 After 100 Years of Heating (Rev A).....164
Figure 6-99 Shear Stress Profiles Along the Liner of Shaft EX_4 After 100 Years of Heating (Case T1).....164
Figure 6-100 Axial Stress Profiles Along the Liner of Shaft IN_2 After 100 Years of Heating (Rev A).....165
Figure 6-101 Axial Stress Profiles Along the Liner of Shaft IN_2 After 100 Years of Heating (Case T1).....165
Figure 6-102 Shear Stress Profiles Along the Liner of Shaft IN_2 After 100 Years of Heating (Rev A).....166
Figure 6-103 Shear Stress Profiles Along the Liner of Shaft IN_2 After 100 Years of Heating (Case T1).....166
Figure 6-104 Axial Stress Profiles Along the Liner of Shaft EX_3S After 100 Years of Heating (Rev A).....167
Figure 6-105 Axial Stress Profiles Along the Liner of Shaft EX_3S After 100 Years of Heating (Case T1).....167

Figure 6-106 Shear Stress Profiles Along the Liner of Shaft EX_3S After 100 Years of Heating (Rev A) 168
Figure 6-107 Shear Stress Profiles Along the Liner of Shaft EX_3S After 100 Years of Heating (Case T1) 168
Figure 6-108 Bending Normal Stresses Induced Along the Shaft IN_4 After 100 Years of Heating Considering 0.3-m Liner Thickness (Rev A) 170
Figure 6-109 Bending Normal Stresses Induced Along the Shaft IN_4 After 100 Years of Heating Considering 0.3-m Liner Thickness (Case T1) 170
Figure 6-110 Bending Shear Stresses Induced Along the Shaft IN_4 After 100 Years of Heating Considering 0.3-m Liner Thickness (Rev A) 171
Figure 6-111 Bending Shear Stresses Induced Along the Shaft IN_4 After 100 Years of Heating Considering 0.3-m Liner Thickness (Case T1) 171
Figure 6-112 Bending Normal Stresses Induced Along the Shaft EX_4 After 100 Years of Heating Considering 0.3-m Liner Thickness (Rev A) 172
Figure 6-113 Bending Normal Stresses Induced Along the Shaft EX_4 After 100 Years of Heating Considering 0.3-m Liner Thickness (Case T1) 172
Figure 6-114 Bending Shear Stresses Induced Along the Shaft EX_4 After 100 Years of Heating Considering 0.3-m Liner Thickness (Rev A) 173
Figure 6-115 Bending Shear Stresses Induced Along the Shaft EX_4 After 100 Years of Heating Considering 0.3-m Liner Thickness (Case T1) 173
Figure 6-116 Bending Normal Stresses Induced Along the Shaft IN_2 After 100 Years of Heating Considering 0.3-m Liner Thickness (Rev A) 174
Figure 6-117 Bending Normal Stresses Induced Along the Shaft IN_2 After 100 Years of Heating Considering 0.3-m Liner Thickness (Case T1) 174
Figure 6-118 Bending Shear Stresses Induced Along the Shaft IN_2 After 100 Years of Heating Considering 0.3-m Liner Thickness (Rev A) 175
Figure 6-119 Bending Shear Stresses Induced Along the Shaft IN_2 After 100 Years of Heating Considering 0.3-m Liner Thickness (Case T1) 175
Figure 6-120 Bending Normal Stresses Induced Along the Shaft EX_3S After 100 Years of Heating Considering 0.3-m Liner Thickness (Rev A) 176
Figure 6-121 Bending Normal Stresses Induced Along the Shaft EX_3S After 100 Years of Heating Considering 0.3-m Liner Thickness (Case T1) 176
Figure 6-122 Bending Shear Stresses Induced Along the Shaft EX_3S After 100 Years of Heating Considering 0.3-m Liner Thickness (Rev A) 177
Figure 6-123 Bending Shear Stresses Induced Along the Shaft EX_3S After 100 Years of Heating Considering 0.3-m Liner Thickness (Case T1) 177
Figure B-1 No plastic failure observed at T-type Intersections Located in TSw2_Nonlithophysal Rock Mass Category 1 after excavation shown on the vertical plane containing the axis of the drift....196
Figure B-2 No plastic failure observed at T-type Intersections Located in TSw2_Nonlithophysal Rock Mass Category 1 after excavation shown on the vertical plane containing the axis of the shaft and perpendicular to the axis of

the drift 197
Figure B-3 Contours of magnitude of displacements (m) at T-type Intersections Located in TSw2_Nonlithophysal Rock Mass Category 1 after excavation shown on the vertical plane containing the axis of the shaft and 198
Figure B-4 Contours of magnitude of displacements (m) at T-type Intersections Located in TSw2_Nonlithophysal Rock Mass Category 1 after excavation shown on the vertical plane containing the axis of the shaft and perpendicular to the axis of the drift 199
Figure B-5 No plastic failure observed at L-type intersection Located in TSw2_Nonlithophysal Rock Mass Category 1 after excavation shown on the vertical plane containing the axis of the drift 200
Figure B-6 No plastic failure observed at L-type Intersections Located in TSw2_Nonlithophysal Rock Mass Category 1 after excavation shown on the vertical plane containing the axis of the shaft 201
Figure B-7 Shown in Red is an Extent of plastic failure at L-type Intersections Located in TSw2_Nonlithophysal Rock Mass Category 1 after excavation shown on the vertical plane containing both the axis of the shaft and axis of the drift and perpendicular to the Main. 202
Figure B-8 Extent of plastic failure at L-type Intersections Located in TSw2_Nonlithophysal Rock Mass Category 1 after excavation shown on a horizontal plane containing the axis of the drift and the effect of connection between shaft and drift and drift and Main. 203
Figure B-9 Contours of the vertical normal stress (MPa) at L-type Intersections Located in TSw2_Nonlithophysal Rock Mass Category 1 after excavation represented on a horizontal plane containing the axis of the drift and the connection between shaft and drift and drift and Main 204
Figure B-10 Contours of magnitude of displacement (m) at L-type Intersections Located in TSw2_Nonlithophysal Rock Mass Category 1 after excavation represented on a vertical plane containing the axis of the drift 205
Figure B-11 Contours of magnitude of displacement (m) at L-type Intersections Located in TSw2_Nonlithophysal Rock Mass Category 1 after excavation represented on a vertical plane containing the axis of the shaft 206
Figure B-12 Contours of magnitude of displacements (m) at L-type Intersections Located in TSw2_Nonlithophysal Rock Mass Category 1 after excavation represented on a vertical plane containing the axis of the drift and the connection between shaft and drift. 207

TABLES

Page

Table 4-1 List of Qualified Software 27
Table 4-2 Boundary Conditions for FLAC Analysis 34
Table 4-3 Summary of Simulation Cases Analyzed for Seismic Loads 38
Table 4-4 Temperature Differences After 100 Years of Heating Obtained for Various Rock Strata Interfaces from, FLUENT and FLAC3D Codes and Values Used In Current Simulations 45
Table 4-5 Summary of the Simulation Cases Analyzed Under Thermal Loading Conditions 45
Table 5-1 List of Attachments 46
Table 6-1 Comparison of Several Stratigraphic Subdivisions of Mid-Tertiary Volcanic Rocks at Yucca Mountain. 48
Table 6-2 Shaft Collar and Station Coordinates and Shaft Name Nomenclature 54
Table 6-3 Lithostratigraphic Column at Each Proposed Shaft Location 55
Table 6-4 Generic Shaft Stratigraphy 56
Table 6-5 Rock Mass Properties for Representative TM Units 58
Table 6-6 Properties of Unreinforced Concrete Liner 59
Table 6-7 Extent of Failure Zone Rpl and Radial Displacements ur for Shaft Sections in Different Rock Mass Units and Categories Obtained Using Analytical Solution 64
Table 6-8 Base Case Configuration for the Generic Shaft Modeling Analysis 66
Table 6-9 Extent of Scaled Failure Zone Rpl and Radial Displacements ur for Shaft Sections in Different Rock Mass Units and Categories Obtained for Shaft Sections Modeled Using FLAC3D 67
Table 6-10 Scaled Maximum Radial Displacement Behind the Advancing Shaft Excavation and Distance to the Shaft Bottom Obtained from FLAC3D Models of Shafts in the Different Stratigraphic Units. 72
Table 6-11 Details of Seismic Load Cases Analyzed Under Seismic Loading Using FLAC3D 124
Table 6-12 Summary of Maximum and Minimum Values of Forces and Moments at Various Points in Level 1 for Location 1 (PTn and TSw1 Contact) – Rev A 134
Table 6-13 Summary of Maximum and Minimum Values of Forces and Moments at Various Points in Level 2 for Location 1 (PTn and TSw1 Contact) – Rev A 134
Table 6-14 Summary of Maximum and Minimum Values of Forces and Moments at Various Points in Level 3 for Location 1 (PTn and TSw1 Contact) – Rev A Case S1 135
Table 6-15 Summary of Maximum and Minimum Values of Forces and Moments at Various Points in Level 1 for Location 2 (TCw) – Rev A 135
Table 6-16 Summary of Maximum and Minimum Values of Forces and Moments at Various Points in Level 1 for Location 3 (TSw1_Lith) – Rev A 136

Table 6-17 Maximum Values of Bending Moments and Shear Forces and Associated Values of Normal Stresses in the Liner for the Different Locations Analyzed – Rev A 137
Table 6-18 Maximum Values of Normal Forces and Associated Values of Normal Stresses in the Liner for the Different Locations Analyzed – Rev A 137
Table 6-19 Summary of Maximum and Minimum Values of Forces and Moments Due to Seismic Loading at Various Points in Level 1 for Location 1 (PTn and TSw1 Contact) – Case S1 139
Table 6-20 Summary of Maximum and Minimum Values of Forces and Moments Due to Seismic Loading at Various Points in Level 2 for Location 1 (PTn and TSw1 Contact) –Case S1 140
Table 6-21 Summary of Maximum and Minimum Values of Forces and Moments Due to Seismic Loading at Various Points in Level 3 for Location 1 (PTn and TSw1 Contact) – Case S1 140
Table 6-22 Summary of Maximum and Minimum Values of Forces and Moments Due to Seismic Loading at Various Points in Level 1 for Location 2 (TCw) – Case S1 141
Table 6-23 Summary of Maximum and Minimum Values of Forces and Moments Due to Seismic Loading at Various Points in Level 1 for Location 3 (TSw1_Lith) – Case S1 141
Table 6-24 Maximum Values of Bending Moments Due to Seismic Loading and Shear Forces and Associated Values of Normal Stresses in the Liner for Different Locations Analyzed – Case S1 142
Table 6-25 Maximum Values of Normal Forces and Associated Values of Normal Stresses in the Liner for the Different Locations Analyzed – Case S1 142
Table 6-26 Summary of Maximum and Minimum Values of Forces and Moments at Various Points in Level 1 for Location 1 (PTn and TSw1 Contact) – Case S2 146
Table 6-27 Summary of Maximum and Minimum Values of Forces and Moments at Various Points in Level 2 for Location 1 (PTn and TSw1 Contact) – Case S2 147
Table 6-28 Summary of Maximum and Minimum Values of Forces and Moments at Various Points in Level 3 for Location 1 (PTn and TSw1 Contact) – Case S2 147
Table 6-29 Summary of Maximum and Minimum Values of Forces and Moments at Various Points in Level 1 for Location 2 (TCw) – Case S2 148
Table 6-30 Summary of Maximum and Minimum Values of Forces and Moments at Various Points in Level 1 for Location 3 (TSw1_Lith) – Case S2 148
Table 6-31 Maximum Values of Bending Moments and Shear Forces and Associated Values of Normal Stresses in the Liner for the Different Locations Analyzed – Case S2 149
Table 6-32 Maximum Values of Normal Forces and Associated Values of Normal Stresses in the Liner for the Different Locations Analyzed – Case S2 149
Table 6-33 Summary of Maximum and Minimum Values of Forces and Moments on Points of the Liner for Location 3 (Unit TSw2_Nonlith) – Case S3 152
Table 6-34 Maximum Values of Bending Moments and Shear Forces and Associated

Values of Normal Stresses in the Liner Analyzed – Case S3 152
Table 6-35 Maximum Values of Normal Forces and Associated Values of Normal Stresses in the Liner Analyzed – Case S3.....152
Table 6-36 Maximum Values of Normal Forces and Associated Values of Normal Stresses in the Liner Under Seismic Loading for the Rock Strata Analyzed 154
Table 6-37 Maximum Values of Bending Moments and Shear Forces and Associated Values of Normal Stresses in the Liner Due to Seismic Loading for the Rock Strata Analyzed.....155
Table 6-38 Tangential Force Nt and Axial Force Na at Step 3 After 100 Years of Heating in Rev A and Current Rev B Analysis (Cases T1, T2, and T3).....158
Table 6-39 Tangential (Ny/t) and Axial (Na/t) Stresses at Step 3 After 100 Years of Heating For Cases Analyzed.....159
Table 6-40 Maximum Axial and Shear Stresses in Liner After 100 Years of Heating.....160
Table 6-41 Maximum Bending Induced Stresses in Liner After 100 Years of Heating.....169
Table 6-42 Allowable Compressive Strength Criteria 178
Table 6-43 Summary of Stresses at TSw1_Lithophysal Unit Obtained from Rev A and T1 Cases (Rev B).....179
Table 6-44 Summary of Results Obtained from Numerical Simulations 181

ACRONYMS AND ABBREVIATIONS

AISC	American Institute of Steel Construction
APE	Annual Probability of Exceedance
ASTM	American Society for Testing and Materials
BDBGM	Beyond design basis ground motion
BOD	Basis of Design for the TAD Canister-Based Repository Design Concept
BSC	Bechtel SAIC Company, LLC
CTE	Coefficient of Thermal Expansion
CRWMS M&O	Civilian Radioctive Waste Management System Management and Operating Contractor
DBGM	Design Base Ground Motion
DOE	U. S. Department of Energy
DTN	Data Tracking Number
E	Elastic Modulus
ECRB	Enhanced Characterization of the Repository Block
ESF	Exploratory Studies Facility
FLAC3D	Fast Lagrangian Analysis of Continua in 3 Dimensions
GFM	Geologic Framework Model
GPa	Giga Pascal
K_o	Horizontal-to-vertical stress ratio
LA	License Application
MPa	Mega Pascal
NRC	U. S. Nuclear Regulatory Commission
NUFT	Nonisothermal Unsaturated-Saturated Flow and Transport - Software Used for Thermal-Hydrological Modeling
Pa	Pascal
PDC	Project Design Criteria
QARD	Quality Assurance Requirements and Description
RDTME	Repository Design and Thermal-Mechanical Effects
RHH	Repository Host Horizon
RMC	Rock Mass Quality Category
RPC	Record Processing Center

SCM	Software Configuration Management
SGPR	Subsurface Geotechnical Parameters Report
TM	Thermal Mechanical
TSPA	Total System Performance Assessment
TDMS	Technical Data Management Systems
UCS	Uniaxial Compressive Strength
YMP	Yucca Mountain Project

1 PURPOSE

The purpose of this calculation is to evaluate the shaft stability, to analyze shaft ground control and reinforcement, and to calculate the parameters of shaft liner required to maintain the long-term shaft operation. The rock strata response is evaluated by considering a range of rock material properties and major loading cases. As a result, evaluations can be made regarding conservatism of solutions obtained.

The Rev. A of this calculation (Reference 2.2.14) presents the results of the shaft stability analysis including the analysis of shaft ground control based on the thermal line load of 1.45 kW/m and seismic load of $1x10^{-4}$ APE ground motion provided in DTN MO0306SDSAVDTH.000 (Reference 2.2.31). For Section 8.2.1.5 of *Basis of Design for the TAD Canister-Based Repository Design Concept,* referred to as BOD (Reference 2.2.9), a maximum thermal line load of 2.0 kW/m is required to be considered in subsurface facility design. In addition, the time histories of velocity for $1x10^{-4}$ ground motion are updated and presented in MO0707THRB1E4A.000 (Reference 2.2.33). In this revision, the cases of thermal line load of 2.0 kW/m and updated seismic parameters (Reference 2.2.33) are analyzed and compared to the results presented in Rev A (Reference 2.2.14) in order to evaluate the performance of the shaft liner under this new range of thermal and dynamic loading conditions.

It should be noted that the ventilation scenario considered in the Rev A and current analysis (Rev B) are not the same. In Rev A, the first 50 years of the 100-year preclosure period are considered forced ventilation having an air flow rate of 15 m^3/s, while for the second 50 years the ventilation is considered with natural ventilation. The thermally induced stresses in the rock and concrete liner due to temperature raise during the second 50 years are, in essence, corresponding to an off-normal scenario. The ventilation scenario in the current analysis considers 100 years of continuous forced ventilation at the rate of 15 m^3/s.

Throughout this calculation the term “model” refers to the FLAC 3D numerical representation of the shaft and shaft/drift intersection.

Design Criteria

The design criteria are as follows:

- Allow for geological mapping, performance confirmation activities (which may include remote observation and possible field testing), waste retrieval operations, and closure operations (which may include installation of permanent drip shields) Reference 2.3.1, Section 63.111(e)(1))
- Account for the appropriate worst possible case in terms of combinations of in situ, thermal, seismic, construction, and operation loads (Reference 2.2.13, Section 4.5.2.1)
- Prevent rock falls that could potentially result in personnel injury (Reference 2.2.13, Section 4.5.2.2)
- Use the site-specific geotechnical data that are obtained from rock at Yucca Mountain (Reference 2.2.13, Section 4.5.2.7)

- Interface with the subsurface development and emplacement drift subsystems to accommodate opening orientation, configuration, and excavated opening sizes (Reference 2.2.13, Section 4.5.2.11).
- Interface with Total System Performance Assessment (TSPA) to ensure general acceptance of committed ground support materials (Reference 2.2.13, Section 4.5.2.12)
- Shaft ground support will function without planned maintenance during the operational life, while providing for the ability to perform unplanned maintenance in the non-accessible non-emplacement areas on as-needed basis (Reference 2.2.13, Section 4.5.2.13)
- Ground support will accommodate the maintenance of accessible non-emplacement openings (Reference 2.2.13, Section 4.5.2.14)

Objectives

The specific objectives of the Shaft Liner Design analysis are:

- To develop a typical shaft configuration arrangement,
- To provide a rationale for shaft design calculations,
- To select appropriate input data, including rock and ground control component properties, in situ stress, and thermal and seismic loading conditions,
- To develop a baseline case involving a case of an unlined shaft for analysis,
- To perform analysis of the proposed ground control means to verify shaft performance under an anticipated in situ condition,
- To perform a series of calculations utilizing the numerical modeling technique and typical shaft station arrangements,
- To provide an assessment of shaft design input and modeling adequacy, and
- To provide assessment of future data needs and methods of shaft design methodology, verification and enhancements.

Activities documented in this report involve developing a procedure for the shaft ground control and the shaft liner design. The design process includes evaluation of the following aspects of shaft design:

- Development of the base case scenario, involving the shaft without rock reinforcement.
- Develop typical design models representing common shaft configurations located within the site-specific geology and subjected to the baseline loading conditions.

The results of the analysis presented in this report are applicable for the lithophysal and nonlithophysal rock units of the repository strata. Shaft response to the thermal loads serves as a relative measure of shaft stability in an environment subjected to the long-term exposure to heat generated by the emplaced waste.

2 REFERENCES

2.1 PROCEDURES /DIRECTIVES

2.1.1 BSC (Bechtel SAIC Company) 2008. *Quality Management Directive*. QA-DIR-10, Rev. 2. Las Vegas, Nevada: Bechtel SAIC Company. ACC: DOC.20080103.0002.

2.1.2 EG-PRO-3DP-G04B-00037, Rev: 010, ICN 0. *Calculations and Analyses*. Las Vegas, Nevada: Bechtel SAIC Company. ACC: ENG.20071018.0001

2.1.3 IT-PRO-011, Rev. 007. *Software Management*. Las Vegas, Nevada: Bechtel SAIC Company. ACC: DOC.20070905.0007.

2.2 DESIGN INPUTS

2.2.1 ACI 318-02/318R-02. 2002. *Building Code Requirements for Structural Concrete (ACI 318-02) and Commentary (ACI 318R-02).* Farmington Hills, Michigan: American Concrete Institute. [ISBN: 0-087031-065-8]

2.2.2 Board, M. 2003. *Resolution Strategy for Geomechanically-Related Repository Design and Thermal-Mechanical Effects (RDTME).* REV 00. Las Vegas, Nevada: Bechtel SAIC Company. ACC: MOL.20030708.0153.

2.2.3 BSC 2003. *Underground Layout Configuration*. 800-P0C-MGR0-00100-000-00E. Las Vegas, Nevada: Bechtel SAIC Company. ACC: ENG.20031002.0007.

2.2.4 BSC 2003. *Scoping Analysis on Sensitivity and Uncertainty of Emplacement Drift Stability.* 800-K0C-TEG0-00600-000-000. Las Vegas, Nevada: Bechtel SAIC Company. ACC: ENG.20031125.0002.

2.2.5 BSC 2004. *Drift Degradation Analysis.* ANL-EBS-MD-000027 REV 03. Las Vegas, Nevada: Bechtel SAIC Company. ACC: DOC.20040915.0010; DOC.20050419.0001; DOC.20051130.0002; DOC.20060731.0005. [DIRS 166107]

2.2.6 BSC 2004. *Geologic Framework Model (GFM2000).* MDL-NBS-GS-000002 REV 02. Las Vegas, Nevada: Bechtel SAIC Company. ACC: DOC.20040827.0008. [DIRS 170029]

2.2.7 BSC 2004. *Yucca Mountain Site Description.* TDR-CRW-GS-000001 REV 02 ICN 01. Two volumes. Las Vegas, Nevada: Bechtel SAIC Company. ACC: DOC.20040504.0008. [169734]

2.2.8 BSC 2005. *Q-List*. 000-30R-MGR0-00500-000-003. Las Vegas, Nevada: Bechtel SAIC Company. ACC: ENG.20050929.0008. [DIRS 175539]

2.2.9 BSC 2007. *Basis of Design for the TAD Canister-Based Repository Design Concept.* 000-3DR-MGR0-00300-000-001. Las Vegas, Nevada: Bechtel SAIC Company. ACC: ENG.20071002.0042; ENG.20071026.0033; ENG.20071108.0002;

ENG.20071109.0001; ENG.20071120.0023; ENG.20071126.0049; ENG.20071214.0009; ENG.20071213.0005; ENG.20071227.0018; ENG.20080207.0004; ENG.20080212.0003.

2.2.10 BSC 2007. *Ground Control for Emplacement Drifts for LA*. 800-K0C-SSE0-00100-000-00C. Las Vegas, Nevada: Bechtel SIAC Company. ACC: ENG.20070921.0001.

2.2.11 BSC 2007. *Ground Control for Non-Emplacement Drifts for LA.* 800-K0C-SSD0-00400-000-00A. Las Vegas, Nevada: Bechtel SAIC Company. ACC: ENG.20071001.0042; ENG.20071218.0001.

2.2.12 BSC 2007. *Ground Support Maintenance Plan.* 800-30R-SSD0-00100-000-00B. Las Vegas, Nevada: Bechtel SAIC Company. ACC: ENG.20070807.0016.

2.2.13 BSC 2007. *Project Design Criteria Document.* 000-3DR-MGR0-00100-000-007. Las Vegas, Nevada: Bechtel SAIC Company. ACC: ENG.20071016.0005; ENG.20071108.0001; ENG.20071220.0003; ENG.20080107.0001; ENG.20080107.0002; ENG.20080107.0016; ENG.20080107.0017; ENG.20080131.0006.

2.2.14 BSC 2007. *Shaft Liner Design.* 860-K0C-SSD0-00100-000-00A. Las Vegas, Nevada: Bechtel SAIC Company. ACC: ENG.20071002.0059.

2.2.15 BSC 2007. *Subsurface Construction Methods.* 800-KMR-MGR0-00100-000-002. Las Vegas, Nevada: Bechtel SAIC Company. ACC: ENG.20071116.0008.

2.2.16 BSC 2007. *Subsurface Geotechnical Parameters Report.* ANL-SSD-GE-000001 REV 00. Las Vegas, Nevada: Bechtel SAIC Company. ACC: ENG.20070115.0006. [DIRS 178693]

2.2.17 BSC 2007. *Subsurface Ventilation Airflow Arrangement for LA Full Emplacement.* 800-KV0-VUE0-00101-000 REV 00A. Las Vegas, Nevada: Bechtel SAIC Company. ACC: ENG.20070220.0007. [DIRS 179877].

2.2.18 BSC 2007. *Supplemental Earthquake Ground Motion Input for a Geologic Repository at Yucca Mountain, NV.* MDL-MGR-GS-000007 REV 000. Las Vegas, Nevada: Bechtel SAIC Company. Under Development.

2.2.19 BSC 2007. *Typical Ground Support For Ventilation Shafts*, 800-K00-SSD0-00101-000-00A, Las Vegas, Nevada: Bechtel SAIC Company. ACC: ENG.20070515.0001.

2.2.20 BSC 2007. *Underground Layout Configuration for LA.* 800-KMC-SS00-00200-000-00B. Las Vegas, Nevada: Bechtel SAIC Company. ACC: ENG.20070727.0004; ENG.20071214.0002.

2.2.21 BSC 2008. *FLUENT THERMAL CALCULATION FOR 2.0 KW/M THERMAL LOAD.* 800-KVC-VUE0-00800-000-00A. Las Vegas, Nevada: Bechtel SAIC Company. ACC: ENG.20080124.0007.

2.2.22 BSC 2008. *IED Geotechnical and Thermal Parameters II.* 800-IED-MGR0-00402-000 REV 00B. Las Vegas, Nevada: Bechtel SAIC Company. ACC: ENG.20080128.0008.

2.2.23 BSC 2008. *IED Geotechnical and Thermal Parameters IV*. 800-IED-MGR0-00404-000 REV 00B. Las Vegas, Nevada: Bechtel SAIC Company. ACC: ENG.20080128.0009. [DIRS 184955]

2.2.24 Carranza-Torres, C 2003. *"Dimensionless Graphical Representation of the Exact Elasto-Plastic Solution of a Circular Tunnel in a Mohr-Coulomb Material Subject to Uniform Far-Field Stresses."* Rock Mechanics & Rock Engineering, 36, 237-253. New York, New York: Springer-Verlag. TIC: 255410.

2.2.25 CRWMS M&O 1997. *Yucca Mountain Site Geotechnical Report*. B00000000-01717-5705-00043 REV 01. Two volumes. Las Vegas, Nevada: CRWMS M&O. ACC: MOL.19971017.0736; MOL.19971017.0737.

2.2.26 CRWMS M&O 1999. *DP for Determination of Available Repository Siting Volume for the Site Recommendation.* Development Plan TDP-NBS-GS-000027 REV 00. Las Vegas, Nevada: CRWMS M&O. ACC: MOL.19991220.0323.

2.2.27 FLAC3D V. 2.1 Sub Release 2.10.196. 2002. WINDOWS 2000/NT 4.0. STN: 10502-2.1-00. [DIRS 161947]

2.2.28 Itasca Consulting Group. [2002]. *Itasca Software–Cutting Edge Tools for Computational Mechanics*. Minneapolis, Minnesota: Itasca Consulting Group. TIC: 252592.

2.2.29 Kosmatka, S.H. and Panarese, W.C. 1994. *Design and Control of Concrete Mixtures.* 13th Edition. Skokie, Illinois: Portland Cement Association. [ISBN: 0-89312-087-1]

2.2.30 Merritt, F.S., ed. 1983. *Standard Handbook for Civil Engineers*. 3rd Edition. New York, New York: McGraw-Hill. [ISBN: 0-07041515-3].

2.2.31 MO0306SDSAVDTH.000. Seismic Design Spectra and Acceleration, Velocity, and Displacement Time Histories for the Emplacement Level at 10^{-4} Annual Exceedance Frequency. Submittal date: 06/26/2003. [DIRS 164033]

2.2.32 MO0408MWDDDMIO.002. *Drift Degradation Model Inputs and Outputs. Submittal date: 08/31/2004.* [DIRS 171483].

2.2.33 MO0707THRB1E4A.000. *Time Histories for the Repository Block at $1E^{-4}$ APE*. Submittal date: 07/26/2007. [DIRS 183200].

2.2.34 Richardson, A. 1990. *Preliminary Shaft Liner Design Criteria and Methodology Guide. SAND88-7060*. Albuquerque, New Mexico: Sandia National Laboratories. ACC: NNA.19900305.0001. [DIRS 103588]

2.2.35 SNF37100195002.001. Hydraulic Fracturing Stress Measurements in Test Hole: ESF-AOD-HDFR1, Thermal Test Facility, Exploratory Studies Facility at Yucca Mountain. Submittal date: 12/18/1996. [DIRS 131356]

It should be noted that the use of Data Tracking Number (DTN): MO0408MWDDDMIO.002 (Reference 2.2.32), and SNF37100195002.001 (Reference 2.2.35) have been approved by inclusion on the information exchange drawing (IED), *IED Geotechnical and Thermal Parameters IV [Sheet 1 of 1]*. (Reference 2.2.23) and *IED Geotechnical and Thermal Parameters II* (Reference 2.2.22), respectively. DTN MO0707THRB1E4A.000 (Reference 2.2.33) is current unqualified however, is being tracked via TBV (TBV-9269). In addition, Reference 2.2.18 cited limitation of the seismic data (DTN MO0707THRB1E4A.000 (Reference 2.2.33)). This limitation is being tracked via TBV (TBV-9268).

2.3 DESIGN CONSTRAINTS

2.3.1 10 CFR 63. 2006. *Energy: Disposal of High-Level Radioactive Wastes in a Geologic Repository at Yucca Mountain*, Nevada. Internet Accessible. [DIRS 180319]

2.4 DESIGN OUTPUTS

The design output is the methodology of shaft ground control and will be used to revise drawing *Typical Ground Support for Ventilation Shafts*, 800-K00-SSD0-00101-000-00A (Reference 2.2.19).

3 ASSUMPTIONS

3.1 ASSUMPTIONS THAT REQUIRE VERIFICATION

3.1.1 Use of DTNs: MO0707THRB1E4A.000 for Seismic Velocities

Assumption: It is assumed that DTN MO0707THRB1E4A.000 (Reference 2.2.33) will be qualified and will be referenced on an IED in the future. It is further assumed that the limitation on this DTN (Reference 2.2.18) will not impact the shaft liner analysis.

Rationale: The data from the source is used as input, because this data is the most recent seismic data. The current status of this data is unqualified and preliminary. The future qualification of this DTN and its inclusion on an IED is being tracked in the Document Input Reference System database via TBV-9269. Furthermore, the assessment of the adequacy, conservatism and risk in the shaft liner analysis by using this data is provided in Section 6.4.9.

This assumption is used in Section 6.

3.2 ASSUMPTIONS THAT DO NOT REQUIRE VERIFICATION

3.2.1 Simultaneous Emplacement

Assumption: Thermal calculation results used in this report are based on assumption that generation of heat from the waste packages occurs simultaneously throughout the repository. The entire repository begins heating at the same time since sequential emplacement of waste packages has not been considered.

Rationale: This assumption is used indirectly to properly interpret the magnitude of thermally induced stresses and is necessary since design information is available only for the emplacement drift layout (Reference 2.2.20), but not for the waste emplacement schedule. This assumption does not require further confirmation, since results from the thermal-mechanical calculation should be the most conservative based on this assumption (i.e., the assumption produces increased heat and greater stresses in the rock mass).

Use in the Analysis: This assumption is used in the base case thermal calculations throughout this calculation.

3.2.2 Generic Shaft Collar Elevation and Depth of RHH

Assumption: A generic shaft as shown in Figure 6-2 and with stratigraphy described in Table 6-4 is assumed to be representative for the purpose of this calculation.

Rationale: Depths of shafts vary, ranging from 278.8 m to 427.71 m. An average shaft depth is equal to 346.3 m (Reference 2.2.3, p. 54, Table 7). This assumption is necessary to develop the design methodology consistent and applicable for all shafts. The thermal mechanical (TM) units as shown in Figure 6-2 are typical units encountered throughout the repository area. A typical or generic shaft collar elevation is 1422.29 m and the depth

used in the current calculation equals to 400 m and is considered reasonable for this calculation. This depth is consistent with other geotechnical calculations, i.e., *Ground Control for Emplacement Drift for LA* (Reference 2.2.10), and *Ground Control for Non-Emplacement Drifts for LA* (Reference 2.2.11). The collar elevations and depths of individual shafts are different and the distance between each shaft and emplacement drifts varies as well. The elevation of the generic shaft collar was selected to fall within a range of other shaft collars listed in Table 6-3. It is the results of decision to locate the shaft station at elevation equal to 1022.29 m (the deepest among all other shafts listed in Table 6-3). A 27.71 m difference between the assumed typical shaft depth and the deepest among the nine shafts planned for the repository ventilation is small (7% approximately) (Reference 2.2.3, p. 54, Table 7) and its impact on results obtained from a 400 m deep shaft are not significant.

Use in the Analysis/Model: This assumption is used in the model development and all subsequent modeling tasks throughout this calculation.

3.2.3 Horizontal-To-Vertical In Situ Stress Ratios

Assumption: The horizontal-to-vertical in situ stress ratio (K_o) is assumed to be equal to 0.5.

Rationale: According to the in situ stress measurement by hydraulic fracturing in a test hole located in the TSw2 unit, the vertical stress equals 4.7 MPa, while maximum and minimum horizontal stresses are equal to 1.7 MPa and 2.9 MPa (Reference 2.2.35), corresponding to the minimum and maximum K_o values equal to 0.36 and 0.62, respectively. The base case is equal to approximately the average of the minimum and maximum K_o values. The K_o value equal to 0.5 lies about in the middle between the two measured values of horizontal stresses. Since the purpose of this calculation is to develop a preliminary shaft design, the K_o value used here is acceptable within a scope of work for this calculation.

Use in the Analysis/Model: This assumption is used throughout this calculation.

3.2.4 Ground Relaxation Prior to Installation of Shaft Liner

Assumption: It is assumed that the concrete liner will be installed after 100 percent of stress-relaxation. This assumption is reasonable since the liner will be installed at some distance away from the advancing shaft bottom where a complete stress relaxation has already taken place. Furthermore, the final results for each shaft are not expected to vary significantly in comparison to those obtained utilizing this assumption.

Use in the Analysis/Model: This assumption is used in throughout this calculation.

3.2.5 Dilation Angle

Assumption: Dilation angle is assumed to be equal to zero.

Rationale: The zero value of the dilation angle is conservative in modeling of structures developed in hard rock formations. The use of this assumption is appropriate for this calculation and does not require further validation.

Use in the Analysis/Model: This assumption is used throughout this calculation.

3.2.6 Duration of Thermal Load

Assumption: The 100 years duration of thermal load resulting from an instantaneous emplacement of nuclear waste in all drifts is assumed.

Rationale: The 100 years duration of thermal load throughout the repository is considered here as a conservative assumption, where the heating period is interpreted to last throughout the preclosure period, in BOD (Reference 2.2.9, Section 8.2.2.1) specified as 100 years. The thermal impact caused by instantaneous emplacement of nuclear waste in all drifts is considered the most conservative as it yields highest transient thermal impact and continuous source of heat in the volume of the rock mass surrounding entire repository. The use of this assumption is appropriate for this calculation and does not require further validation.

Use in the Analysis/Model: This assumption is used throughout this calculation..

3.2.7 Propagation of Seismic Waves

Assumption: Seismic waves are assumed to propagate vertically upwards.

Rationale: Upward propagation of seismic waves applied at the model base represents potentially most severe loading condition and consequently the most pronounced impact on the shaft stability analysis.

Use in the Analysis/Model: This assumption is used throughout this calculation.

4 METHODOLOGY

4.1 QUALITY ASSURANCE

This calculation was prepared in accordance with EG-PRO-3DP-G04B-00037, *Calculations and Analyses* (Reference 2.1.2). The design calculation methodology presented in this report will be used mainly to design ground support systems in ventilation shafts. The ground support system is classified as a non-Safety Category item on the *Q-List* (Reference 2.2.8, Table A-1, p. A-11). Therefore, this document is subject to the requirements of the BSC *Quality Management Directive* (Reference 2.1.1, Section 2.1.C.1.1. and 17.E) and the approved version is designated as QA:N/A.

4.2 USE OF SOFTWARE

All software documented in this section is appropriate for applications used in this calculation. The software is managed under IT-PRO-0011 (Reference 2.1.3), *Software Management*, and was obtained from Software Configuration Management (SCM) in accordance with IT-PRO-0011 (Reference 2.1.3).

4.2.1 Specialized Level 1 Software Usage

The Level 1 software used in this calculation is identified in Table 4-1.

Table 4-1 List of Qualified Software

Software Title / Version	Software Tracking Number	Brief Description of Software Use
Fast Lagrangian Analysis of Continua in 3 Dimensions (FLAC3D) V 2.1	10502-2.1-00	FLAC3D was used to analyze the seismic and thermal effects on block movement in the lithophysal rock units.

The FLAC3D Version 2.1 (Reference 2.2.27) is a three-dimensional explicit finite difference program for solving complex problems in geotechnical, civil, and mining engineering. FLAC3D simulates the behavior of three-dimensional structures built of soil, rock, or other materials that undergo plastic flow when a limiting yield condition is reached. Problems involving thermomechanical coupled effects can be solved readily. The explicit, Lagrangian calculation scheme and the mixed discretization zoning technique ensure that plastic collapse and flow are modeled very accurately. A detailed discussion on the general features and areas of the FLAC3D computer code applications is presented in the User's Manual (Reference 2.2.28, User's Manual of FLAC3D). In this calculation FLAC3D was used to perform coupled mechanical analysis. The input and output files generated during modeling are archived on a CD (see Table 5-1 and Attachment D) and processed as discussed above. The results of modeling are presented and discussed in Section 6.

FLAC3D Version 2.1 was obtained from the SCM in accordance with the IT-PRO-0011 procedure (Reference 2.1.3). FLAC3D is installed and run on stand-alone PCs with windows 2000/NT 4.0 operating system. FLAC3D Version 2.1 was qualified for use in design in accordance with the IT-PRO-0011 procedure (Reference 2.1.3). Use of FLAC3D was

appropriate for this application, and the code was applied within the range of validation as specified in the software qualification documentation.

4.2.2 Level 2 Software Usage

4.2.2.1 Microsoft Excel 2000

Microsoft Excel is the Level 2 controlled software that is commercially available and is not required to be qualified per IT-PRO-0011, *Software Management* (Reference 2.1.3, Attachment 12).

Excel 2000 SP-3 (STN: 003743-E) was used to perform support calculation activities and visual representation as described in Section 6 and associated attachments.

Excel 2000 SP-3 operations were performed on personal computers with a Pentium microprocessor and Microsoft Window 2000 operating system. Excel working file is included in Attachment D and also archived on a CD. The Excel computations were confirmed using hand calculations as presented in Section 6 and figures and graphical information were verified by visual inspection.

4.2.2.2 Mathcad

Mathcad is the Level 2 controlled software that is commercially available and is not required to be qualified per IT-PRO-0011, *Software Management* (Reference 2.1.3, Attachment 12).

Mathcad is a computational engine accessed through conventional math notation. It is designed for engineering problem solving and presentation of results. Here Mathcad was used to obtain closed-form solutions for an unlined shaft problem.

Mathcad working file is included in Attachment D and also archived on a CD. The Mathcad computations were confirmed using numerical calculations as presented in Section 6 and figures and graphical information were verified by visual inspection.

4.3 DESIGN METHODOLGY

Typically, shaft analyses include a section with calculations of shaft deformations resulting from the in situ stresses present at a particular shaft depth. These deformations depend on rock properties and shaft diameter as well as the type of the shaft liner and other ground support measures used to maintain stability of the shaft excavation.

Although current concepts indicate that the Yucca Mountain shafts will be concrete-lined after their excavation, it is necessary to establish a baseline case. This baseline case is analyzed by evaluating the performance of shaft excavation without ground support. The shaft support is then introduced, considering that entire strata deformation due to excavation has already occurred (Assumption 3.2.4). This case is used as a benchmark of shaft performance to which the performance of the shaft with the shaft liner installed is compared. This consideration is justified as the common experience with excavations developed in hard rock at shallow-to-

moderate depths shows very small deformations of rock strata and overall rock strata stabilizing at a short distance away from the advancing shaft bottom.

This analysis is performed utilizing a set of geotechnical data characterizing the behavior of distinct stratigraphic units in terms of five rock mass categories, where category 1 refers to the lowest (poorest) rock mass quality while the best rock quality is represented by category 5. The bounding variability of strata properties are captured by considering an extreme range of rock properties characterizing rock mass quality 1 and 5.

It should be noticed that no credit is taken for an initial ground support. Installation of the initial ground support is dictated by the construction method used in excavating the shaft.

Field experience supported by the measured magnitude of in situ stresses in combination with the layered and generally tectonically little disturbed rock strata causes, that potential for the locked-up stresses that can be released in the form of violent, uncontrolled deformation (e.g. rock bumps) are not expected. Modeling and field experience at the Yucca Mountain site also indicates that the rockbolts and wire mesh used typically as an initial ground support in combination with the major portion of displacement associated with the stress rearrangement occurring prior to applying the final support will not cause the stress to become locked up in the rock mass due to excavation.

4.3.1 Analysis

For the purpose of this analysis, shaft names have been simplified and are assigned as either intake shafts (IN_X), or exhaust shafts (EX_X), with “X” representing the sequence number or shaft location.

4.3.1.1 Unlined Shaft - Baseline

The baseline case was analyzed using the closed-form method and was confirmed by using the numerical solution method.

4.3.1.1.1 Closed-Form Solution

Calculations of shaft closure for shaft segments located in the different TM units were performed using closed form solution, as discussed by Carranza-Torres (Reference 2.2.24).

The shaft deformation was calculated as a function of depth and applied confining pressure. The product of these calculations is a ground reaction curve, which in its basic form illustrates the magnitude of deformation as a function of radial stress and shaft internal pressure. Details of the closed form calculation are presented in Section 6.5.1.1.

4.3.1.1.2 Numerical Solution

To supplement the analytical solution, the numerical solution was obtained for identical conditions. The modeling methodology applied in the current study is based on the scenario, which results in selecting thickness and elevation representative for the weaker strata, such that

potentially the most unfavorable effects of in situ stresses on shaft stability could be evaluated. Details of numerical analysis are presented in Section 6.5.1.2.

4.3.1.1.3 Timing of Ground Support Installation

The analysis was performed to evaluate the shaft deformation occurring at various stages of excavation. The purpose for this analysis was to establish the distance above the shaft bottom, at which the entire deformation has taken place, such that the shaft liner installed at this distance would accrue no load due to in situ stress readjustments. This standoff distance will vary depending on the depth (magnitude of stresses) and properties of rocks constituting the given geological unit.

Mechanical models of the unsupported bottom region of the advancing shaft have been developed with FLAC3D as shown in Figure 4-1. The model dimensions are 80m x 80 m x160 m (WxLxH). The axisymmetric configuration allows the use one quarter of the shaft cross-section and appropriate depth to obtain the required results. The purpose of these models is to obtain the distribution of the shaft wall convergence behind the advancing shaft bottom for shafts excavated in different rock strata units. The construction sequence has not been finalized at this time. Of interest, however, is the standoff distance required such that the final liner be placed behind the face after the maximum wall closure has occurred.

Undertaken here was an estimation of the distance between the shaft bottom and the liner, with the liner installed after 100% of the deformation due to excavation has taken place (Assumption 3.2.4). This task was accomplished by using the profiles of radial deformation obtained from the FLAC3D models. Details of FLAC 3D analysis are presented in Section 6.5.1.3.

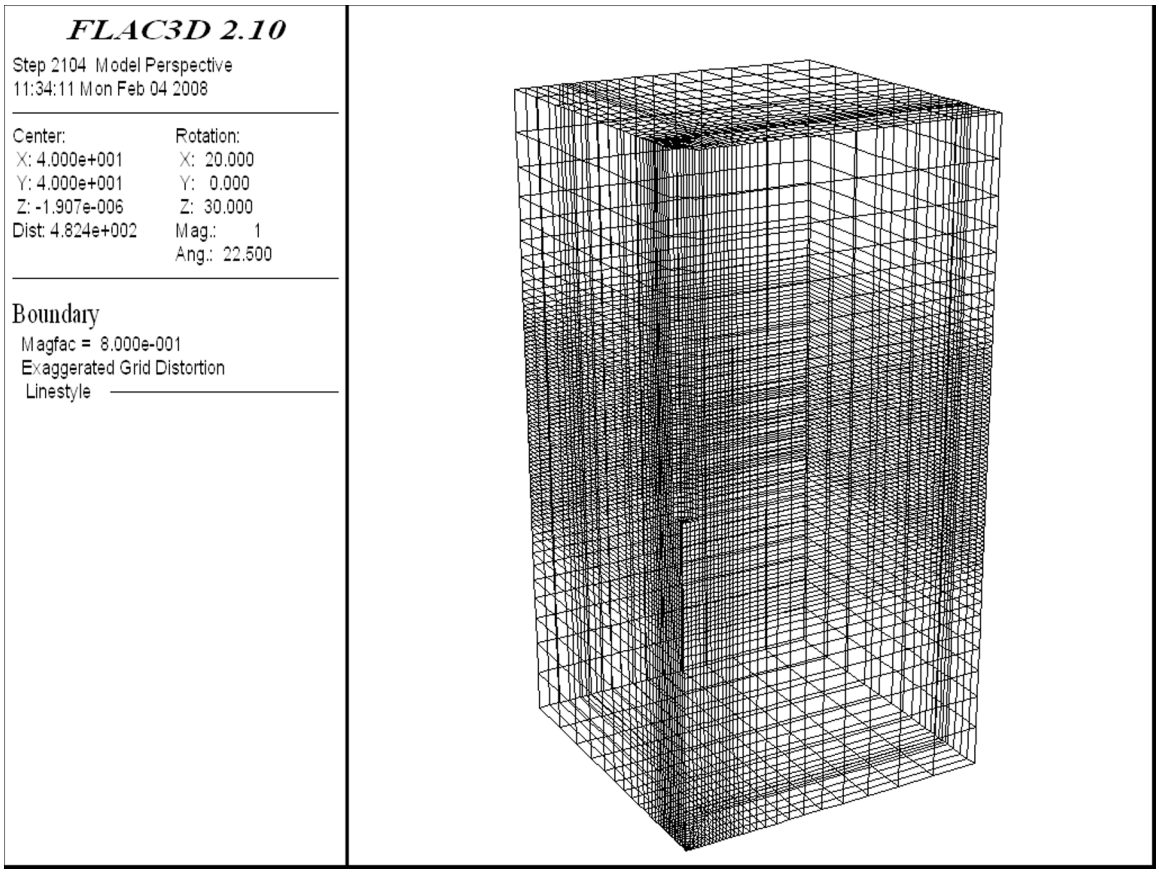

Figure 4-1 FLAC3D Model Used for Evaluating the Minimum Distance from the Advancing Shaft Bottom to the Fully Relaxed Shaft Wall

4.3.1.1.4 Shaft and Drift Intersections

Geometry of the Intersections

Two typical types of shaft/drift intersections are arranged for the purpose of shaft analysis. Figure 4-2 shows these two generalized shaft/drift intersections, further referred to as:

a) "T-type" intersection, and
b) "L-type" intersection.

The initial "L-type" intersection was refined further to provide more details in the shaft station area. Figure 4-3 shows this more refined version including the shaft sump, a short connecting tunnel and the adjacent tunnel, in the ventilation scheme represented by the main ventilation drift.

Figure 4-4 displays the geometry of the FLAC3D numerical model resulting from the subsequent refinements of the initial shaft sketches.

Details of FLAC 3D analysis are presented in Section 6.5.1.4.

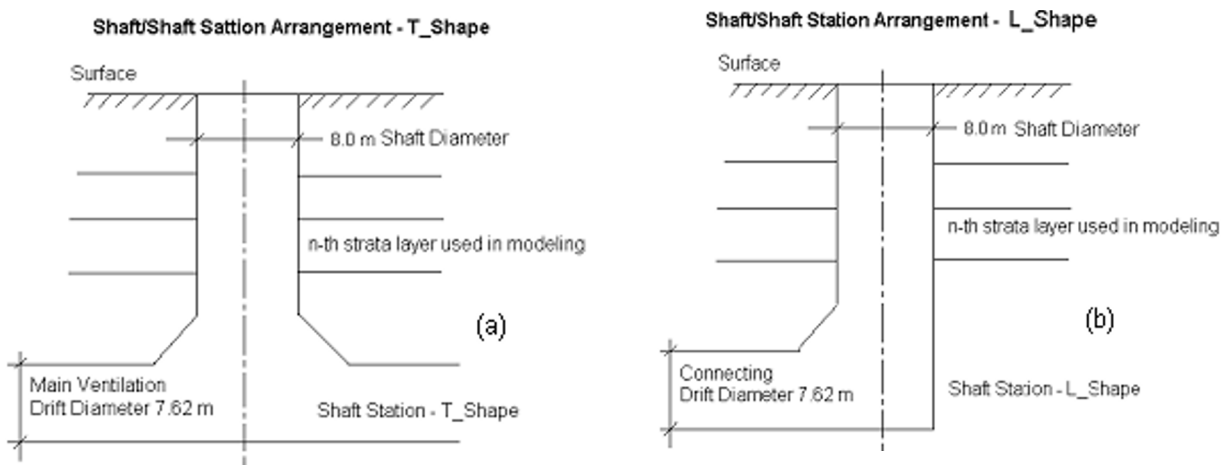

Figure 4-2 Two Typical Shaft/Drift Intersections, (a) T-type, and (b) L-type.

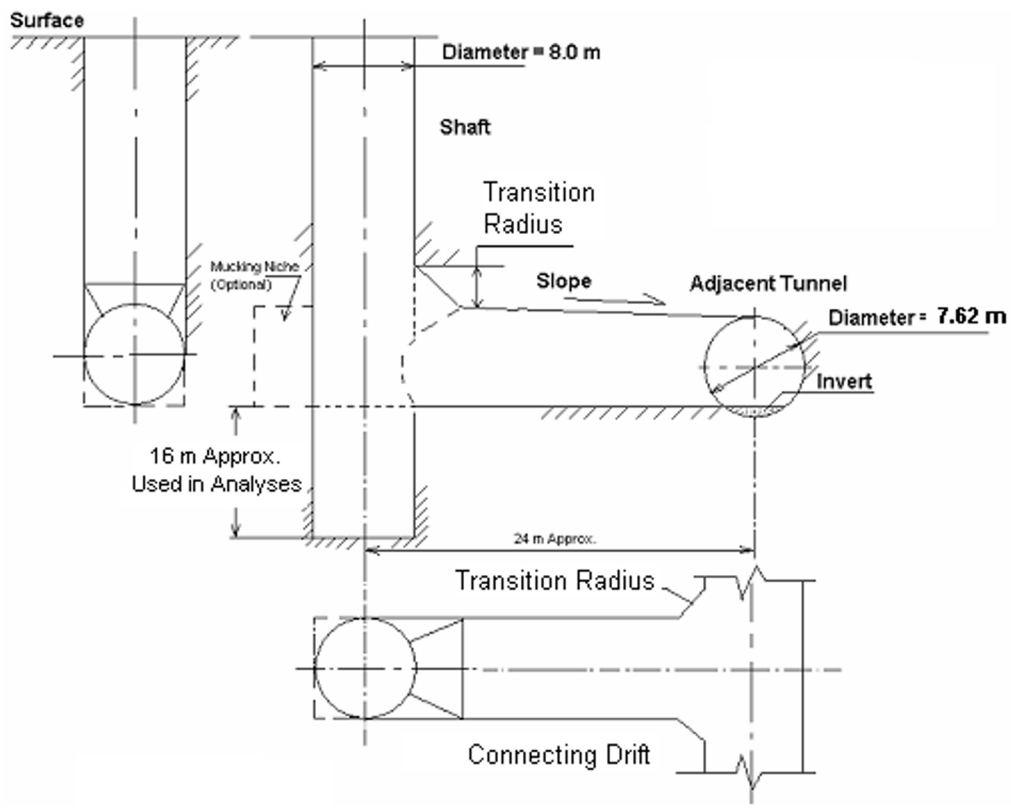

Figure 4-3 Refinement of the “Generic” L-type Intersection Used to Develop the Numerical Model

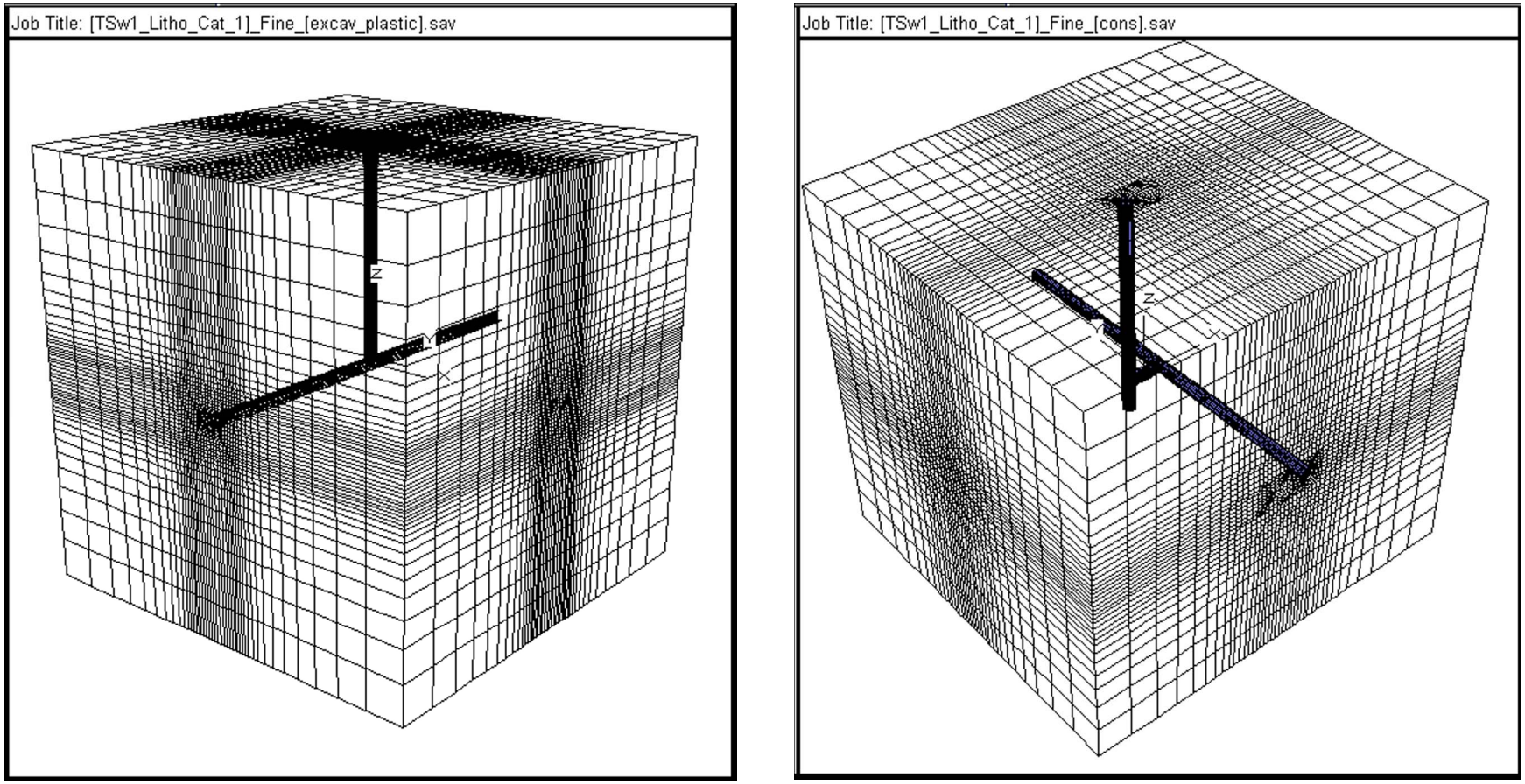

(a) (b)

Figure 4-4 FLAC3D Model of the (a) T-type and (b) L-type Intersections

Model Description

The two FLAC3D models representing two shaft/drift intersections have been assembled for analyses. The purpose for these analyses is to examine the stability of these intersections in response to excavation and seismic loading with time histories of velocity components presented in MO0707THRB1E4A.000 (Reference 2.2.33). Results of FLAC 3D analysis are presented in Section 6.5.1.4.

Model Geometry

Figure 4-5 and Figure 4-6 show views of the detailed FLAC3D models of the "T-type" and "L-type" intersections, respectively. The dimensions of the models are 269 m × 269 m × 269 m for the "T-type" intersection, and 250 m × 250 m × 274 m for the "L-type" intersection. In these models, the origin of the axis of the drift has been located at a depth of 400 m (Assumption 3.2.2), at the station elevation corresponding to the springline of the short tunnel connecting the shaft to the main tunnel.

Model Properties

The shaft intersections have been modeled using rock mass properties presented in Table 6-5. Since the modeling approach involved the FLAC3D code capable of modeling rock strata as a continuum, the nonlithophysal rock mass properties represented by the poorest rock mass quality category 1 (characterized by lower elastic moduli) serve as benchmark for a conservative assessment of ground response.

Model Loading and Boundary Conditions

The boundary conditions applied to models are summarized in Table 4-2. The modeling sequence involved the following steps.

- Simultaneous excavation of drift and shafts.
- Application of the dynamic load at the base of the models.

Table 4-2 Boundary Conditions for FLAC Analysis

Boundary	Initial Consolidation and Excavation Stage	Dynamic Analysis Stage
Lateral	Fixed in the direction normal to the face	Free-Field boundary
Bottom	Fixed in vertical direction	Non-reflecting boundary
Top	Applied pressure in vertical direction	Non-reflecting boundary
Drift Wall	Free	Free

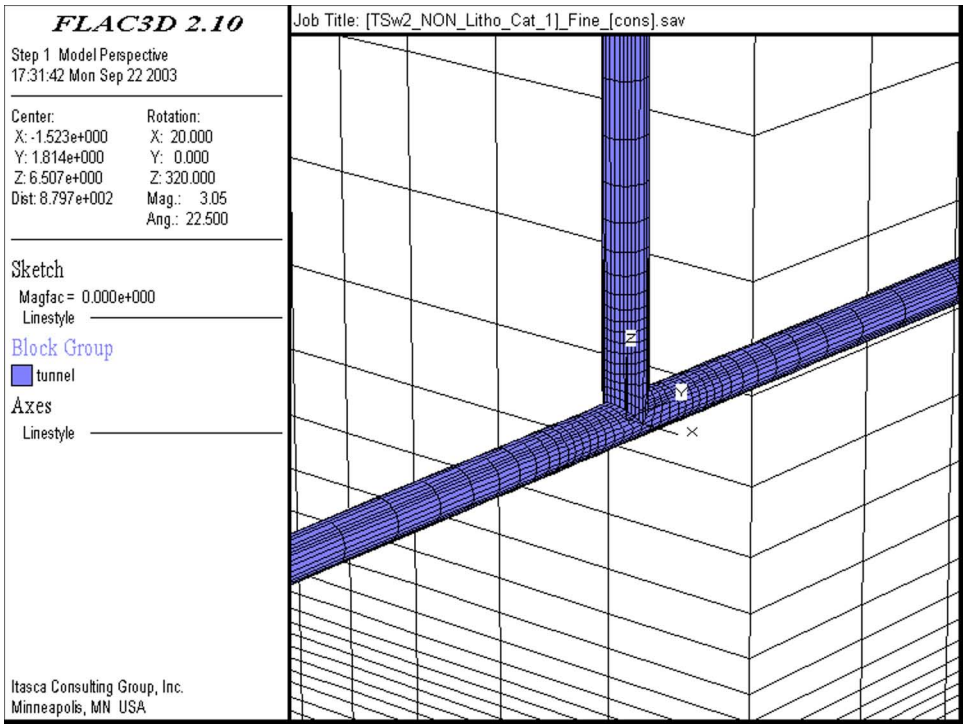

Figure 4-5 Detailed View of the FLAC3D Model for the “T-type” Intersection.

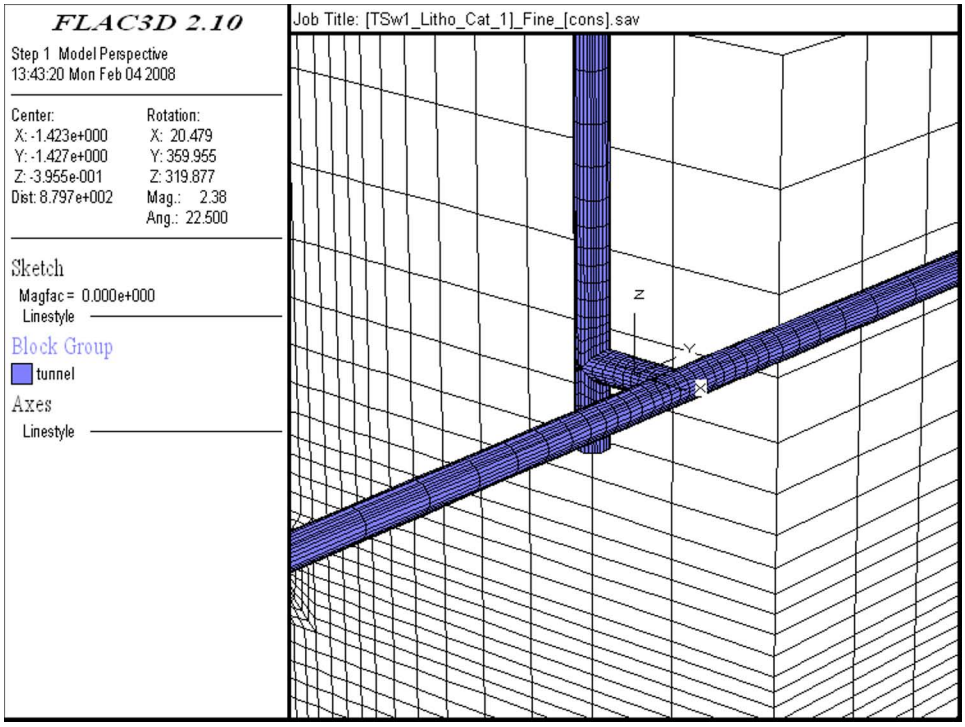

Figure 4-6 Detailed View of the FLAC3D Model for the “L-type” Intersection.

4.3.1.2 Lined Shaft

The location of the shaft can have a substantial impact on its performance. Here, listed in Table 6-2 and Table 6-3 are coordinates and detailed stratigraphy at each shaft location. Since the overall purpose of this analysis is to develop a methodology applicable to any location, a generic shaft was developed, in which attributes of a typical conditions at Yucca Mountain location are incorporated and considered in the design process as a case representative for all shafts Yucca Mountain. The attributes of this generic shaft are listed in Table 6-4.

The lined shafts are evaluated on an 8-m shaft diameter with liner thicknesses of 0.25-m and 0.3-m and 5-m shaft diameter with 0.25-m liner thickness. Details of shaft analysis are presented in Section 6.5.2.

4.3.1.2.1 Stresses Due to Seismic Loads

The behavior of the concrete liner due to seismic excitation has been analyzed with FLAC3D model that considers sections of the shaft located within or at the interface of thermal mechanical units constituting the stratigraphy of the generic shaft. A typical FLAC3D model developed and used for this purpose in the shape of a cube 200 m x 200 m x 100 m (WxLxH) with shaft structure located centrally is shown in Figure 4-7. The model allows for simulation of a 100-m shaft section which can be probed at pre-selected model locations and levels at which shaft performance is evaluated. The performance of the shaft located within a single thermal mechanical unit (e.g., Model Location 2 and 3) is evaluated at a single level (Level 1), while at the Model Location 2 shaft performance is evaluated at the adjacent strata interface (Level 1) and at the Levels 2 and 3 located in each adjacent individual strata.

In this analysis, the concrete liner is installed after 100% relaxation of the initial stresses has occurred (Assumption 3.2.4). In effect, loads associated with the deformation due to excavation are not transmitted to the liner. As shown in Figure 4-8 three different model locations have been considered in the current analysis:

- Location 1 Shaft at the contact between units PTn and TSw1 (Levels 1, 2, and 3)
- Location 2 Shaft in unit TCw (Level 1 only)
- Location 3 Shaft in unit TSw1_Lithophysal (Level 1 only)

At all three locations, the free-field boundary conditions were used along the vertical model boundaries. The quiet, non-reflecting boundary conditions were used at the bottom and at the top model boundaries even at Location 2, in TCw unit, in which the top boundary is a free surface. This procedure is considered appropriate because the base ground motion waveforms already include the effect of reflection of seismic energy from the free surface. The dynamic analysis at all three or at selected model locations was conducted for the poorest rock mass quality, i.e., rock mass Category 1 and are referred to as simulation cases. The various simulation cases analyzed here are summarized in Table 4-3.

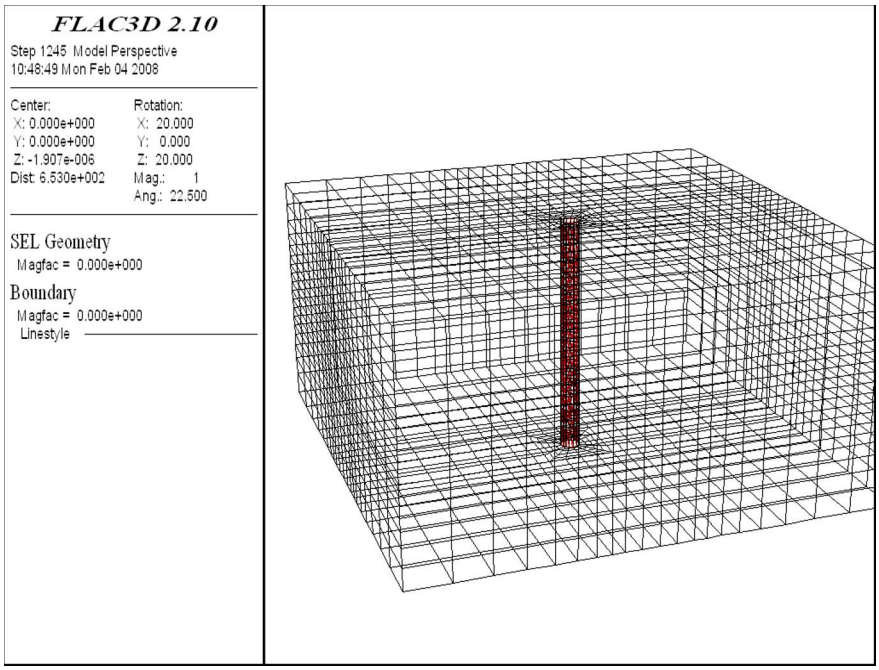

Figure 4-7 Model Geometry of the FLAC3D Model for Evaluating Effects of Seismic Load

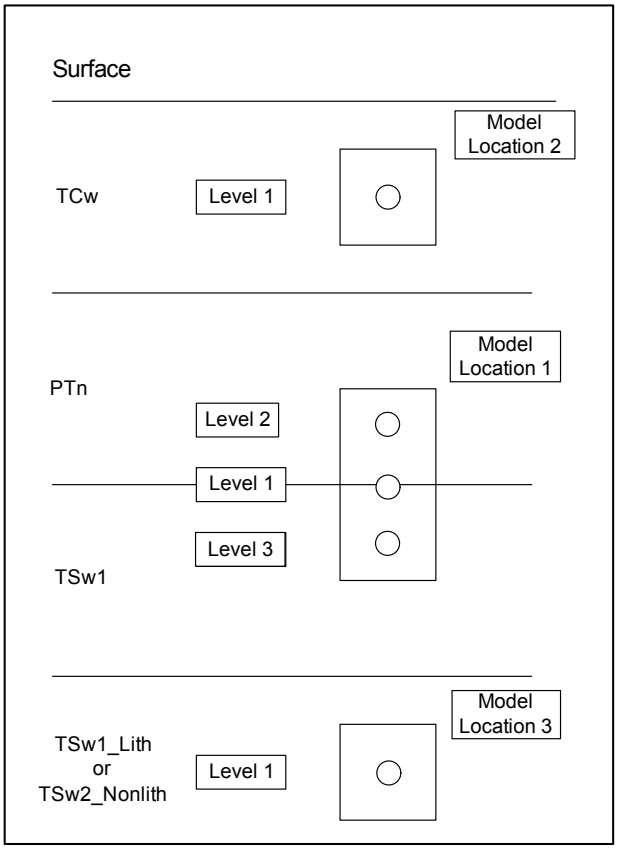

Figure 4-8 Model Location Within Thermal Mechanical Units.

Table 4-3 Summary of Simulation Cases Analyzed for Seismic Loads

Description	Rev A	Case No (Rev B)		
		S1	S2	S3
Seismic Load Source				
MO0306SDSAVDTH.000	X			
MO0707THRB1E4A.000		X	X	X
Rock Strata Considered				
PTn-TSw1	X	X	X	
TCw	X	X	X	
TSw1_Lith	X	X	X	X
Shaft Diameter				
8.0 m	X	X	X	
5.0 m				X
Liner Thickness				
0.30 m	X	X		
0.25 m			X	X

4.3.1.2.2 Stresses Due to Ground and Thermal Loads

Two approaches were applied in the process of evaluating the effect of thermal loads.

The first approach is based on simulation cases involving the FLAC 3D model shown in Figure 4-9. This model developed in a form of a thin slab 160 m x 160 m x 1.25 m (WxLxH) is used for detailed assessment of the thermally-induced liner hoop stresses within individual thermal mechanical unit.

The second approach involves FLAC3D large regional model as shown in Figure 4-10, which considers the development of thermally-induced stresses on the repository scale and was used to calculate axial and shear stresses at shaft locations. These stresses develop as a result of heating the entire block of rock mass surrounding the repository and are different in the middle section and on the periphery of the repository block. In this model, the properties of rock strata have been updated using procedure described in Attachment C and summarized in Table C-1.

Stress changes and deformations presented in Section 6.5.2.1 through Section 6.5.2.3 are calculated for the rock mass along the shafts. The compatibility of elastic moduli of the rock mass and shaft liner concrete and the fact that liners are in an intimate contact with the rock mass makes the rock mass stresses computed from the large model useful in calculating stresses in the liner as displacements generated within the rock mass are transferred to the liner. Discussed below is the use of these results for calculation of stresses and deformations induced in the shaft liners.

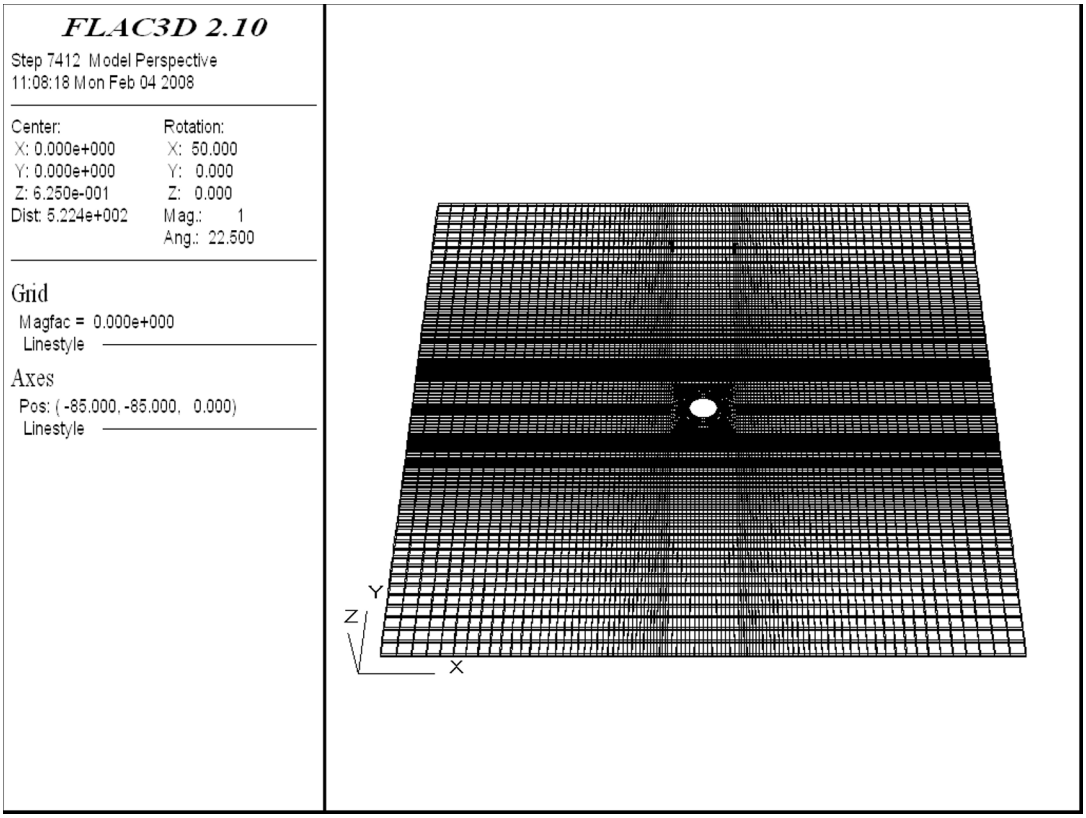

Figure 4-9 Detailed View of the FLAC3D Model for Evaluating Effects of Thermal Load in the Concrete Shaft Liner in Each Individual Rock Strata.

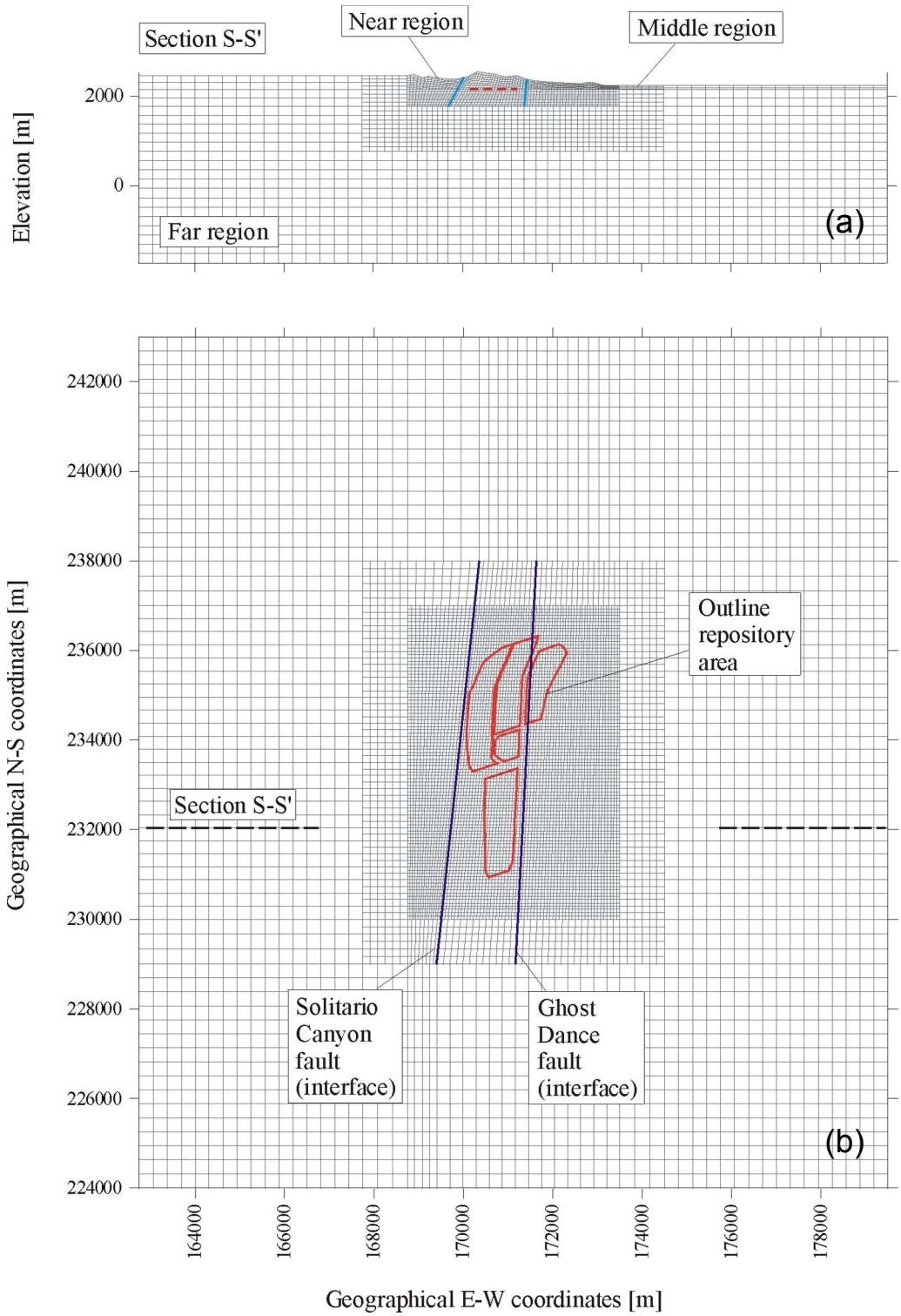

Source: *Drift Degradation Analysis* (Reference 2.2.5)

Notes: a) Cross-Section at the North Coordinate 232,000 Meters.

b) Plan View of the FLAC3D Calculation at the Elevation 1073 Meters.

Figure 4-10 Geometry and Dimensions of the Repository Grid

Hoop Deformation

Thermally induced horizontal normal stresses in the rock mass have the significant effect on stresses in shaft liners. Three-dimensional models in the horizontal slab cross-section normal to the vertical shaft axes are set for different elevations corresponding to geological units at various shaft depths. The analyses were carried out considering plane-strain conditions of deformation.

The large-scale thermo-mechanical model uses the average properties for different TM units. For example, for TSw2, combined lithophysal and non-lithophysal rock mass, Young's modulus or the modulus of deformability of 15 GPa was used. On the other hand, the variability of Young's modulus at RHH is represented by properties of TSw1_Tptpul ranging between 1.9 GPa and 19.7 GPa (Table 6-5). As a result of these differences, stress changes predicted from the large-scale model and shown in Figure 6-59 through Figure 6-66 would overpredict significantly stress changes in poor quality lithophysal rock mass, and underpredict stress changes in good quality non-lithophysal rock mass. Therefore, instead of using thermal stress changes as calculated from the large-scale, three-dimensional model shown in Figure 6-59 through Figure 6-66, the analysis was performed considering isotropic stress change corresponding to a homogeneous temperature increase throughout the horizontal cross-section and rock mass properties for different geological units and categories. This approach results in conservative estimates of thermal loads. This is particularly the case for the thermally induced axial stresses. Plane-strain conditions result in large overestimate of the axial compressive stresses in the liner. Both the liner and the rock mass will deform in the vertical direction relaxing the axial stress. A discussion of the axial stress is also presented in the section below.

Supported sections of the shaft in the different units have been analyzed for ground and thermal loads using FLAC3D. The modeling sequence for all models is as follows:

Step 1 Entirely (100%) relax stresses around periphery of the opening.

Step 2 Install concrete liner (properties as in Table 6-6).

Step 3 Apply increment of temperature due to heating (see Table 6-4).

The analysis of thermal effects was carried out using temperature fields after 100 years of heating (Assumption 3.2.6), as obtained from the FLAC3D mountain-scale model and FLUENT model (Reference 2.2.21). It should be noted that the Rev A analysis of thermal effects was carried out using temperature fields as obtained from two-dimensional code NUFT (Reference 2.2.32).

Therefore, the calculation is representative of the hoop stresses and deformation of the shaft liners in the middle of the repository. Selection of this case for analysis represents the conservative approach.

Axial and Shear Deformation

The axial stress in the shaft liners due to axial deformation is determined based on calculated change in the vertical stress in the rock mass. Considering the values of Poisson's ratios of the rock mass and the concrete are very close, the axial stresses (σ_{zz}) in the shaft liners are calculated using the following simple proportion:

$$\frac{\sigma_{zz}^{liner}}{E^{liner}} = \frac{\sigma_{zz}^{rock}}{E^{rock}} \qquad \text{(Eq. 1)}$$

or

$$\sigma_{zz}^{liner} = \frac{E^{liner}}{E^{rock}} \sigma_{zz}^{rock} \qquad \text{(Eq. 2)}$$

Where: E is the Young's modulus. The maximum increase in the shear stresses in the shaft liner ($\sigma_{\theta z}$) is calculated using the following relation (Reference 2.2.34, Appendix B, p. B-3):

$$\sigma_{\theta z}^{liner} = \frac{2\left(1+\frac{a^2}{r^2}\right)}{\frac{G^{rock}}{G^{liner}}\left(1+\frac{a^2}{R^2}\right)+\left(1-\frac{a^2}{R^2}\right)} \sigma_{xz}^{rock}$$

or (Eq. 3)

$$\sigma_{\theta z}^{liner} = \frac{2\left(1+\frac{a^2}{r^2}\right)}{\frac{G^{rock}}{G^{liner}}\left(1+\frac{a^2}{R^2}\right)+\left(1-\frac{a^2}{R^2}\right)} \sigma_{yz}^{rock}$$

Where: G is the shear modulus, a and R are internal and external radii of the shaft liner, respectively, and r is the radial distance from the shaft center to the point of interest. The maximum stress is obtained for $r = a$. In the analysis, it was considered that $(a/R)^2 \approx 1$. Considering the variability of rock mass properties and its effect on stresses in the liner, the calculation was performed considering two values for the stiffness of the rock mass: (a) 1.9 GPa, resulting in upper bound of stresses in the liner; and (b) 15 GPa. A Young's modulus of rock mass of 15 GPa was selected as being representative of the average rock-mass stiffness at Yucca Mountain, particularly for the RHH lithophysal units. Stresses in the shaft liners calculated using Young's modulus of 15 GPa are referred to in the text and figures as "lower bound" as a contrast to "upper bound", although they are probably more representative of average conditions.

Axial Bending

Deformation of the rock mass due to heating that is somewhat different from the deformation of the shafts due to thermal strains will induce additional stresses in shaft liners. This is particularly the case for horizontal displacement, because the thermal strains will mainly cause axial deformation of the shaft liners. Consequently, the horizontal deformation of the rock mass can cause bending of the liners. Calculation of the bending moments and transverse forces, and corresponding normal and shear stresses in the liner was conducted based on displacement profiles. The axial bending stresses (σ_{zz}) are calculated using the following equation (Reference 2.2.34, Appendix B, pp. B-3 and B-4):

$$\sigma_{zz} = \pm ER \frac{d^2 u_i}{dz^2} \qquad \text{(Eq. 4)}$$

Where u_i is the horizontal displacement (*i* stands for the *x*- or *y* direction). The maximum bending shear stresses (σ_{xi})are calculated using the following relation:

$$\sigma_{xi} = \frac{EI}{A} \frac{d^3 u_i}{dz^3} \qquad \text{(Eq. 5)}$$

The second and the third derivatives were calculated by sequential differencing of the displacement profiles.

4.3.2 Loading Cases

4.3.2.1 Ground Stresses and Other Loads

Two types of loads are considered: (1) thermal loads and (2) seismic loads.

4.3.2.2 Seismic Loads

To confirm the performance and to gain confidence in the proposed design of the shaft/drift intersection system, seismic analysis was carried out for the $1x10^{-4}$ APE, a 10,000 years earthquake. In this calculation, time histories of velocity components presented in DTN MO0707THRB1E4A.000 (Reference 2.2.33) are used. It should be noted that the Rev A seismic analysis was carried using the time histories of velocity components presented in DTN MO0306SDSAVDTH.000 (Reference 2.2.31).

The full signal duration corresponds to a record of ground motions of duration equal to 75 seconds. The duration of the seismic loads imposed on the model is somewhat shorter and is equal to 45 seconds approximately. In the current analysis this duration equals to the time interval resulting from the portion of the total signal between 10.6 and 55.03 seconds (Reference 2.2.33). The seismic signal duration is selected based on the input energy content. Established modeling routine requires that simulation be performed for the portion of the seismic record, of which beginning and end correspond to 5% and 95% of the total seismic energy carried by this seismic event. Seismic waves are assumed to propagate vertically upwards (Assumption 3.2.7).

The seismic load is imposed by means of applying a full three-dimensional seismic wave ground motion at the model base. Stress waves, equivalent to the seismic velocity histories, were applied at the bottom boundary of the model. The non-reflecting, quiet boundary condition was applied on the top model boundary. The free-field boundary condition was used on all vertical model boundaries.

Table 4-3 lists the summary of cases analyzed under seismic loading conditions in both Rev A and current Rev B analysis. Details of this analysis and results are presented in Section 6.5.2.2.

4.3.2.3 Induced Thermal Loads

Further details pertaining to calculations of thermal loads according to the methodology discussed earlier in Section 4.3.1.2.2 are provided in this Section.

Temperature Distribution and Parameters Used in Calculation

As stated in Section 4.3.1.2.2, current analysis of thermal effects was carried out using temperature fields after 100 years of heating, as obtained from the FLAC3D mountain-scale model and FLUENT model (Reference 2.2.21). The results of temperature differences at each rock strata interfaces obtained from FLUENT and FLAC3D simulations are summarized in Table 4-4. Thermal mechanical and physical parameters used in this calculation are obtained from the *Subsurface Geotechnical Parameters Report* (SGPR) Rev 00 (Reference 2.2.16) and are considered conservative. The transient temperature field generated by the emplaced waste in the repository rock strata (see Table 4-5) and within the rock mass surrounding the repository at Yucca Mountain, will cause the deformation and stress changes in the rock mass. These changes cause deformation and stress changes in the shaft liners. The finite size and shape of the repository and the topography at Yucca Mountain site will result in a three-dimensional and complex temperature-induced stresses and deformation fields around the repository.

The locations of nine shafts are shown in the plan view in Figure 6-3. Shafts IN_4, EX_1 and EX_4 are close to the center of the heated area of the repository, while the remaining shafts IN_2, IN_3, EX_2, EX_3N, EX_3S and EX_ECRB, are located at the edge of the repository. Here, no distinction is made between the intake and exhaust shafts. The differences in thermally induced stresses depend on the location of the shaft in the layout, in particular, the distance between the shaft and the center of the heated area. Determining of the deformation and stress changes along different shafts, and especially at shaft station levels, requires that a three-dimensional, thermo-mechanical numerical model be developed.

The analysis was carried out using FLAC3D computer code and model shown in Figure 4-10. The code description and typical results are documented in Reference 2.2.28. Here, the deformation and stresses of the rock mass along the axes of the shafts were extracted from the modeling results at several time intervals. The time interval equal to 100 years after waste emplacement was used to assess the temperature-related impact on shaft liner performance considering the repository scale.

The temperature differences listed in Table 4-4 are used in detailed evaluations of thermal effects within particular rock strata using the FLAC3D model shown in Figure 4-1. Table 4-5 provides a summary of the simulation cases analyzed under thermal loading conditions in both Rev A and Rev B analysis using this detailed model. Further details pertaining to this analysis and results are presented in Section 6.5.2.1.

Table 4-4 Temperature Differences After 100 Years of Heating Obtained for Various Rock Strata Interfaces from, FLUENT and FLAC3D Codes and Values Used In Current Simulations

Rock Strata / Interface	Elev. Above RHH	FLUENT	FLAC3D	Values To Be Used In Simulations
Thermal Load		2.0 kW/m	2.0 kW/m	2.0 kW/m
PTn-TSw1 Contact	211.5	2.6	1.0	2.6
TSw1	95.5	6.8	8.0	8.0
TSw1_Lith or TSw2_Nonlith	0.0	27.2	15.9	27.2

Table 4-5 Summary of the Simulation Cases Analyzed Under Thermal Loading Conditions

Revision	Case Number	Thermal Mechanical Unit	Rock Mass Categories	Shaft Diameter D, (m)	Liner Thickness, t, (m)	Temperature Difference, Delta T, (°C)
Rev A	Rev A	TCw	1 and 5	8.0	0.30	0.0
		PTn	1 and 5	8.0	0.30	0.0
		TSw1	1 and 5	8.0	0.30	5.0
		TSw1_Lith	1 and 5	8.0	0.30	40.0
		TSw2_Nonlth	1 and 5	8.0	0.30	40.0
Rev B	T1	TCw	1 and 5	8.0	0.30	0.0
		PTn	1 and 5	8.0	0.30	2.6
		TSw1	1 and 5	8.0	0.30	8.0
		TSw1_Lith	1 and 5	8.0	0.30	27.2
		TSw2_Nonlth	1 and 5	8.0	0.30	27.2
	T2	TCw	1 and 5	8.0	0.25	0.0
		PTn	1 and 5	8.0	0.25	2.6
		TSw1	1 and 5	8.0	0.25	8.0
		TSw1_Lith	1 and 5	8.0	0.25	27.2
		TSw2_Nonlth	1 and 5	8.0	0.25	27.2
	T3	TCw	1 and 5	5.0	0.25	0.0
		PTn	1 and 5	5.0	0.25	2.6
		TSw1	1 and 5	5.0	0.25	8.0
		TSw1_Lith	1 and 5	5.0	0.25	27.2
		TSw2_Nonlth	1 and 5	5.0	0.25	27.2

5 LIST OF ATTACHMENTS

Table 5-1 List of Attachments

Attachment	Description	No. of Pages
A	Derivation of Closed-Form Solution for Unlined Shaft	4
B	Results for T-type and L-type Intersections Located in TSw2_Nonlithophysal Rock Mass Category 1	13
C	Derivation of Equivalent Material Properties for Mountain-Scale Model	3
D	List of CD Files	8

6 BODY OF CALCULATION

6.1 INTRODUCTION

The Rev. A of this calculation (Reference 2.2.14) presents the results of the shaft stability analysis including the analysis of shaft ground control based on the thermal line load of 1.45 kW/m and seismic load of $1x10^{-4}$ APE ground motion provided in DTN MO0306SDSAVDTH.000 (Reference 2.2.31). For Section 8.2.1.5 BOD (Reference 2.2.9), a maximum thermal line load of 2.0 kW/m is required to be considered in subsurface facility design. In addition, the time histories of velocity for $1x10^{-4}$ ground motion are updated and presented in MO0707THRB1E4A.000 (Reference 2.2.33). In this section, the cases of thermal line load of 2.0 kW/m and updated seismic parameters (Reference 2.2.33) are analyzed and compared the cases presented in Rev A (Reference 2.2.14), to evaluate the performance of shaft liner under this new range of thermal and dynamic loading conditions.

6.2 YUCCA MOUNTAIN GEOLOGY

Shaft design must include consideration of the rock stratigraphy as various strata units may differ substantially in terms of strength and other characteristics. This section presents an overview of Yucca Mountain geology.

The geologic framework of the Yucca Mountain region is described in detail in Section 3 of the *Yucca Mountain Site Description* (Reference 2.2.7). In general, the Tertiary volcanic rocks comprising Yucca Mountain have been differentiated into lithostratigraphic units based on three principal criteria: 1) Lithology and rock properties, 2) Mineralogy, and 3) Geophysical log characteristics. Table 6-1 and Figure 6-1 provide a tabular and visual summary of the several stratigraphic subdivisions of mid-tertiary volcanic rocks at Yucca Mountain. Also presented in Table 6-3 are stratigraphic units encountered at the potential locations of the future repository shafts.

Geological and geotechnical characterization of the repository host rock is provided in Section 3 of the *Resolution Strategy for Geomechanically-Related Repository Design and Thermal-Mechanical Effects* (RDTME) (Reference 2.2.2). The SGPR Rev 00 (Reference 2.2.16) is the source of rock strength property data used in current analysis. Here, the repository host rock is represented by one of two volcanic tuff units, i.e., either the lithophysal rock units, or the nonlithophysal rock units.

Nonlithophysal units are generally hard, strong, fractured rocks with matrix porosities of 10 percent or less. The primary structures in these units are fractures that formed during the cooling process that followed volcanic eruption and have undergone little to no post-formation shearing. The lithophysal units, on the other hand, have fewer fractures of significant continuous length, but have a relatively uniformly distributed porosity in the form of lithophysal cavities. Approximately 85 percent of the repository emplacement drifts are located within the lithophysal rock units; with the remaining 15 percent drifts located within the nonlithophysal units (Reference 2.2.16, Section 6.4).

Table 6-1 Comparison of Several Stratigraphic Subdivisions of Mid-Tertiary Volcanic Rocks at Yucca Mountain.

Lithostratigraphic Units [a,e,f,g]		Thermal-Mechanical Units [a,b]	Hydrogeologic Units [c]
Timber Mountain Group (Tm)	Rainier Mesa member (Tmr)	Undifferentiated overburden (UO)	Unconsolidated Surficial Materials (UO)
	Pre-Rainier Mesa bedded tuff (Tmbt1)		
PAINTBRUSH GROUP (Tp)			
	rhyolite of Comb Peak (Tpk); includes the pyroclastic flow deposit (TpKi) that is informally referred to as tuff unit "X" (Tpki)		
	Post-Tiva Canyon bedded tuff (Tpbt5)		
Tiva Canyon Tuff (Tpc)	crystal-rich member (Tpcr) vitric zone (Tpcrv) -nonwelded subzone (Tpcrv3) -moderately welded subzone (Tpcrv2) -densely welded subzone (Tpcrv1) nonlithophysal zone (Tpcrn) lithophysal zone (Tpcrl)	Tiva Canyon welded (TCw)[d]	Tiva Canyon welded (TCw)[d]
	crystal-poor member (Tpcp) upper lithophysal zone (Tpcpul) middle nonlithophysal zone (Tpcpmn) lower lithophysal zone (Tpcpll) lower nonlithophysal zone (Tpcpln) -hackly subzone (Tpcplnh) -columnar subzone (Tpcplnc) vitric zone (Tpcpv) -densely welded subzone (Tpcpv3) -moderately welded subzone (Tpcpv2) -nonwelded subzone (Tpcpv1)	Paintbrush nonwelded (PTn)	Paintbrush nonwelded (PTn)
	pre-Tiva Canyon bedded tuff (Tpbt4)		
Yucca Mountain Tuff (Tpy)	Yucca Mountain Tuff (Tpy)		
	pre-Yucca Mountain bedded tuff (Tpbt3)		
Pah Canyon Tuff (Tpp)	Pah Canyon Tuff (Tpp)		
	pre-Pah Canyon bedded tuff (Tpbt2)		
Topopah Spring Tuff (Tpt)	crystal-rich member (Tptr) -vitric zone (Tptrv) -nonwelded subzone (Tptrv3) -moderately welded subzone (Tptrv2) -densely welded subzone (Tptrv1) nonlithophysal zone (Tptrn) lithophysal zone (Tptrl)	Topopah Spring welded. Lithophysae-rich (TSw1)	Topopah Spring welded (TSw)
	crystal-poor member (Tptp) upper lithophysal zone (Tptpul) [upper part]		
REPOSITORY HOST HORIZON[e]	upper lithophysal zone (Tptpul) [lower part] middle nonlithophysal zone (Tptpmn) lower lithophysal zone (Tptpll) lower nonlithophysal zone (Tptpln)	Topopah Spring welded. Lithophysae-poor (TSw2)	
	vitric zone (Tptpv) -densely welded subzone (Tptpv3) -moderately welded subzone (Tptpv2) -nonwelded subzone (Tptv1)	Topopah Spring welded vitrophyre (TSw3)	Topopah Spring basal vitrophyre (TSbv)
	pre-Topopah Spring bedded tuff (Tpbt1)		
Calico Hills (Tac)	Calico Hills Formation (Tac)	Calico Hills Nonwelded (CHn)	Calico Hills Nonwelded (CHn)
	pre-Calico Hills bedded tuff (Tacbt)		

Source: Reference 2.2.25, Table 3-1

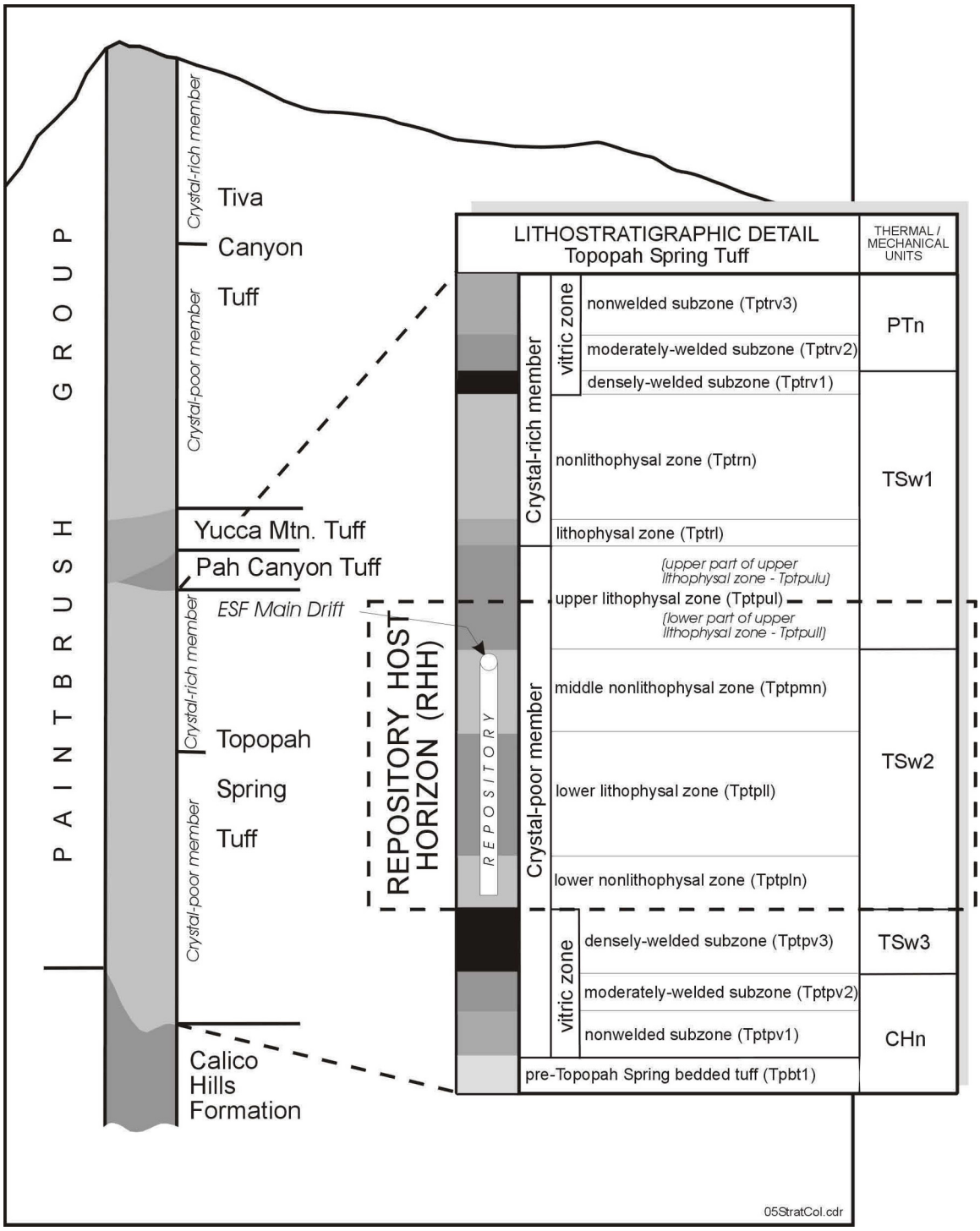

Source: Reference 2.2.26, Figure 5.

Figure 6-1 General Stratigraphic Column for Yucca Mountain

6.2.1 Generic Stratigraphy

For the purpose of shaft analysis, the lithostratigraphic units presented in Table 6-1 have been grouped into five major TM units, namely: 1) TCw, 2) PTn, 3) TSw1, 4) TSw1_Lithophysal, and 5) TSw2_Nonlithophysal.

This selection was further refined by considering the rock strength properties and the stress sustained by each unit in the Exploratory Studies Facility (ESF) ramps and the Main tunnel. For example, the properties of the PTn unit are represented by the properties of the 13_PTn_Tpcpv1 strata as listed in SGPR Rev 00 (Reference 2.2.16, Table 6-66). By combining the geotechnically similar units, the development of a numerical model could be simplified considerably. This simplification has a negligible consequence on the results as the associated model contains all the geotechnically significant features, and the range of conservative rock strength properties characterizing each stratum provides for a conservative assessment of shaft performance.

Figure 6-2 shows a sketch in which a L-type shaft/drift intersection arrangement is used as an example to show the relative location of TM units used in the current analysis. This generic stratigraphic represents a typical stratigraphic column used in the current shaft stability analysis.

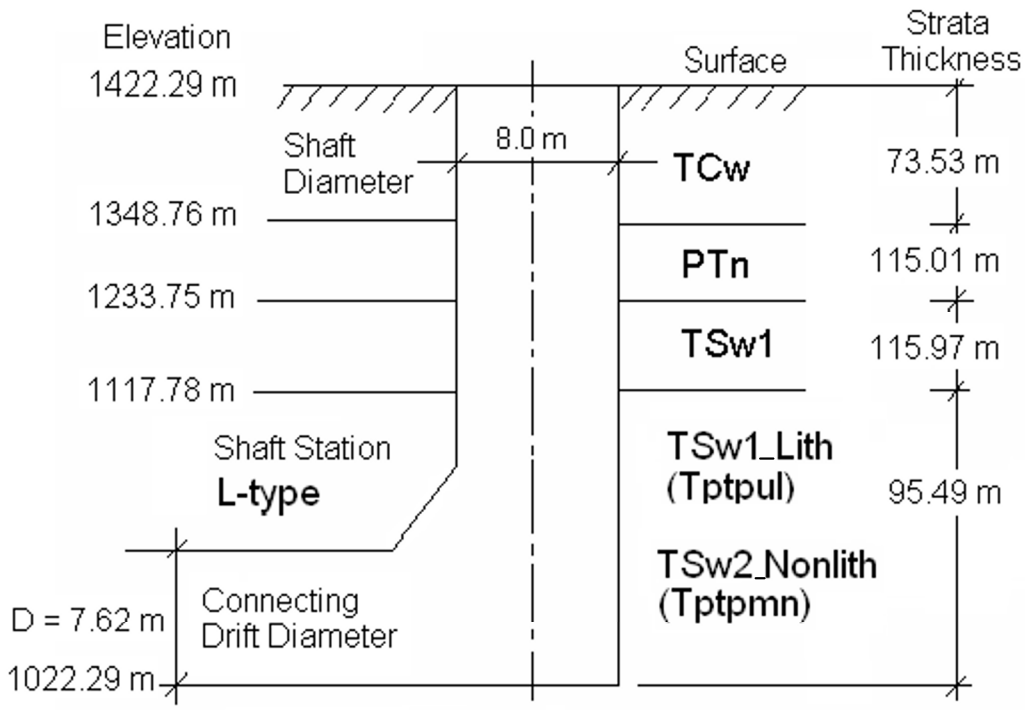

Figure 6-2 Thermal Mechanical Units Used in Numerical Model to Represent the Rock Strata

6.3 REPOSITORY LAYOUT AND SHAFT CONFIGURATIONS

The overall plane view of the repository layout and shaft locations shown in Figure 6-3. Shown in Figure 6-4 is a 3-D view of waste emplacement panels and associated shafts, displaying the flow of air and shaft functions. There are two types of ventilation shafts, 1) intake shafts, and 2) exhaust shafts. A typical intake shaft will operate at ambient temperature that will vary seasonally. Due to the heat generated by the emplaced waste, each exhaust shaft will operate at an elevated temperature. Calculations performed using FLUENT code (Reference 2.2.21) indicate that during the preclosure period of repository operation, the maximum operational drift temperature does not exceed 103 °C within the first 50 years of operation. It is reasonable to expect that the exhaust shafts will operate at the temperature level not higher than that of the emplacement drift.

Table 6-2 and Table 6-3 summarize the shaft-related data. Table 6-2 lists the shaft coordinates as well as individual shaft depths and diameters. Stratigraphic units and their elevations at each shaft location are listed in Table 6-3. The thickness of each TM unit was selected to represent the representative depth of that unit among all shaft locations listed in Table 6-3.

Generic Shaft

The stratigraphy used in the current analysis is performed for the generic shaft as presented in Table 6-4. This shaft is assembled such that it contains the stratigraphy representative for all shafts, and its collar elevation and depth of 400 m are selected to correspond to be on the conservative side in comparison to those of other repository shafts (Assumption 3.2.2). The shaft is considered to represent an average case and no distinction is made for this shaft to be either the intake or an exhaust type shaft.

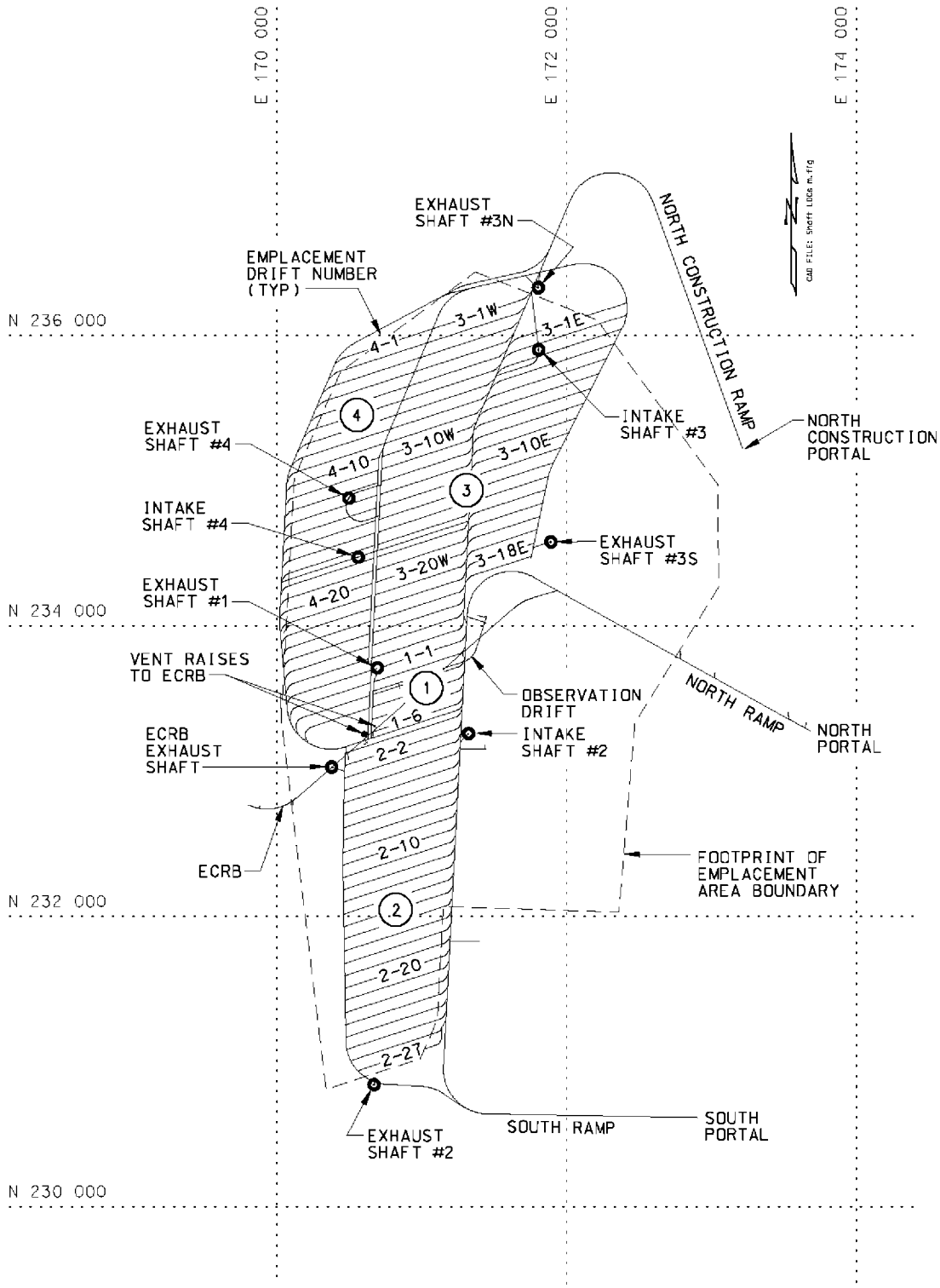

Source: Reference 2.2.20, Figure 11

Figure 6-3 Repository Footprint and Shaft Locations

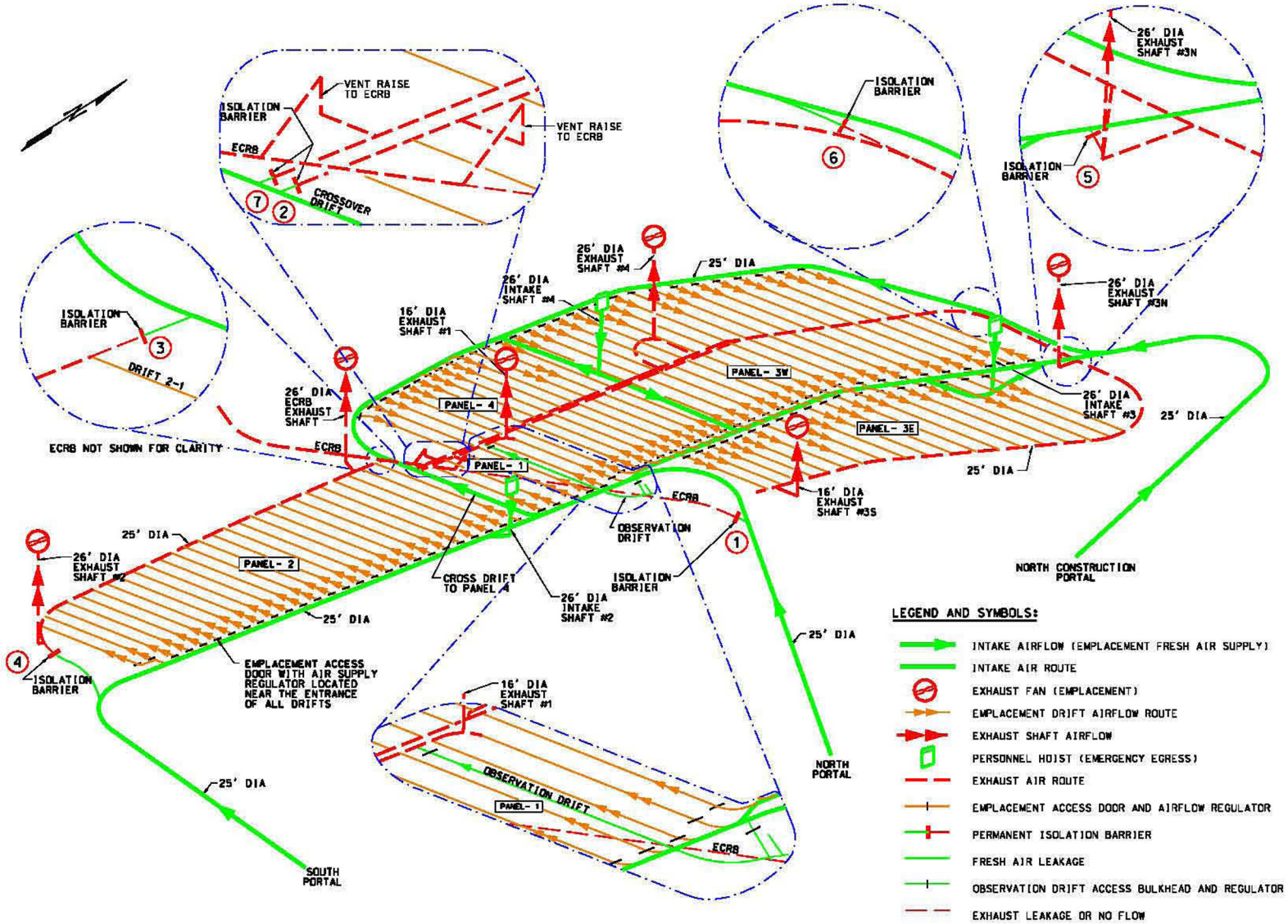

Source: Reference 2.2.17

Figure 6-4 Repository Ventilation System, Shaft Locations and Functions

Table 6-2 Shaft Collar and Station Coordinates and Shaft Name Nomenclature

Shaft Name	Assigned Short Name	Shaft Location	Shaft Coordinates			Shaft Depth (m)	Shaft Diameter[1] (m)	Shaft/Drift Configuration
			Northing (m)	Easting (m)	Elevation (m)			
Intake Shaft #2	IN_2	Collar	233,260.25	171,322.50	1,325.00	248.10	8.0	L
		Station	233,260.25	171,322.50	1,076.90			
Intake Shaft #3	IN_3	Collar	235,903.43	171,805.96	1,410.00	350.47	8.0	T
		Station	235,903.43	171,805.96	1,059.54			
Intake Shaft #4	IN_4	Collar	234,474.45	170,560.87	1,450.00	377.98	8.0	T
		Station	234,474.45	170,560.87	1,072.02			
Exhaust Raise 1 (Old)		Collar	234,010.00	170,690.00	1,435.00	370.91	5.0	T
		Station	234,010.00	170,690.00	1,064.09			
Exhaust Shaft #1 (New)	EX_1	Collar	233,713.00	170,692.00	1,425.00	356.00	5.0	T
		Station	233,713.00	170,692.00	1,069.00			
Exhaust Shaft #2	EX_2	Collar	230,842.86	170,669.24	1,400.00	292.13	8.0	L
		Station	230,842.86	170,669.24	1,107.87			
Exhaust Shaft #3N	EX_3N	Collar	236,330.29	171,803.38	1,450.00	427.71	8.0	L
		Station	236,330.29	171,803.38	1,022.29			
Exhaust Shaft #3S	EX_3S	Collar	234,580.00	171,890.00	1,340.00	278.80	5.0	T
		Station	234,580.00	171,890.00	1,061.20			
Exhaust Shaft #4	EX_4	Collar	234,880.59	170,495.70	1,470.00	405.02	8.0	T
		Station	234,880.59	170,495.70	1,064.98			
ECRB Exhaust Shaft	EX_ECRB	Collar	233,029.53	170,378.51	1,475.00	365.60	8.0	T
		@ECRB	233,029.53	170,378.51	1,109.41	32.84		
		Station	233,029.53	170,378.51	1,076.56	398.44		
Construction Vent. Raise to ECRB						29.0	3.75	
Construction Vent. Raise to ECRB						29.0	8.0	

Sources: Reference 2.2.3, Table 7, Reference 2.2.20, Table 8 and Table 16

Note: 1. Shaft Diameters as listed in Reference 2.2.20, Tables 3, 4, 5, 8 and 9.

Table 6-3 Lithostratigraphic Column at Each Proposed Shaft Location

Layer Number	Lithostratigraphic Unit	TM Units Used in Analysis	Intake Shaft #2, IN_2	Intake Shaft #3, IN_3	Intake Shaft #4, IN_4	Exhaust Raise #1 (OLD), Ex_R_1 (Old)	Exhaust Shaft #1 (NEW), EX_1, (Note 1)	Exhaust Shaft #2, EX_2	Exhaust Shaft #3N, EX_3N	Exhaust Shaft #3S, EX_3S	Exhaust Shaft #4, EX_4	ECRB Exhaust Shaft, EX_ECRB
Collar El. (m) --->			**1325.00**	**1410.00**	**1450.00**	**1435.00**	**1442.50**	**1400.00**	**1450.00**	**1340.00**	**1470.00**	**1475.00**
1	Tpcpv3	TCw	1253.91	1340.76	1349.87	1328.99	1339.43	1316.96	1364.09	1246.06	1367.34	1349.37
2	Tpcpv2		1253.91	1340.76	1349.87	1328.99	1339.43	1315.20	1364.09	1246.06	1367.34	1348.76
3	TPcpv1	PTn	1249.45	1332.87	1345.71	1323.89	1334.80	1312.04	1356.04	1242.54	1363.02	1343.86
4	Tpbt4		1246.81	1327.05	1338.50	1318.18	1328.34	1308.53	1349.26	1237.12	1355.17	1342.19
5	Tpy		1245.50	1324.80	1337.93	1317.79	1327.86	1307.21	1347.78	1234.88	1353.50	1341.14
6	Tpbt3		1244.42	1303.19	1327.05	1308.52	1317.79	1307.21	1326.82	1216.77	1341.78	1335.92
7	Tpp		1239.98	1276.47	1322.42	1304.36	1313.39	1303.43	1295.60	1206.18	1336.93	1330.74
8	Tpbt2		1229.74	1227.96	1296.44	1286.49	1291.47	1301.32	1244.67	1172.22	1300.34	1325.24
9	Tptpv3		1221.28	1219.06	1287.37	1277.02	1282.19	1294.11	1234.38	1163.25	1291.43	1317.23
10	Tptpv2		1217.35	1218.74	1283.89	1272.40	1278.14	1293.18	1234.23	1159.98	1287.28	1313.84
11	Tptpv1	TSw1	1216.93	1218.08	1283.16	1271.78	1277.47	1292.37	1233.75	1158.44	1286.88	1312.90
12	Tptrn		1215.71	1218.01	1281.67	1270.68	1276.17	1292.11	1233.75	1157.87	1285.73	1312.17
13	Tptrl		1170.23	1164.30	1237.57	1223.95	1230.76	1266.42	1179.80	1102.91	1243.91	1275.05
14	Tptpf		1165.16	1156.87	1226.84	1213.65	1220.24	1264.09	1172.80	1091.07	1232.16	1268.18
15	Tptpul		1165.16	1152.52	1226.84	1213.65	1220.24	1264.09	1163.01	1091.07	1232.16	1268.18
16	Tptpul (RHH)	TSw1_Lith	1103.45	1111.58	1184.80	1164.53	1174.66	1232.74	1117.78	1091.07	1194.45	1214.04
17	Tptpmn	TSw2 _nonlith	1088.96	1094.00	1148.97	1135.73	1142.35	1214.48	1107.34	1091.07	1156.19	1197.31
18	Tptpll		1088.96	1063.42	1117.29	1104.79	1111.04	1171.44	1078.21	1091.07	1122.60	1160.66
19	Tptpln		1088.96	1063.42	1117.29	1104.79	1111.04	1171.44	1078.21	1091.07	1122.60	1160.66
Station El. (m) -->			**1076.90**	**1059.54**	**1072.02**	**1064.09**	**1068.06**	**1107.87**	**1022.29**	**1061.20**	**1064.98**	**1076.56**
Shaft Depth (m) ->			**248.10**	**350.47**	**377.98**	**370.91**	**374.44**	**292.13**	**427.71**	**278.80**	**405.02**	**398.44**

Sources: Reference 2.2.6, Reference 2.2.3, Table 7, and Reference 2.2.20, Table 8 and Table 16

Notes:
1. EX_1 stratigraphy interpolated between IN_4 and ECRB Exhaust Shaft.
2. Elevations Shown are at the Top of Each Lithostratigraphic Unit.
3. Indicated in red are strata layers nonexistent at that location.
4. All dimensions expressed in meters.
5. Exhaust Raise #1 (Old) data are used in calculations of average elevations of stratigraphic unit.

Table 6-4 Generic Shaft Stratigraphy

TM Units Used in Analysis	SGPR Rev 00 TM and Lithostratigraphic Designation	Average Saturated Bulk Density, g/cm^3 (Note 5)	Average Saturated Bulk Density Used, g/cm^3 (Note 6)	Elevation Top of Strata Interface, m	Elevation Bottom of Strata Interface, m (Note 7)	Depth Top of Strata Interface, m	Depth Bottom of Strata Interface, m	Individual Strata Thickness m	Distance Top of Strata to Emplac Level, m	Distance Bottom of Strata to Emplac. Level, m	Vertical Stress at Bottom of Each Interface, MPa (Note 8)	RHH to Interface Temp. Diff. in 100 yrs, °C (Note 9)		Empl. Drift Centerline / Pillar Centerline Temp. Diff. in 100 yrs, °C (Note 10)	
												Rev A	Rev B	Rev A	Rev B
Collar Elevation				**1422.29**	1422.29										
				(Note2)											
TCw	04_TCw_Tpcrn	2.12	2.41	1422.29	1348.76	0.00	73.53	73.53	400.00	326.47	1.77	0.0	0.0	N/A	N/A
					(Note 3)										
PTn	18_PTn_Tpbt2	1.73	2.41	1348.76	1233.75	73.53	188.54	115.01	326.47	211.46	4.54	0.0	2.6	N/A	N/A
TSw1	23_TSw1_Tptrl	2.26	2.41	1233.75	1117.78	188.54	304.51	115.97	211.46	95.49	7.34	3.0	8.0	N/A	N/A
Strata at the Repository Host Horizon (RHH)															
TSw1_Lith	25_TSw1_Tptpul	2.41	2.41	1117.78	1022.29	304.51	400.00	95.49	95.49	0.00	9.64	N/A	N/A	40.0	27.2
		(Note 1)					(Note 4)								
TSw2_Nonlith	26_TSw2_Tptpmn	2.41	2.41	1117.78	1022.29	304.51	400.00	95.49	95.49	0.00	9.64	N/A	N/A	40.0	27.2

Notes:

1. Conservative value of Saturated Bulk Density for RHH TM units taken as equal to 2.41 g/cm^3, (density of Tptpln, highest among RHH units, Reference 2.2.16, Table 6-67, p. 6-22).
2. Elevation 1422.29 m considered as collar elevation to account for shaft depth used in calculation (Assumption 3.2.2).
3. Elevation 1348.76 taken to provide a more even representation of the TCw strata in calculations (Assumption3.2.2).
4. A reference depth established at 400 m at the centerline of the drift connecting the Shaft Station and the Exhaust Main, at the lowest elevation of RHH strata in all shafts.
5. Average Saturated Bulk Density data used for thermal and seismic calculations.
6. Conservative values of density (2.41 g/cm^3) used for all strata for calculating in-situ stresses.
7. The elevations of TCw/PTn and PTn/TSw1 contacts are identical to those used in *Shaft Liner Design*, Rev A (Reference 2.2.14). The surface elevation changed from 1475.0 m to 1422.29 m and the elevation of the shaft station was established at 1022.29 m to maintain the same as in *Shaft Liner Design*, Rev A (Reference 2.2.14).
8. Values of vertical stresses calculated using the gravity g=10 m/s^2.
9. Source: Reference2.2.14
10. Source: Reference 2.2.21

6.4 INPUT DATA AND PARAMETERS

6.4.1 Rock Properties

As stated in Section 6.2.1, the detailed stratigraphy of the generic shaft has been simplified to be represented by five TM units: TCw, PTn, TSw1, TSw1_Lithophysal and TSw2_Nonlithophysal and summarized in Table 6-4. As described in detail in *Drift Degradation Analysis* (Reference 2.2.5, Section 4.1.4.2), the mechanical properties of rocks within each of these units are classified into five categories, with Category 1 characterizing the poorest rock-mass quality and Category 5 characterizing the best rock-mass quality as encountered in the ESF and Enhanced Characterization of the Repository Block (ECRB) Cross Drift. Table 6-5 lists mechanical properties for the five representative TM units, each characterized by rock mass category 1 and 5. Unless otherwise noted, the rock property data were extracted from SGPR Rev 00 (Reference 2.2.16).

6.4.2 Shaft Diameters

In general, the shaft dimensions considered for the repository shafts, are vary ranging from small, 3.75 m diameter for construction raise to 8 m diameter for the typical intake and exhaust shafts. The stability of a shaft depends on several factors such as rock mass properties, in situ stresses and other, e.g., thermal and seismic loading conditions. Under given local conditions, however, the major discriminating factor is the shaft diameter. The larger the diameter, the more pronounced impact other factors will have upon its stability and overall performance. Therefore, for the purpose of this study, the largest shaft diameter among all planned repository shafts equal to 8.0 m is considered in general case of liner design analysis. In addition, liner design analysis for 5-m shaft diameter is analyzed using the shaft liner thickness of 0.25-m. When the drift connected to the shaft has been modeled the diameter of the drift is equal to 7.62 m, the largest already existing tunnel boring machine-excavated diameter (Reference 2.2.3, Section 8.4).

Table 6-5 Rock Mass Properties for Representative TM Units

TM Units Used in Analysis	SGPR Rev 00 TM and Lithostratigraphic Designation	Rock Mass Quality Category	Intact Rock UCS, σ_{ci}, MPa	Lithophysal Porosity, %	Hoek-Brown Class. GSI	Mohr-Coulomb Parameters		Rock Mass Tensile Strength, σ_t, MPa	Rock Mass Global Strength, σ_{cm}', MPa	Rock Mass Modulus of Deformability, Em, GPa	Rock Mass Poisson's Ratio, ν	Rock Mass Dilation Angle, Degrees	CTE, 10^{-6} /°C.
						C, MPa	ϕ, degrees						
TCw	04_TCw_Tpcrn	1	36.02	N/A	56	1.63	26.18	0.27	5.24	8.48	0.20	0.0	7.34
		5			80	3.25	32.09	1.65	11.76	33.75			
PTn	18_PTn_Tpbt2	1	2.92	N/A	63	0.18	33.13	0.02	0.65	3.61	0.21	0.0	7.34
		5			78	0.25	37.23	0.06	1.00	8.56			
TSw1	23_TSw1_Tptrl	1	38.06	N/A	42	1.54	26.14	0.06	4.93	3.89	0.30	0.0	7.34
		5			64	2.27	32.45	0.32	8.27	13.81			
Rock Mass Strength Properties for the RHH Strata													
TSw1_Lith	25_TSw1_Tptpul	1	97.13	>30	42	2.60	35.0	1.00	10	1.9	0.22	0.0	8.99
		5		<10	69	7.81	35.0	3.00	30	19.7			
TSw2_Nonlith	26_TSw2_Tptpmn	1	136.36	N/A	51	7.36	32.64	0.27	26.90	10.59	0.19	0.0	8.99
		5			72	10.52	38.79	1.33	43.90	35.48			

Source: Data based on merged SGPR Rev 0, Tables 6-66 and 6-67 (Reference 2.2.16)

Notes:

1. GSI values correspond to 5, 20, 40, 70, and 90% of cumulative frequency of occurrence in the tunnels which correspond to rock mass categories 1 through 5.
2. Poisson's ratio taken as equal to that of the intact rock.
3. The properties of Tptpul are considered representative of Lithophysal strata in RHH. Rock mass strength properties for these strata calculated using porosity as a surrogate parameter.
4. The properties of Tptpmn are considered representative of Nonlithophysal strata in RHH.
5. For Tptpul strata cohesion (c) is calculated based on rock mass strength ($\sigma_{cm'}$) and friction angle (ϕ), and Tensile Strength (σ_t) is taken as one-tenth of rock mass strength ($\sigma_{cm'}$).
6. CTE values taken as those for temperature interval 50 to 75 ºC for RHH Units (8.99e-6 1/ºC) and 25 to 50 ºC (7.34e-6 1/ºC) for the strata above RHH (Reference 2.2.16, Table 6-86). It should be noted that the CTE values presented in this Table are based on laboratory testing on specimen from DST and are considered conservative.

6.4.3 Mechanical Properties of Ground Control Components

Properties of the concrete liner used in the current analysis are summarized in Table 6-6. The concrete liner is installed after 100% of stress-relaxation due to excavation takes place (Assumption 3.2.4). In effect, the liner has been considered to take load due to thermal and seismic effects only.

Table 6-6 Properties of Unreinforced Concrete Liner

Concrete Parameter	Value	Source/Remark
Thickness (m)	0.3	Converted from a 12 in. thickness (12.0 in. x 0.0254 m/in. = 0.3 m)
Density (kg/m^3)	2324	Converted from a typical unit weight for concrete 145 lb/ft^3 x 0.454 kg/lb x 35.315 ft^3/m^3 = 2324 kg/m^3 (Reference 2.2.29)
Young's Modulus (GPa)	29	Based on mean value in Sec. 1.7 of ACI, 506R-05 (Reference 2.2.1).
Poisson's Ratio	0.25	Reference 2.2.30, p. 6-8
Compressive Strength (MPa)	40.0	Converted from concrete strength of 6000 psi/(145 psi/MPa) = 40 MPa (approximately) (Reference 2.2.29, Chapter 1 page 5, Section "Unit Weight")
Tensile Strength (MPa)	4.0	10% of Uniaxial Compressive Strength (UCS) or 0.1x40.0 MPa = 4.0 MPa
CTE (1/°C)	9.90E-06	Reference 2.2.30, p. 5-13
Allowable Stress (MPa)	26.0	Applied reduction factor (**0.65** x 40 MPa = 26 MPa), based on ACI 318-02, Sec. 9.3.2.2 (Reference 2.2.1)

6.4.4 Field Stresses

To estimate the initial stress conditions around the shafts, different lengthwise sections of the shaft were considered and the thickness of the overlaying strata computed. Table 6-4 provides the evaluation of the initial vertical stresses for strata in different units. These vertical stresses are computed based on uniform unit weight equal to 0.0241 MN/m^3 (150 lb/ft^3) (Reference 2.2.5, Attachment V, Table V-2).

6.4.5 Horizontal-to-Vertical Stress Ratio

Results of hydraulic fracturing stress measurements indicate that at the Yucca Mountain site the horizontal-to-vertical stress ratio is equal to 0.36 to 0.62 for the minimum and maximum horizontal stress, respectively (Reference 2.2.35). In this calculation the horizontal stresses are computed considering the ratio of horizontal-to-vertical stress equal to 0.5 (Assumption 3.2.3). In effect, the horizontal components of stresses are all equal to each other. Note that for shaft sections in the units of TSw1_lithophysal and TSw2_nonlithophysal, the depth of the section is considered to be equal to 400 m (Assumption 3.2.2).

6.4.6 Rock Thermal Properties Data and Field Temperature Characteristics

In Revision A, the NUFT thermal field data was used as input to FLAC3D code to evaluate the mechanical effect and responses of the associated ground support due to temperature change in the rock mass. The NUFT analysis has been performed to obtain the temperature distribution within the mountain-scale model of rock strata based on the thermal line load of 1.45 kW/m.

In this revision, the distribution of temperature within the mountain-scale model has been evaluated using FLAC3D mountain-scale model and FLUENT model (Reference 2.2.21) with a thermal line load of 2.0 kW/m and adds the evaluation of the mechanical effect and responses of the associated ground support due to temperature change in the rock mass. The effects of the increased thermal line load from 1.45 kW/m to 2.0 kW/m on shaft stability are also included in this revision.

It should be noted that the ventilation scenario considered in the Rev A and current analysis (Rev B) are not the same. In Rev A, first 50 years of 100-year preclosure period are considered forced ventilation with air flow rate of 15 m^3/s, while the second 50 years the ventilation is considered natural ventilation only with the minimum flow rate of 0.0 m^3/s. The thermally induced stresses in the rock and concrete liner due to temperature raise during the second 50 years are, in essence, corresponding to an off-normal scenario. Ventilation scenario in current analysis considers 100 years continuous forced ventilation at the rate of 15 m^3/s.

In general, the value of CTE is a function of temperature. In the current analysis the CTEs as listed in Table 6-5 are considered to be constant, independent of temperature. From the FLAC3D generated input, a value was selected corresponding to the temperature changes 100 years after waste emplacement.

The temperature changes for the shaft sections located within the TSw1_Lith or TSw2_Nonlith unit were calculated while considering the two shaft locations; 1) the shaft located in the center of the repository, and 2) the shaft located in the center of the pillar separating two adjacent emplacement drifts. For other units located at larger vertical distance from the repository horizon, it is considered that the shafts are located along the axes of emplacement drifts. As a result of this conservative approach, predicted temperature changes are only few degrees higher.

The temperature changes at various shafts depend on the distance between the individual shaft-location and the heat source, i.e., emplacement drift, as well as the elevation of the point of interest along the shaft axis, e.g., rock mass temperature at the repository level will be different than temperature at other elevations along the shaft axis. Table 6-4 summarizes the temperature changes associated with relative location of the shaft and heat sources. Temperature changes relative to the ambient in-situ temperature state are provided for temperature states at 100 years of heating. The distances selected for this analysis represent a scenario, where the elevations for individual interfaces between the overlaying strata were selected at the elevations considered representative among all shaft locations and the associated strata elevations listed in Table 6-4.

6.4.7 Repository Layout and Shaft Locations

Shaft types were obtained from the drawing entitled: *Subsurface Ventilation Airflow Arrangement for LA Full Emplacement* (Reference 2.2.17). The locations of the all shafts were

obtained from *Underground Layout Configuration* (Reference 2.2.3, Table 7) and location of the new Exhaust Shaft #1, replacing the previously considered Exhaust Raise #1 as well as modifications of the all shaft nomenclature were obtained from *Underground Layout Configuration for LA* (Reference 2.2.20, Table 8 and Table 16). The elevations of rock strata at this location were obtained by simple linear interpolation between elevations of the individual stratigraphic unit at the Intake Shaft #4 and the Exhaust Shaft #1 locations.

6.4.8 Initial Ground Relaxation

The relaxation of rock strata surrounding the shaft due to excavation is considered to be equal to 100% prior to installation of the concrete liner (Assumption 3.2.4). This procedure is consistent with the general approach used in numerical simulations of underground excavations. As a result, the shaft liner is considered to be subject to the thermal and seismically-induced loads only.

6.4.9 Seismic Ground Motion Data

In the current analysis, time histories of velocity components of 1 x 10^{-4} ground motion as presented in Figure 6-6 have been used as input in computer simulations under assumption presented in Assumption 3.1.1. This ground motion is subjected to limitation of frequencies below 0.5 Hz that are not qualified (Reference 2.2.18, Executive Summary, p viii). The following discussions are presented to enhance the understanding of the adequacy, conservatism and risk involved in applying the ground motions documented in DTN MO0707THRB1E4A.000 (Reference 2.2.33).

Dynamic vs Quasi-Static Loading: Ground motion time histories are transient and stochastic in nature, and cover a broad range of wavelength and frequency. The interaction of a seismic wave with an underground opening depends on the ratio of the wavelength to the maximum span of the opening. For large ratios, say, greater than 8, and relatively long ground motion duration, the transient ground motion caused by seismic waves produce basically quasi-static loading, which is the case of current analysis. A typical wave speed of 2,000 m/s with the frequency ranging from 0.5 to 10 Hz will have the wavelengths ranging from 4,000 to 200 m, resulting in a minimum ratio of 25 for an 8-m shaft. Based on the magnitude of this ratio, the shafts analyzed are not anticipated to be sensitive to the low frequency range. It is the peak ground velocity values that have the major impact on seismically induced stresses. Therefore, the limitation presented in Reference 2.2.18 (Executive Summary, p viii) will not impact the current shaft liner analysis.

Conservatism in Seismic Loading: Ground motions with an APE of 1 x 10^{-4} (a 10,000-year return period) are considered to be beyond the preclosure design basis. Therefore, the shaft liner analysis presented in this revision is valid and adequate for supporting the LA.

Conventional Application of Ground Motion Parameters: PGV measures the amplitude of medium frequencies in the ground motion and is used for underground structures in medium to hard rock while the peak ground displacement measures the amplitude of low-frequencies and is mostly used for surface structures. The limitation applies to the frequency at or below 0.5 Hz, which is on the low end of the frequency range of the response spectra. Thus, a low frequency

range is not anticipated to play a significant role in velocity time histories used in subsurface design.

Time histories of velocity components of 1 x 10^{-4} ground motion presented in Figure 6-5 is based on DTN MO0306SDSAVDTH.000 which was used in Rev A analysis and is presented for information only.

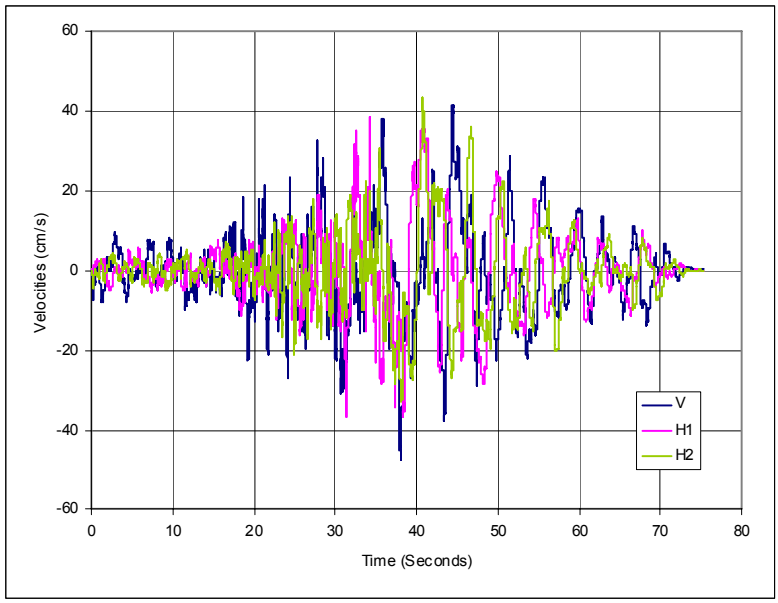

Source: MO0306SDSAVDTH.000 (Reference 2.2.31)

Figure 6-5 Time Histories of Velocity Components of 1x10^{-4} Seismic Motion at Repository Horizon

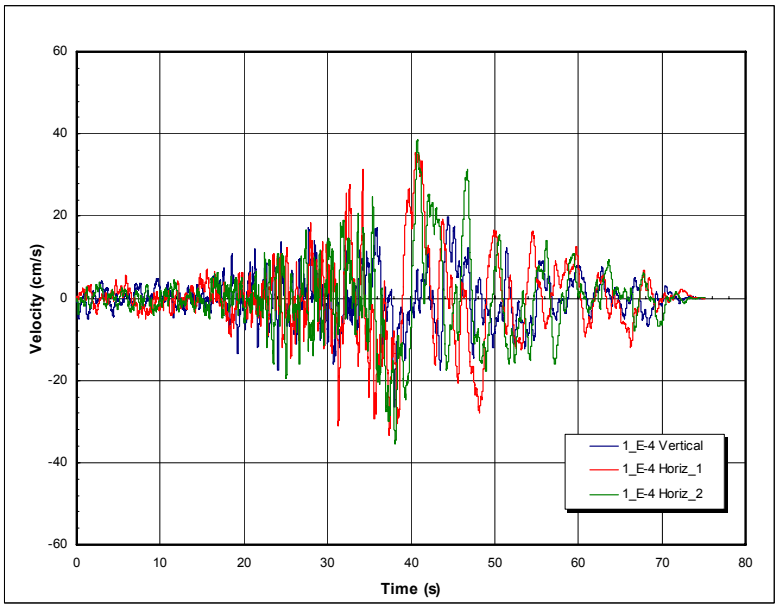

Source: MO0707THRB1E4A.000 (Reference 2.2.33)

Figure 6-6 Updated Time Histories of Velocity Components of 1x10^{-4} Seismic Motion at Repository Horizon

6.5 ANALYSIS

Shaft analysis in Revision A (Reference 2.2.14) was based on the thermal line load of 1.45 kW/m and seismic load of $1x10^{-4}$ APE ground motion with time histories of velocity provided in Figure 6-5. This section presents the results of shaft analysis based on the revised thermal line load (2.0 kW/m) and seismic velocity components provided in DTN MO0707THRB1E4A.000 (Reference 2.2.33). Based on the Rev A and current Rev B shaft analysis, shaft performance and the effects of new thermal line load and seismic load on shaft performance are evaluated and presented in this section.

6.5.1 Solutions for Unlined Shaft – Baseline Case

To develop a more thorough understanding of the excavation process and its impact on shaft stability, it is important to examine the performance of rock strata surrounding the shaft during and after excavation, without support and then with the standard ground reinforcement applied. The following steps involve the development of a numerical model and testing the validity of solution by comparing the closed-form solution results against numerical modeling results.

6.5.1.1 Closed-Form Solution

The initial analysis of rock mass stability and shaft closure was carried out for each TM unit intersected by the shaft. At the interface between each subsequent rock strata unit a depth of the overburden was selected as the representative depth among all nine shafts penetrating that unit as listed in Table 6-3. The data selected is summarized in Table 6-4.

Calculations of shaft closure for shaft segments located in the different units were performed using the closed form solution, as discussed by Carranza-Torres (Reference 2.2.24). Details of the derivation of the closed-forms numerical formulae and the results for PTn unit, rock mass Category 1 are presented in Attachment A.

The analytical results (i.e., the extent of the failure zone and a maximum radial displacement) are summarized in Table 6-7. The shaft deformation was calculated as a function of depth and applied confining pressure. The product of these calculations is a ground reaction curve, which illustrates the magnitude of deformation as a function of radial stress (sig0) and shaft internal pressure (pi). Figure 6-7 shows a ground reaction curve representing the radial shaft closure as a function of decreasing internal pressure computed using the analytical solution. The results shown in Figure 6-7 correspond to the unit PTn represented by the Category 1 rock. For the same PTn unit, Figure 6-8 shows the corresponding relation between the resulting dimensions of the failed zone as a function of internal pressure.

The profile of convergence and radius of plastic zone along the shaft EX_3N are shown in Figure 6-9 and Figure 6-10. The difference between responses of adjacent individual strata assists in focusing design on these transition zones. Field experience indicates that the contrast in response is tempered by a more gradual transitions zone between adjacent stratigraphic and no visible signs of the impact such contrast in response may cause are evident. In addition, as shown further in this analysis, e.g., Section 6.5.1, unlined shaft excavations completed in all stratigraphic units stabilize on their own prior to installation of the final liner.

Table 6-7 Extent of Failure Zone Rpl and Radial Displacements ur for Shaft Sections in Different Rock Mass Units and Categories Obtained Using Analytical Solution

Rock Strata	Rock Mass Category	u_r (m)	R_{pl} (m)	u_r/R (%)	R_{pl}/R
TCw	1	5.04E-04	-	0.013	-
	5	1.27E-04	-	0.003	-
PTn	1	7.90E-03	7.24	0.198	1.81
	5	2.21E-03	5.80	0.055	1.45
TSw1	1	5.22E-03	4.52	0.130	1.13
	5	1.38E-03	-	0.035	-
TSw1_Lithophysal	1	1.24E-02	-	0.310	-
	5	1.19E-03	-	0.030	-
TSw2_Nonlithophysal	1	2.17E-03	-	0.054	-
	5	6.47E-04	-	0.016	-

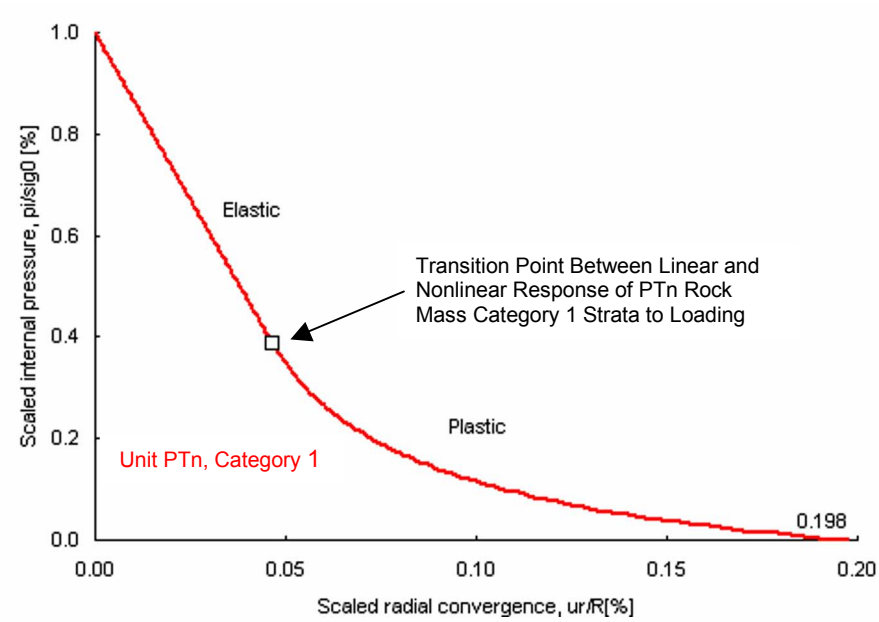

Note: pi=internal pressure; sig0=radial stress

Figure 6-7 Ground Reaction Curve Obtained with an Analytical Solution for a Section of Shaft Excavated in PTn, Category 1

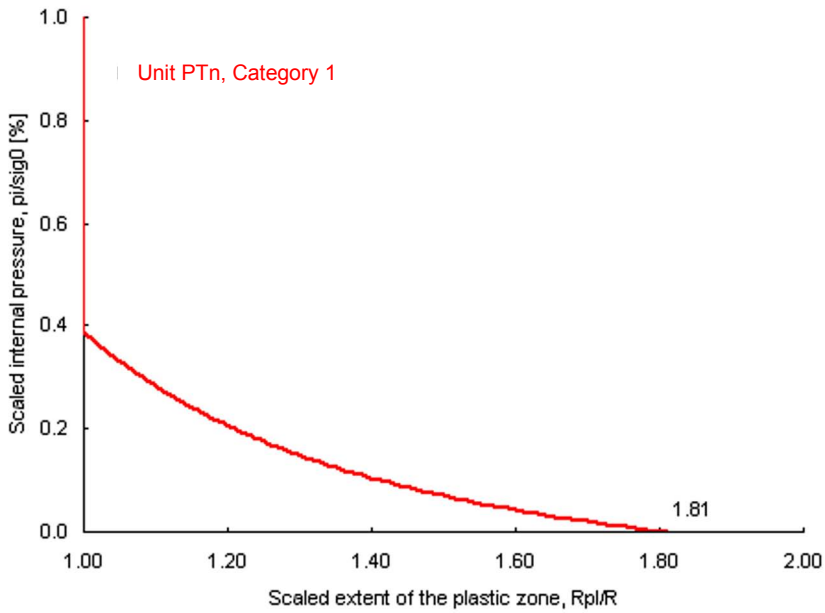

Note: pi=internal pressure; sig0=radial stress

Figure 6-8 Extent of Failure Zone as a Function of Decreasing Internal Pressure as Obtained Analytically for a Section of Shaft Excavated in PTn, Category 1.

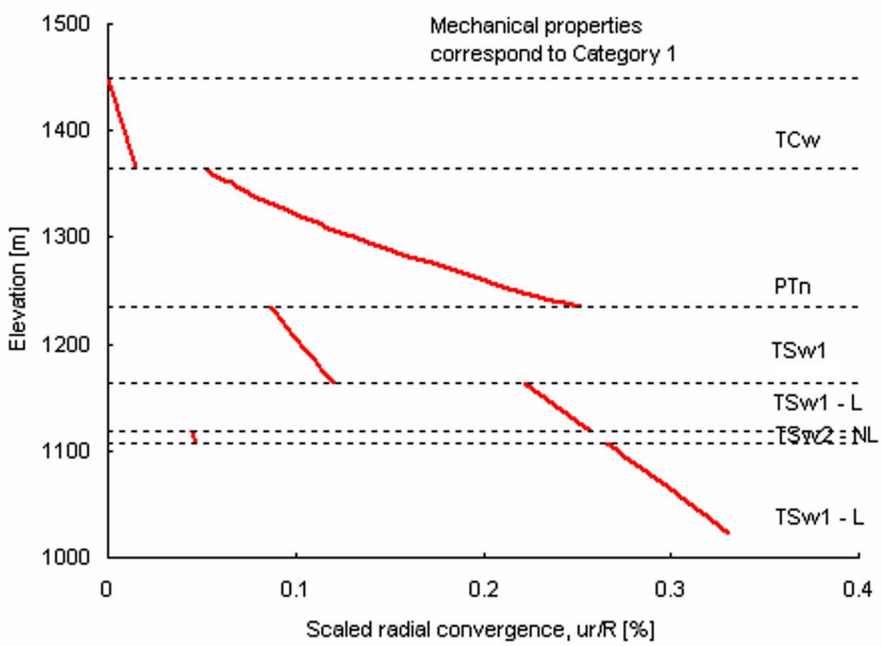

Figure 6-9 Profile of the Maximum Shaft Closure (Scaled to the Shaft Radius) Along the Shaft EX_3N Considering Category 1 Rock Mass in Each Unit

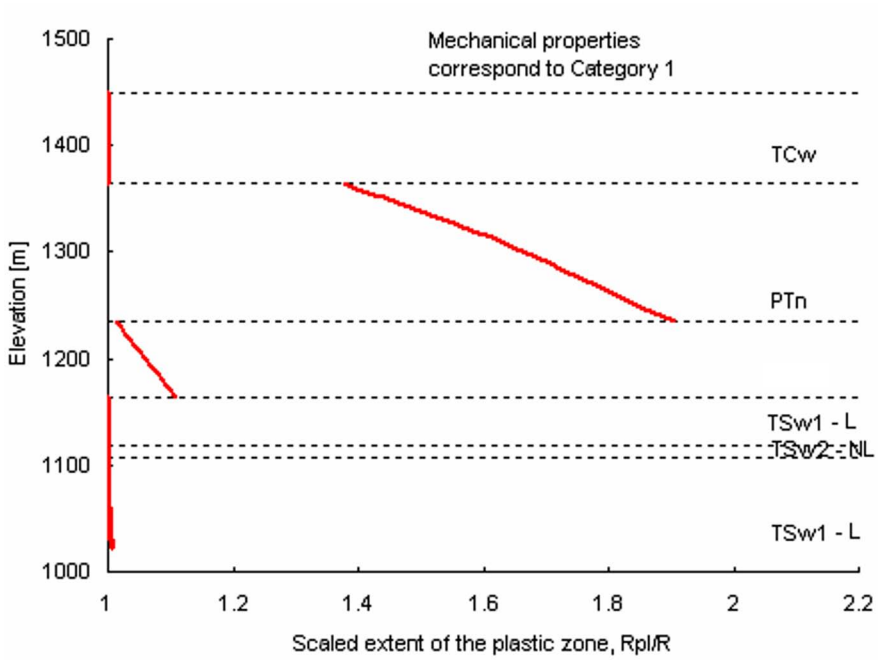

Figure 6-10 Profile of the Normalized Radius of the Plastic Zone along the Shaft EX_3N Considering Category 1 Rock Mass in Each Unit

6.5.1.2 Numerical Solution

To complement the analytical solution (presented in Figure 6-7 through Figure 6-10), the numerical solution was obtained for identical conditions. A procedure leading to the development of the numerical model, followed by comparison of the numerical and analytical results is described below. Table 6-2 and Table 6-3, shown earlier, contain a list of all shafts including coordinates and detailed geology at each shaft location. The modeling methodology applied in the current study is based on the worst-case scenario, which results in selecting thickness and deepest elevation for the weaker strata, such that potentially the most unfavorable effects of in situ stresses on shaft stability could be evaluated. Table 6-8 summarizes the basic parameters of the numerical base case model used in the current analysis.

Table 6-8 Base Case Configuration for the Generic Shaft Modeling Analysis

2D-Model Dimension	80 x 80 x 1.25 m
Overburden Depth to Interface	Variable
Density of Overburden	2410 kg/m^3
In situ K_0 factor	0.5

Table 6-7 summarizes the values of the radial extent of failure zone (Rpl) and radial displacement (ur) for different units and rock categories 1 and 5 as obtained using analytical approach. Table 6-9 summarizes the equivalent results obtained with FLAC3D. These tables also include the scaled magnitudes (Rpl / R) and (ur / R), where R = 4 m is the radius of the

shaft. The table also provides an indication if plasticity is observed in numerical model. The accuracy of the actual radius of plasticity in the numerical model is a function of the zone size in comparison to the size of plastic region. However, qualitative agreement of the analytical and numerical models with regard to prediction of plasticity is evident from the Figure 6-12 and Figure 6-13.

The contours of the displacement calculated in the numerical model for the PTn unit are shown in Figure 6-11. The maximum displacement of 0.009 m compares well with analytically obtained convergence of 0.008 m. Figure 6-12 represents the extent of the failure zone for the shaft section located in PTn, Category 1 unit.

Shaft sections in units PTn, Category 1 and TSw1_Lith, Category 1 show the development of the failure zone after excavation, with TSw1_Lith, Category 1 strata showing the largest value of deformation for both cases. Table 6-7 and Table 6-9 show that the shaft section excavated in TSw1_Lithophysal, Category 1 unit has the largest convergence (ur / R ≈ 0.30%).

Table 6-9 Extent of Scaled Failure Zone Rpl and Radial Displacements ur for Shaft Sections in Different Rock Mass Units and Categories Obtained for Shaft Sections Modeled Using FLAC3D

Rock Strata	Category	u_r (m)	R_{pl} (m)	u_r/R (%)	R_{pl}/R
TCw	1	5.079e-04	-	0.013	-
	5	1.276e-04	-	0.003	-
PTn	1	9.049E-03		0.226	yes
	5	2.334e-03	yes	0.058	yes
TSw1	1	5.092e-03	yes	0.127	yes
	5	1.359e-03	-	0.034	-
TSw1_Lithophysal	1	1.220E-02	-	0.305	-
	5	1.176E-03	-	0.029	-
TSw2_Nonlithophysal	1	2.136e-03	-	0.053	-
	5	4.373e-04	-	0.011	-

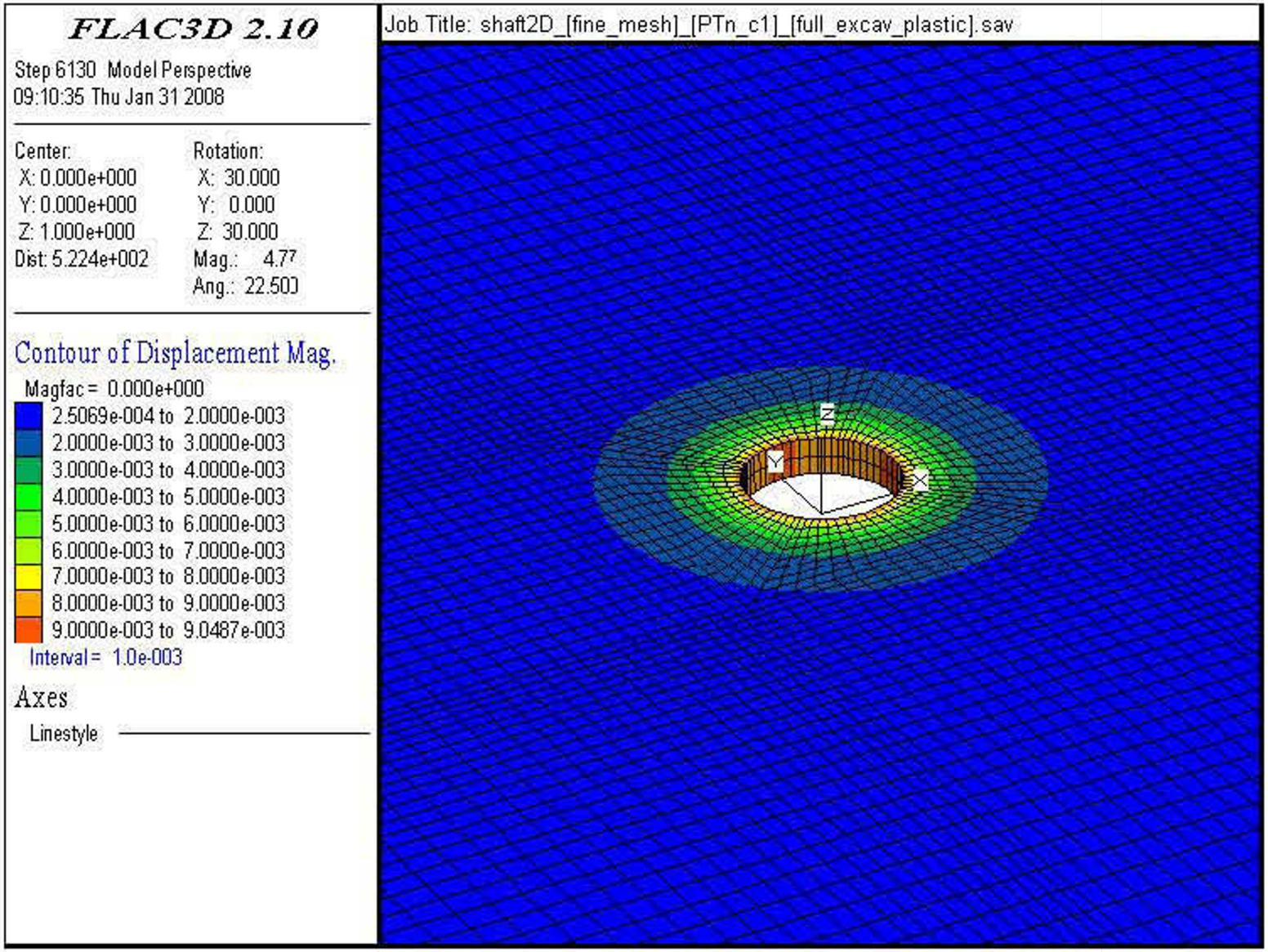

Figure 6-11 FLAC3D Model of a Section of Shaft in Unit PTn, Category 1, Showing Magnitude of Displacement (m) After Excavation (i.e., internal pressure equal to zero).

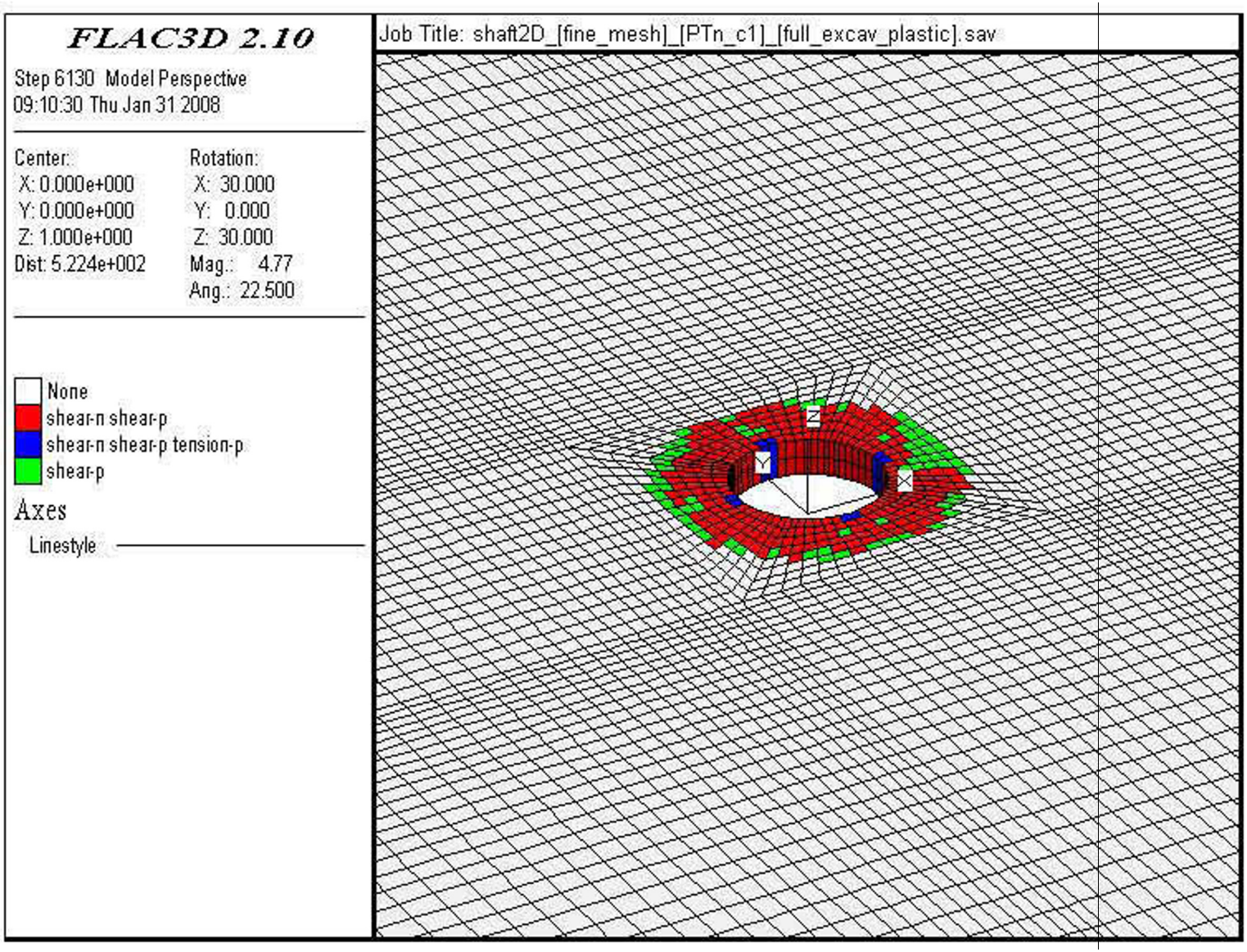

Figure 6-12 FLAC3D Model of a Section of Shaft in Unit PTn, Category 1, Showing Zones in Failure State After Excavation - Internal Pressure Equal to Zero.

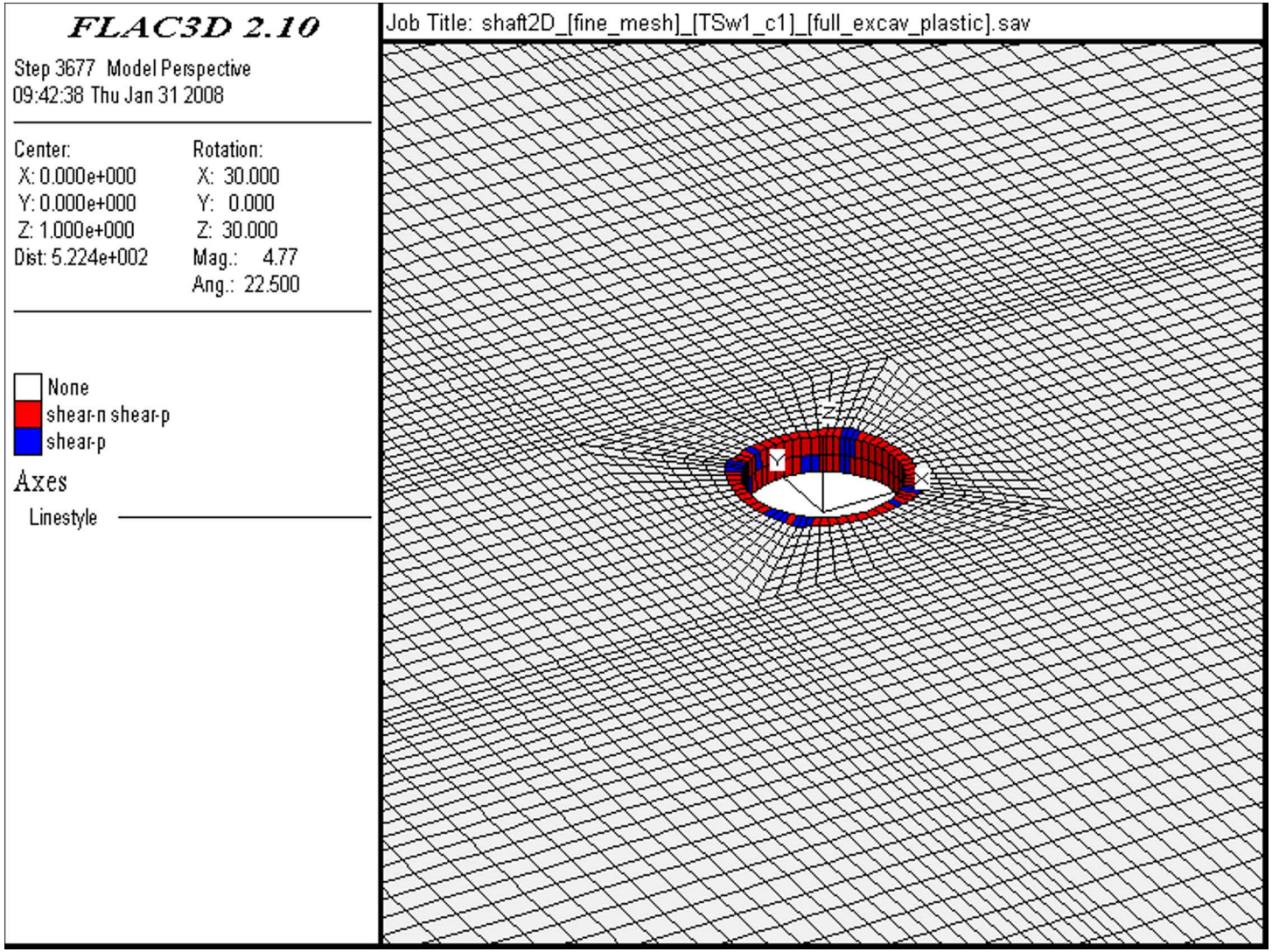

Figure 6-13 FLAC3D Model of a Shaft Section in Unit TSw1, Category 1, Showing Zones in a Failure State After Excavation - Internal Pressure Equal to Zero.

The results of modeling indicate that under ground conditions considered in this calculation, shaft excavations are expected to be fairly stable along their entire depths. The calculated rock mass deformations are generally elastic. Plastic deformations around shafts might occur in the poor quality rock mass, e.g., Category 1 of PTn and TSw1_Lith units, however, their extent is limited. The expected shaft closure is relatively small. There are no indications of major stability problems that might be encountered during shaft sinking, provided the field conditions are not significantly different from those considered in the analysis.

The relatively low level of in situ horizontal stresses at Yucca Mountain, acting perpendicular to the shaft axes result in favorable conditions from the stability standpoint. It should be noted that this analysis was conducted considering an isotropic stress conditions, with the coefficient of lateral stress K_o equal to 0.5. Although the anisotropic horizontal stress condition that exists at Yucca Mountain will have an effect on the extent of the plastic zone and maximum shaft closure, however, those effects will not be significant and would not change conclusions about stability of shaft excavations derived on the basis of results obtained from this analysis.

6.5.1.3 Timing of Ground Support Installation

The void created by the shaft excavation and stresses in the rock mass surrounding it cause the deformation of the rock mass towards the opening to occur both ahead and behind the advancing shaft bottom. The stress relaxation causes stress redistribution in the rock mass adjacent to the excavated opening. The maximum deformation of shaft walls occurs some short distance above the shaft bottom. If the ground support is installed too close to the advancing shaft bottom, stress redistribution may cause the shaft liner to take a substantial load due to the rock mass displacement following the relaxation of in situ stress.

Mechanical models of the unsupported bottom region of the advancing shaft have been set up with FLAC3D. The purpose of these models is to obtain the distribution of the shaft wall convergence above the advancing shaft bottom for shafts excavated in different stratigraphic units. Of interest is the standoff distance required such that the final liner be placed behind the face after the maximum wall closure has occurred. Undertaken here was an estimation of the distance between the shaft bottom and the liner, with the liner installed after 100% of the deformation due to excavation has taken place. This task was accomplished by using the profiles of radial deformation obtained from the FLAC3D models of the advancing shaft.

The modeling has been performed to evaluate the amount of shaft deformation occurring at various stages of excavation. The purpose for this modeling effort was to establish the distance above the shaft bottom, at which the entire deformation has taken place. The shaft liner installed at this distance would accrue no load due to in situ stress readjustments. This standoff distance will vary depending on the depth (magnitude of stresses) and properties of rocks constituting the given geological unit.

Figure 6-14 and Figure 6-15 show the extent of the failure zone and contours of displacements for a shaft excavated in PTn, Category 1 unit, while Figure 6-16 presents the corresponding distribution of the wall convergence, u_r, as a function of the distance to the shaft bottom, d. The diagram in the Figure 6-16 shows that the scaled radial displacement, u_r, reaches its peak equal to 0.178% at a distance to the shaft bottom equal to 2.22 times the radius of the shaft. Beyond

this distance, the radial displacements start to decrease. This decrease is the result of redistribution of the initial stresses, which are governed by a lithostatic gradient and, therefore, decrease in the upward direction.

Table 6-10 summarizes the values of the calculated scaled maximum radial displacement, (u_r^{max}/R), and the scaled distance behind the shaft bottom (d / R), at the location where the maximum radial displacement occurs, as obtained from the FLAC3D models for the different units. From the Table 6-10, it can be observed that 100% of the deformation behind the front occurs at a distance of approximately 3 times the radius away from the shaft bottom. The liner load due to relaxation following the advancing shaft bottom can be reduced to zero if, according to the current calculation, the liner is installed at a minimum distance equal to 3 times the radius of the shaft away from the shaft bottom.

Table 6-10 Scaled Maximum Radial Displacement Behind the Advancing Shaft Excavation and Distance to the Shaft Bottom Obtained from FLAC3D Models of Shafts in the Different Stratigraphic Units.

Unit (Category 1)	u_r^{max}/R (%)	d/r
TCw	0.009	1.667
PTn	0.178	2.222
TSw1	0.109	2.5
TSw1_Lithophysal	0.274	3.055
TSw2_Nonlithophysal	0.048	3.055

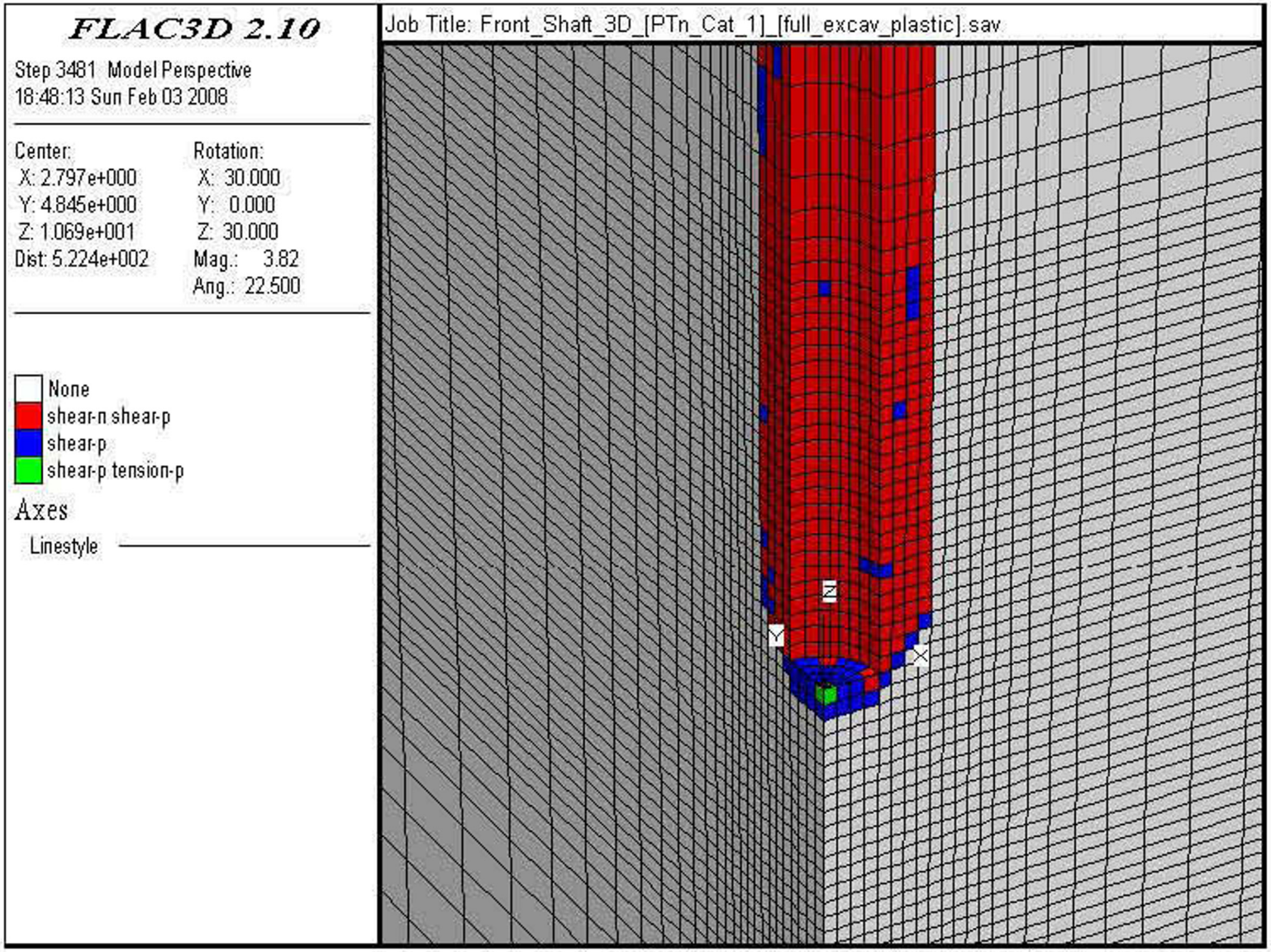

Figure 6-14 Extent of Plastic Failure from the FLAC3D Model of the Advancing Shaft in the PTn, Category 1.

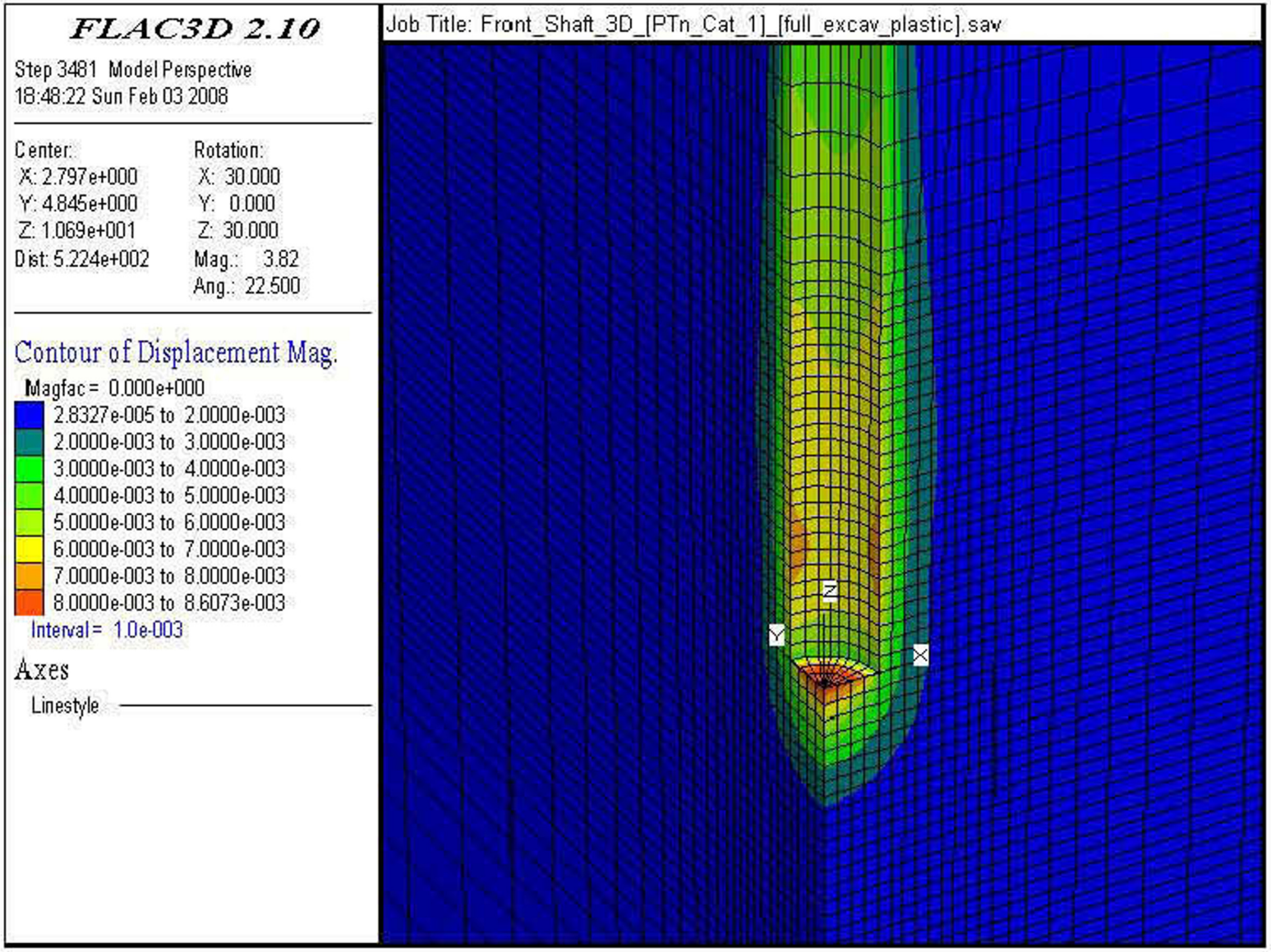

Figure 6-15 Contours of Displacements (M) from the FLAC3D Model of the Advancing Shaft in the PTn, Category 1.

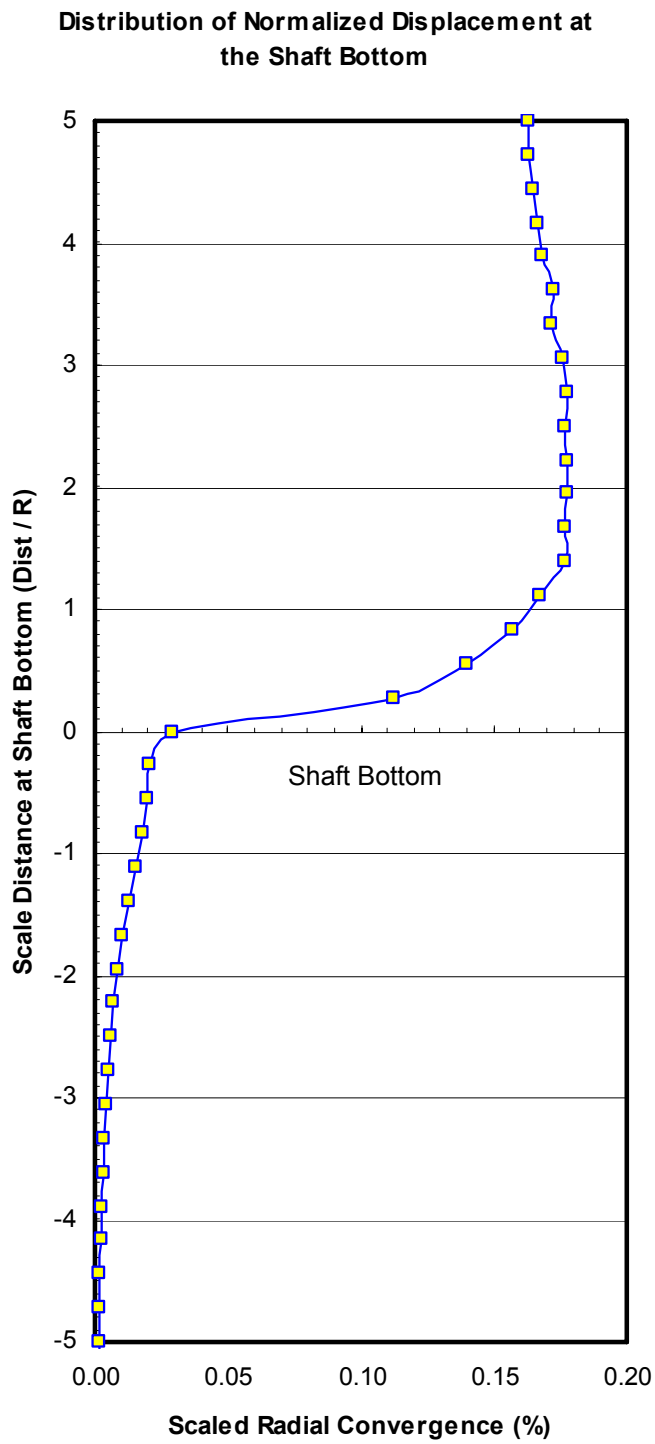

Figure 6-16 Distribution of Radial Displacements Behind the Front Obtained from the FLAC3D Models of the Advancing Shaft in the PTn, Category 1. (ur/R=0.178 %, Dist/R = 2.22)

6.5.1.4 Analysis of Shaft/Drift Station Intersections

The geometry and an overall numerical model features have been introduced in Section 4.3. Presented in this Section are the results of numerical simulations performed on two intersections, i.e., a "T-type" intersection, and an "L-type" intersection.

It should be noted that this section presents a summary of results of numerical simulations for intersections excavated in TSw1_Lithophysal strata. For completeness, the complementary set of figures presenting the results for TSw2_Nonlithophysal strata for both types of intersections is included in Attachment B.

6.5.1.4.1 Results for "T-type" Intersection

Figure 6-17 and Figure 6-18 show two different views of the extent of the plastic zone after excavation of the drifts and shaft (Step 1) is completed. Figure 6-19 and Figure 6-20 show the corresponding displacements, with maximum displacement occurring in the horizontal drift and equal to 0.03 m, which indicates that the intersection is stable. By comparison, deformations occurring in the shaft alone, are shown earlier in Table 6-9 and Table 6-10. A limited zone of the failed rock ranging from 0.5 m to 1.0 m develops mostly in the walls of the drift at the shaft/drift intersection, however, the magnitude of the associated deformation is small.

Figure 6-21 and Figure 6-22 show locations of several points in the intersection region. At these locations, the rock strata velocities resulting from applying the seismic load (Step 2) have been recorded. Figure 6-23 represents the 3D record of input velocities introduced at the base of the model in the x-, y- and z- directions. Here, the y-direction coincides with the axis of the drift and the z-direction coinciding with the axis of the shaft. Figure 6-24 through Figure 6-30 represent the resulting velocities recorded at points 1, 4 and 6 for both (Rev A and Rev B) time histories of velocity components of 1×10^{-4} ground motion as presented in Figure 6-5 and Figure 6-6, respectively, which locations are shown earlier in Figure 6-21 and Figure 6-22. Note that input signals (Figure 6-23 and Figure 6-27) and recorded signals at various points within the intersection (Figure 6-24 though Figure 6-26 and Figure 6-28 through Figure 6-30) are similar in shape and magnitude, with the maximum velocity being less than 0.6 m/s. This indicates that at shaft location all strata points move in unison, showing no evidence of irreversible deformation accumulation in the intersection region. This suggests that the intersection is stable.

Figure 6-31 and Figure 6-34 show the extent of failure zone after the application of the seismic load. Comparison of the results depicted in these figures with the results shown earlier in Figure 6-17 and Figure 6-18, corresponding to the plastic failure before application of the seismic load, serves as further proof that the intersection is stable. No additional plasticity in the region of the intersection is generated as a result of the imposed seismic load.

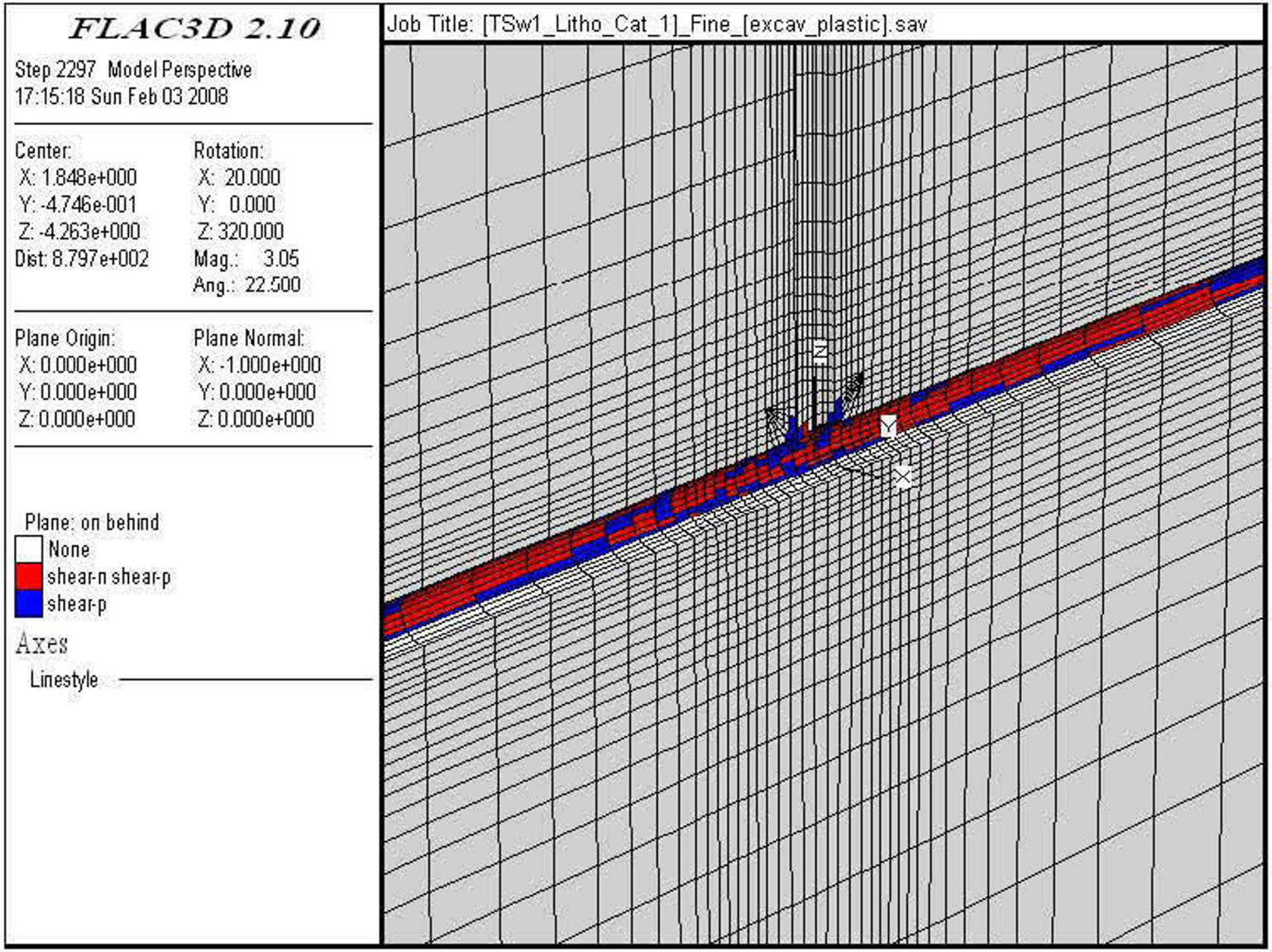

Figure 6-17 Extent of Plastic Failure at T-type Intersection After Excavation Represented on a Vertical Plane Containing the Axis of the Drift

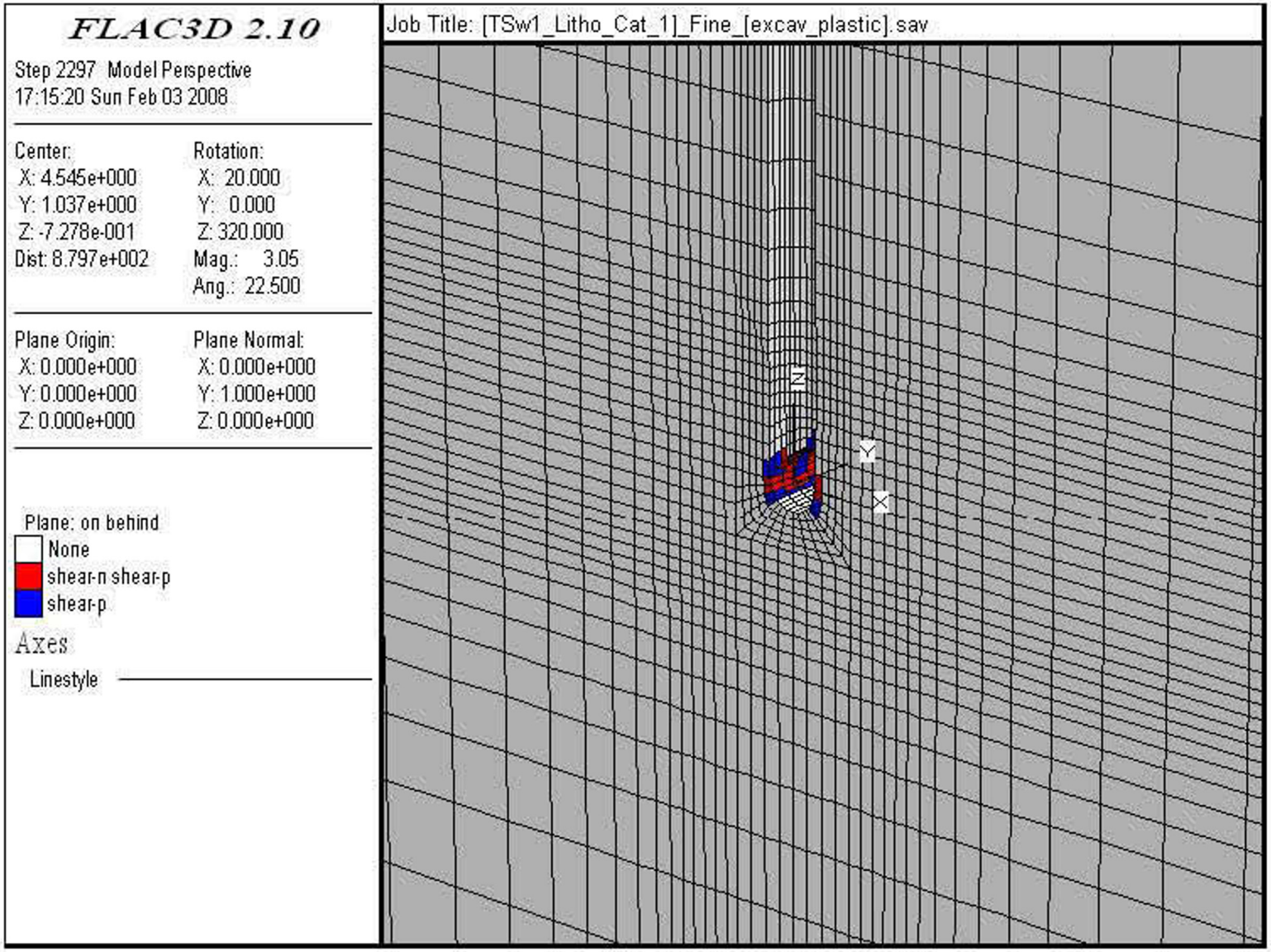

Figure 6-18 Extent of Plastic Failure at T-type Intersection After Excavation Represented on a Vertical Plane Perpendicular to the Axis the Drift And Containing the Axis of the Shaft

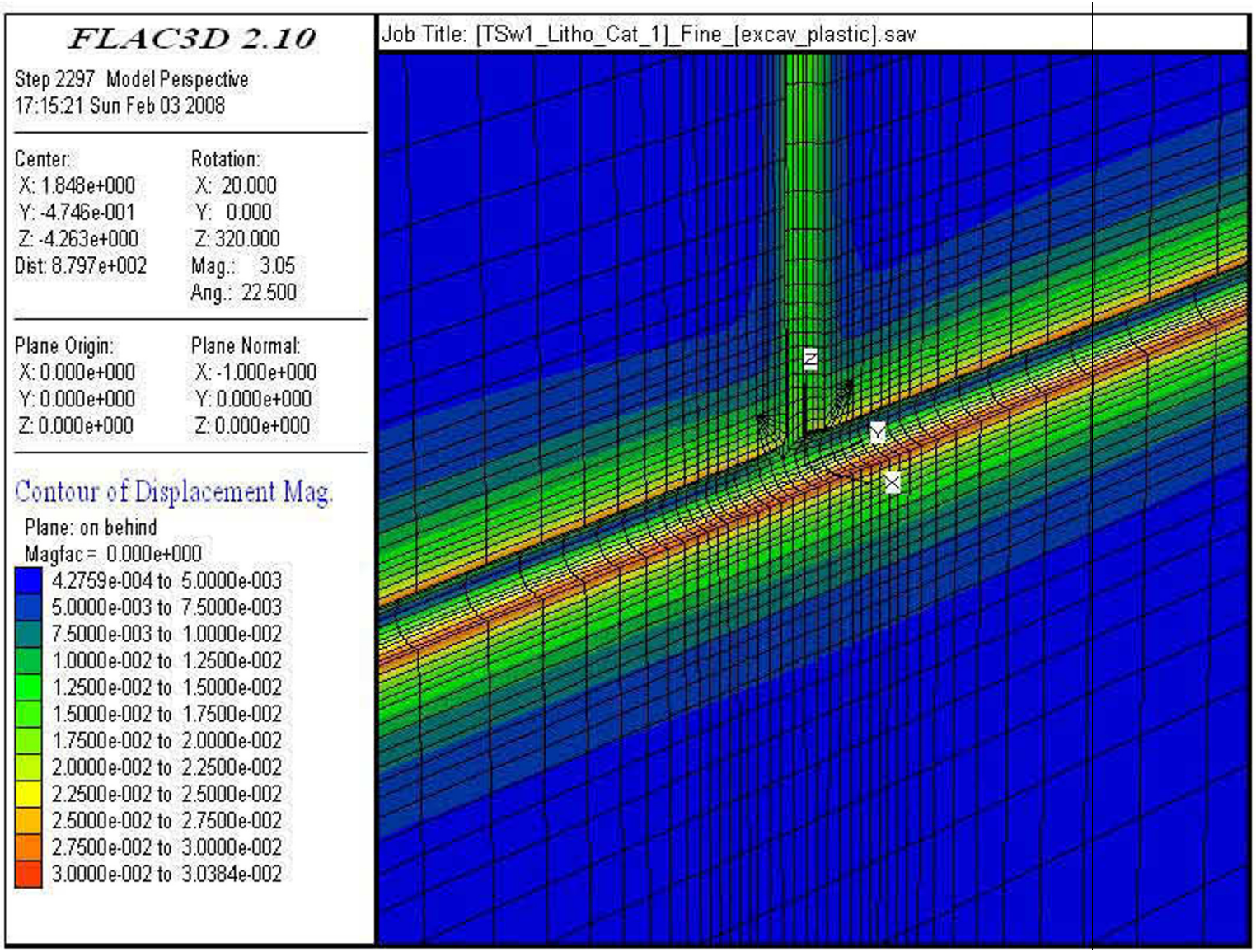

Figure 6-19 Contours of Magnitude of Displacement (m) at T-type Intersection After Excavation Represented on a Vertical Plane Containing the Axis of the Drift

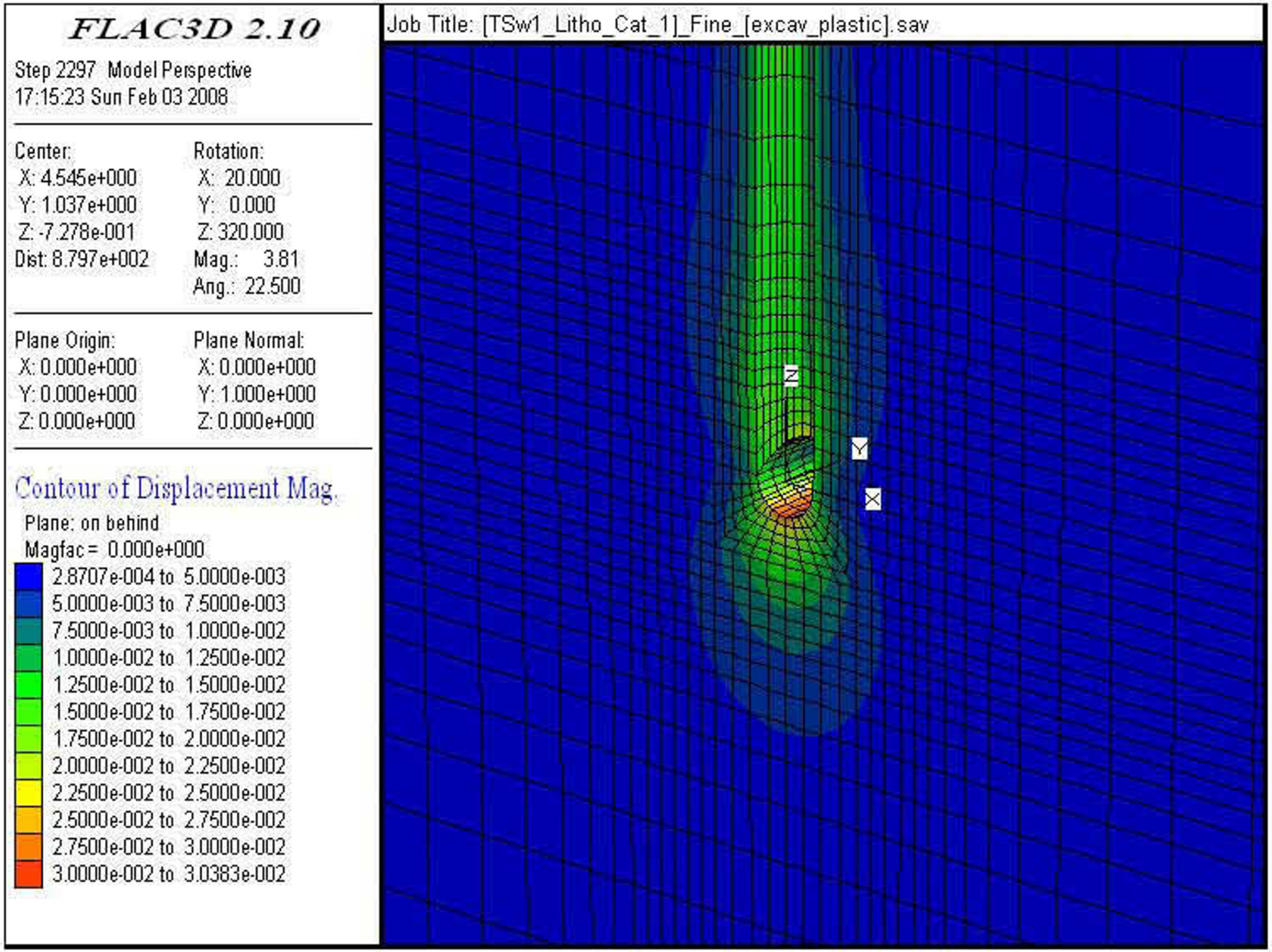

Figure 6-20 Contours of Magnitude of Displacement (m) at T-type Intersection After Excavation Represented on a Vertical Plane Perpendicular to the Axis of the Drift and Containing the Axis of the Shaft

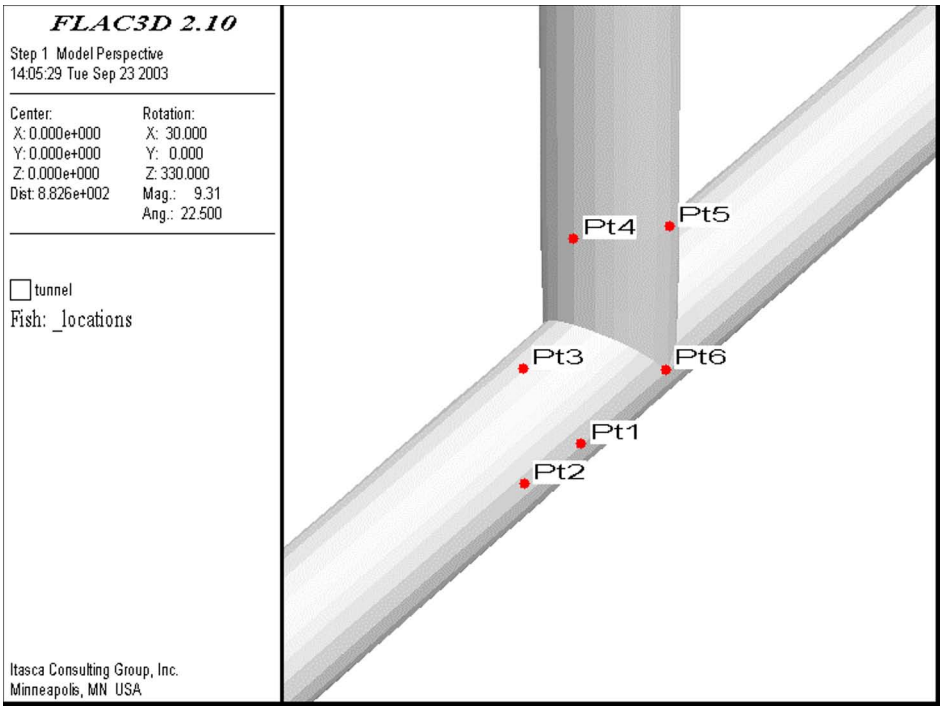

Figure 6-21 T-type Intersection - View 1 Showing Points, Where Velocities Induced by Seismic Excitation Have Been Calculated and Recorded During Simulations

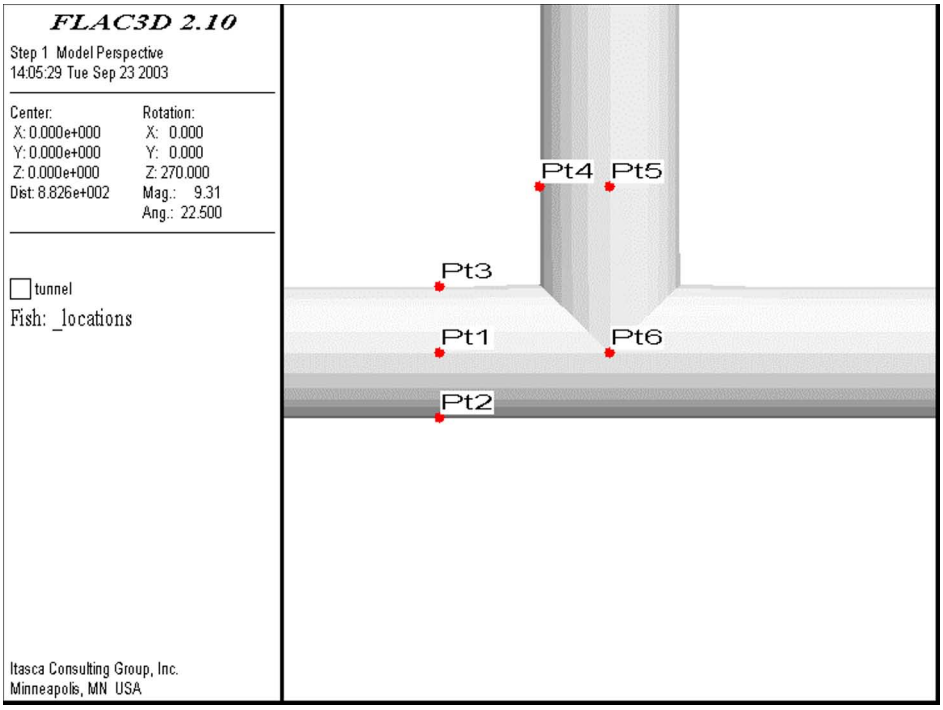

Figure 6-22 T-type Intersection - View 2 Showing Points, Where Velocities Induced by Seismic Excitation Have Been Calculated and Recorded During Simulations

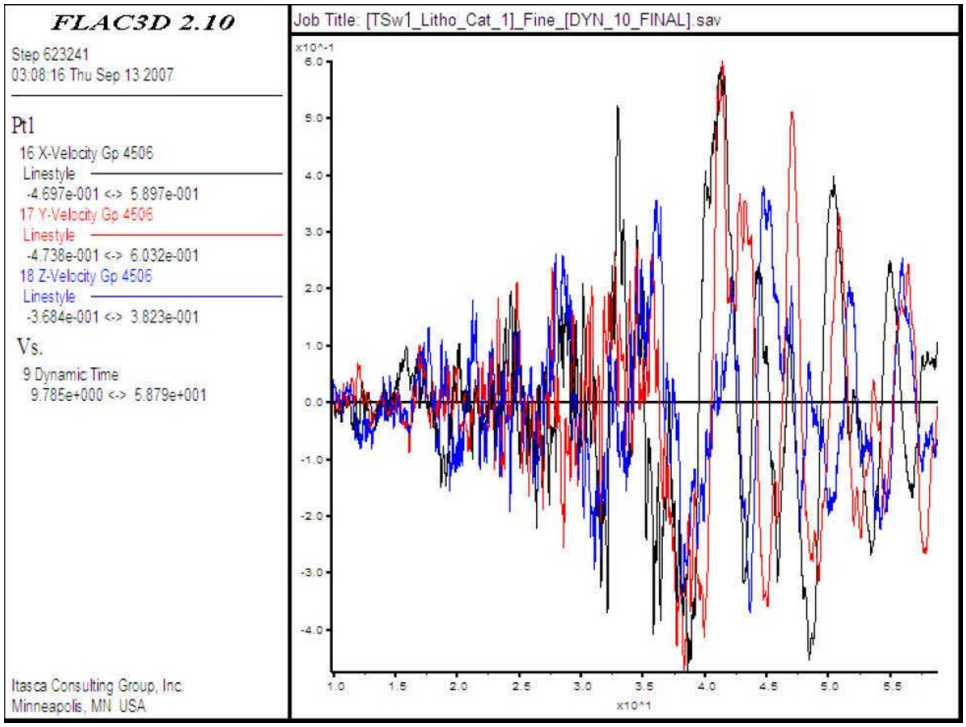

Source: Rev A (Reference 2.2.14)

Figure 6-23 T-type Intersection - Record of Input Velocities (m/s) in the X-, Y- and Z-Directions at the Base of the Model

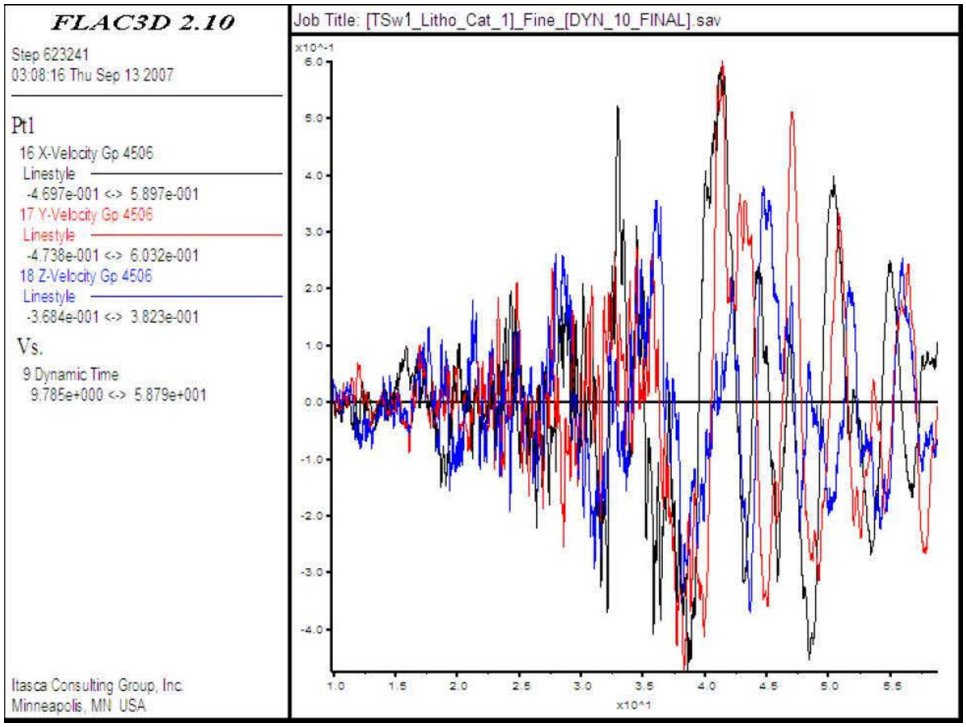

Source: Rev A (Reference 2.2.14)

Figure 6-24 T-type Intersection - Record of Velocities (m/s) at Point 1 in the “T-type” Intersection Induced by Application of Seismic Excitation.

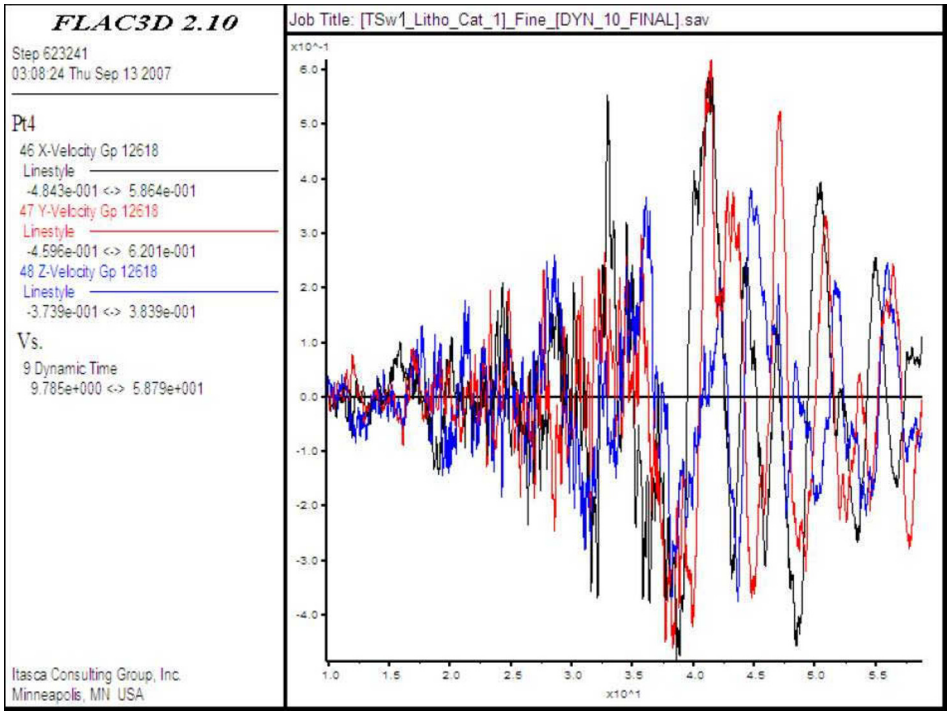

Source: Rev A (Reference 2.2.14)

Figure 6-25 T-type Intersection - Record of Velocities (m/s) at Point 4 in the "T-type" Intersection Induced by Application of Seismic Excitation

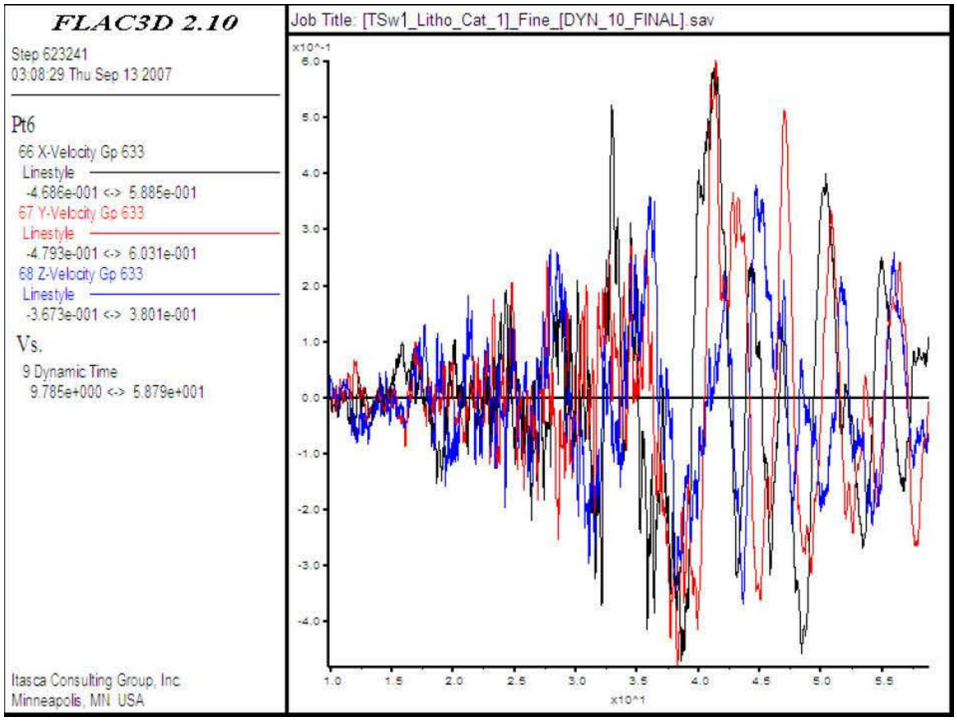

Source: Rev A (Reference 2.2.14)

Figure 6-26 T-type Intersection - Record of Velocities (m/s) at Point 6 in the "T-type" Intersection Induced by Application of Seismic Excitation

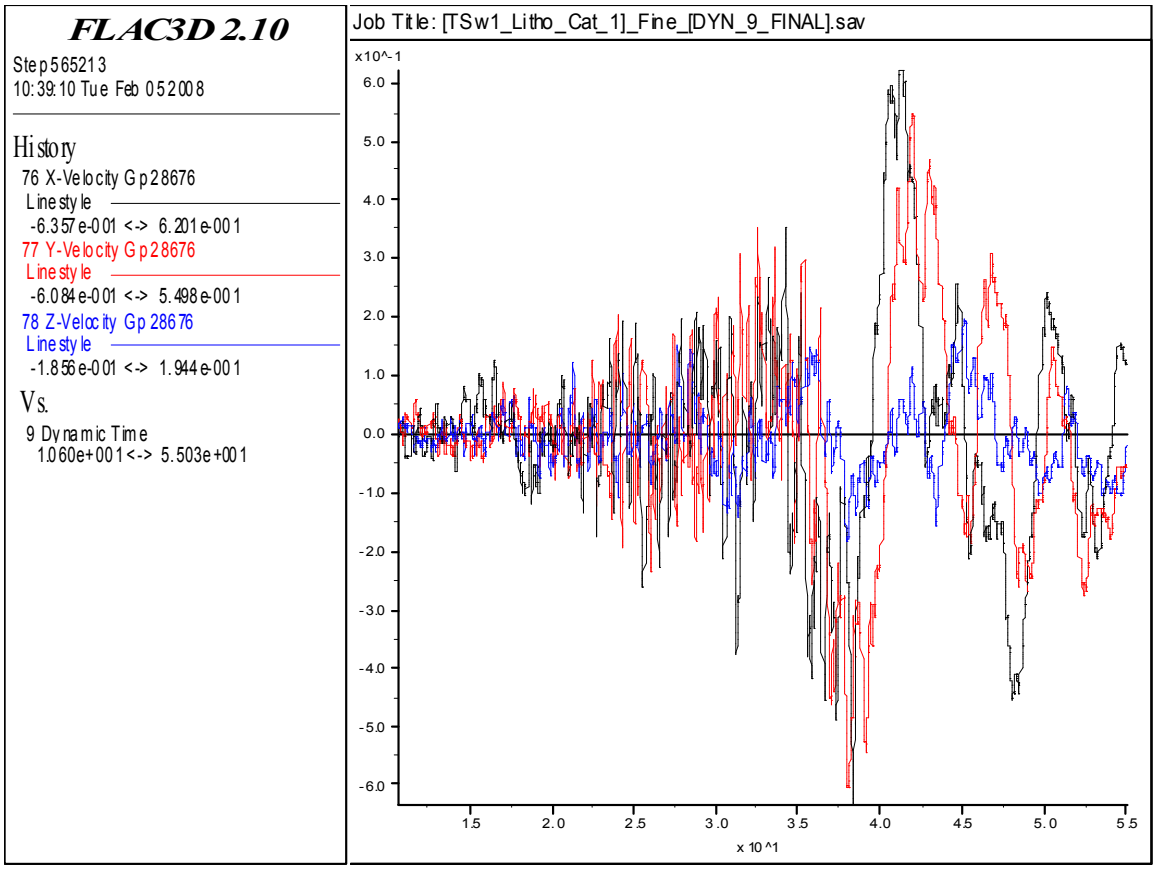

Source: MO0707THRB1E4A.000 (Reference 2.2.33)

Figure 6-27 T-type Intersection - Record of Input Velocities (m/s) in the X-, Y- and Z-Directions at the Base of the Model

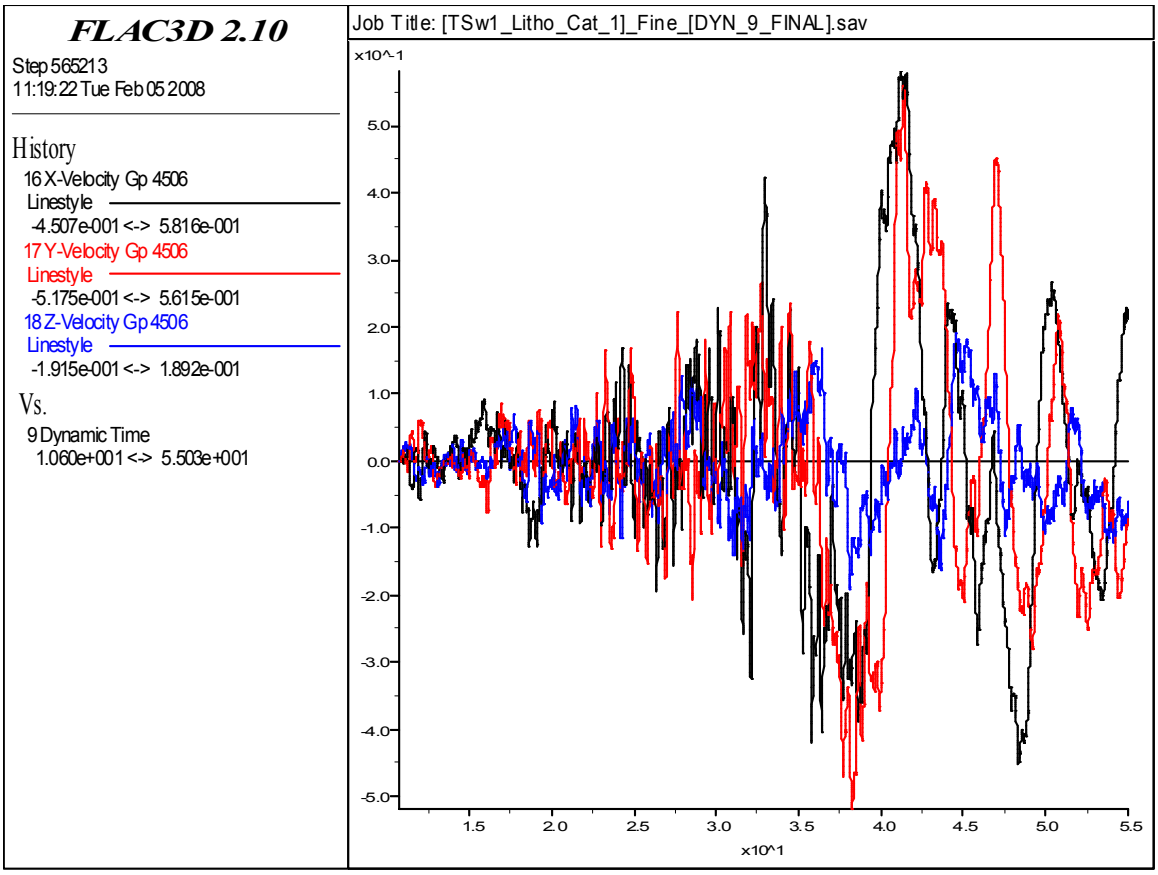

Source: MO0707THRB1E4A.000 (Reference 2.2.33)

Figure 6-28 T-type Intersection - Record of Velocities (m/s) at Point 1 in the “T-type” Intersection Induced by Application of Seismic Excitation.

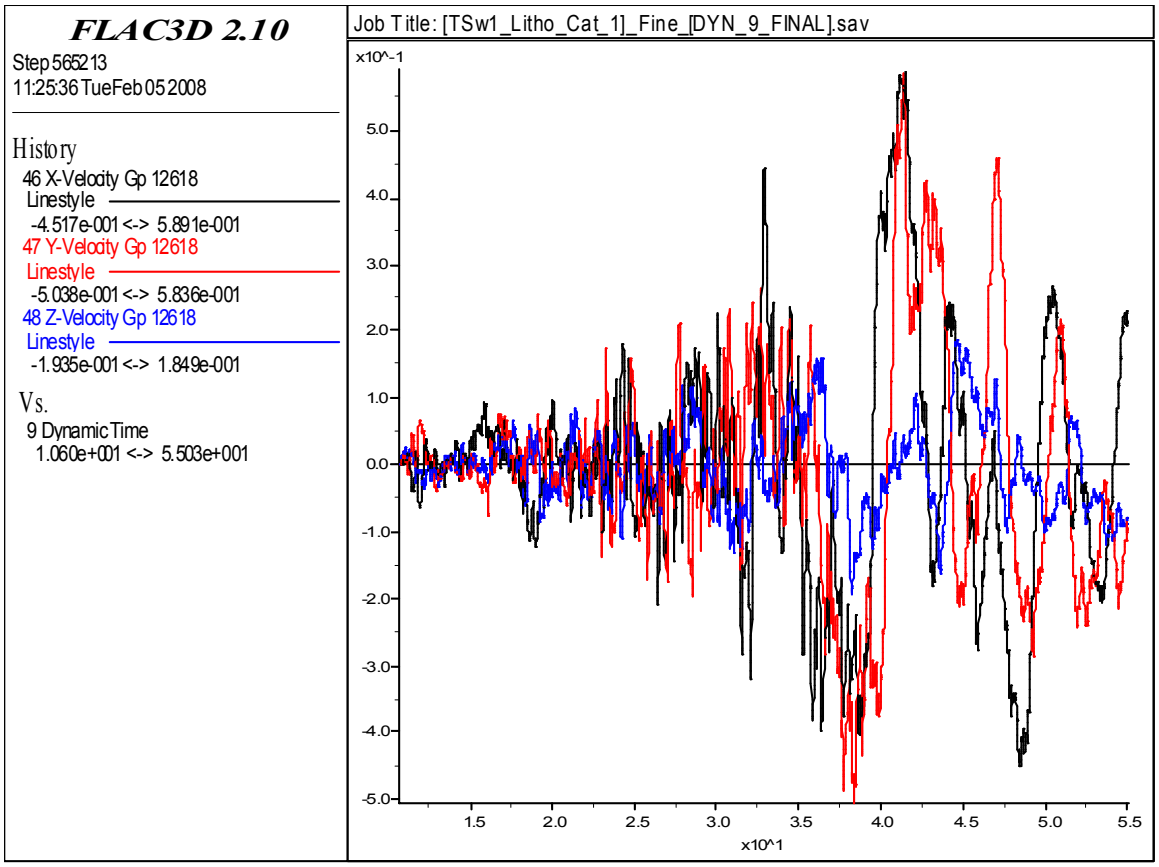

Source: MO0707THRB1E4A.000 (Reference 2.2.33)

Figure 6-29 T-type Intersection - Record of Velocities (m/s) at Point 4 in the “T-type” Intersection Induced by Application of Seismic Excitation

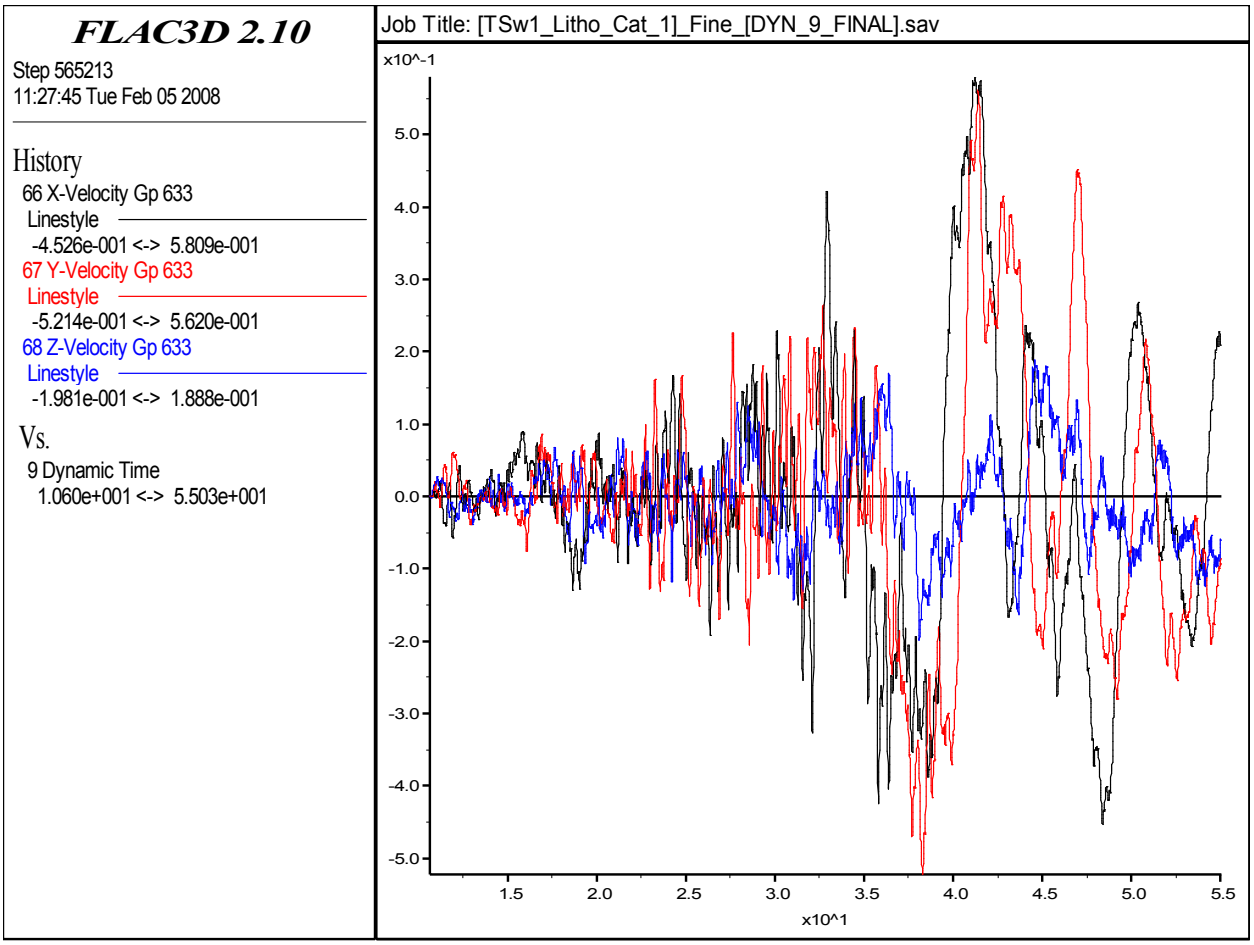

Source: MO0707THRB1E4A.000 (Reference 2.2.33)

Figure 6-30 T-type Intersection - Record of Velocities (m/s) at Point 6 in the “T-type” Intersection Induced by Application of Seismic Excitation

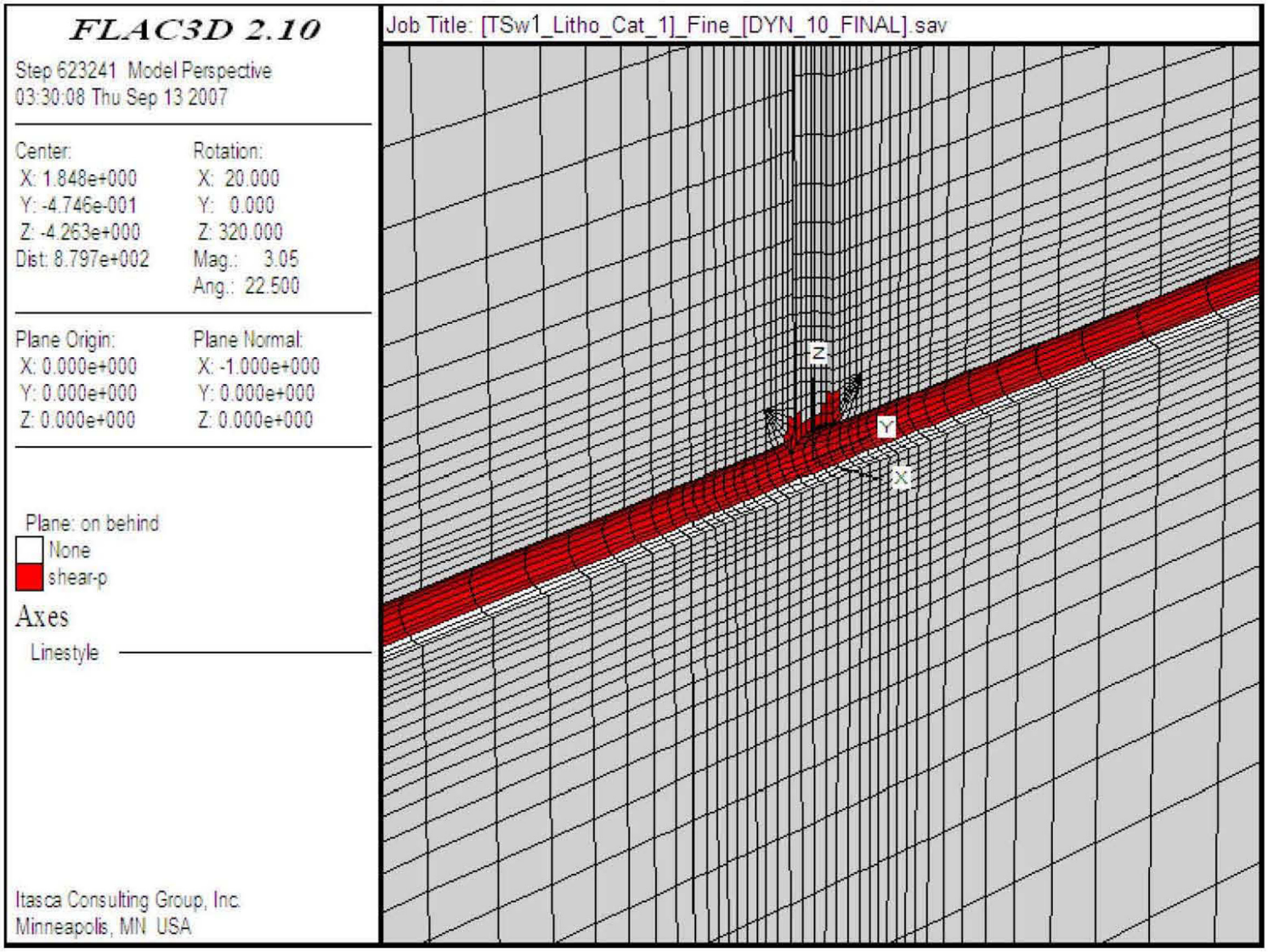

Source: Rev A (Reference 2.2.14)

Figure 6-31 T-type Intersection - View of Extent of the Failure Zone After Application of the Seismic Load in the “T-type” Intersection (The vertical plane cutting the model contains the axis of the drift.)

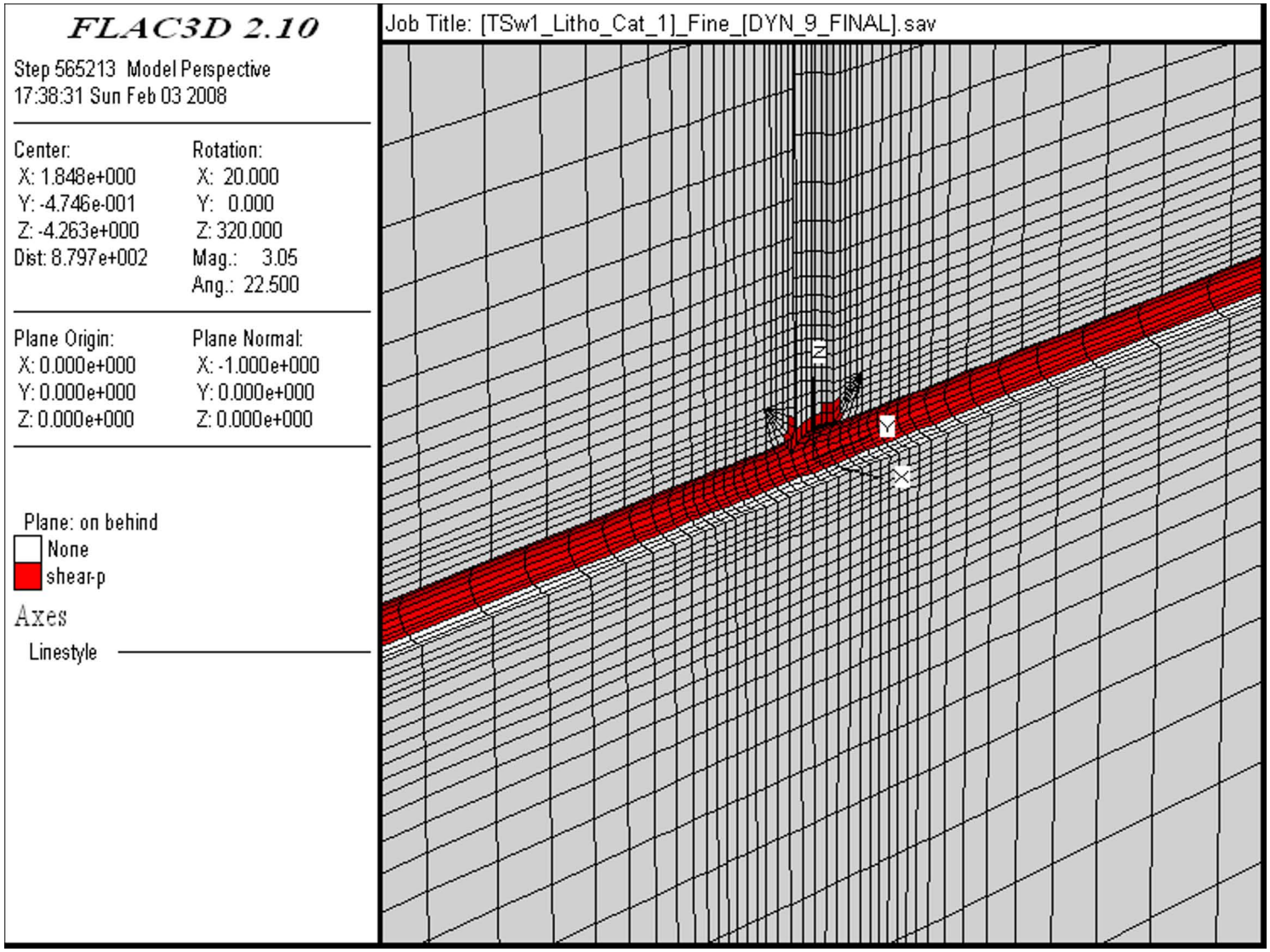

Source: MO0707THRB1E4A.000 (Reference 2.2.33)

Figure 6-32 T-type Intersection - View of Extent of the Failure Zone After Application of the Seismic Load in the “T-type” Intersection (The vertical plane cutting the model contains the axis of the drift.)

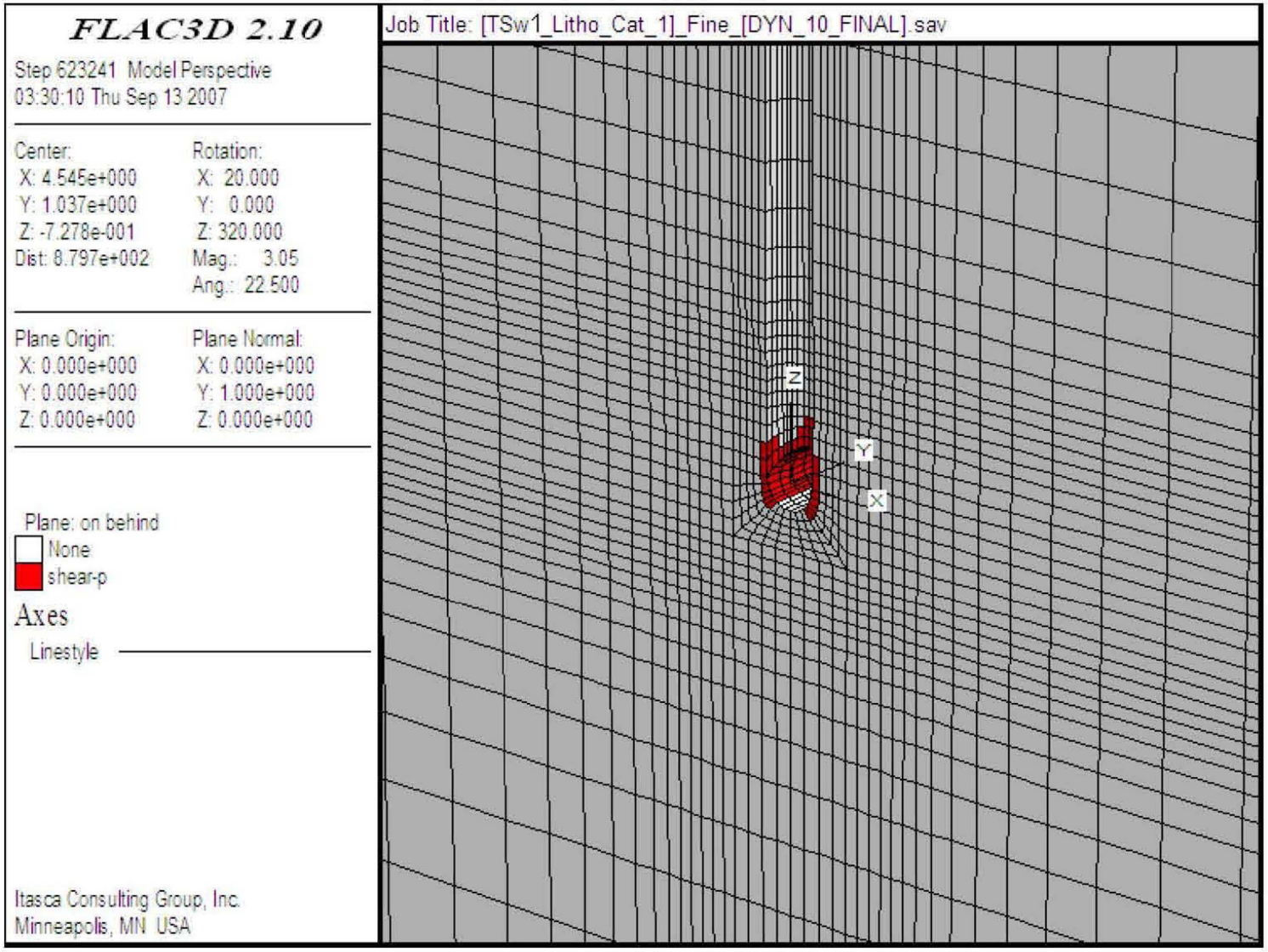

Source: Rev A (Reference 2.2.14)

Figure 6-33 T-type Intersection - View of Extent of the Failure Zone After Application of the Seismic Load in the “T-type” Intersection (The vertical plane cutting the model contains the axis of the shaft and is perpendicular to the axis of the drift.)

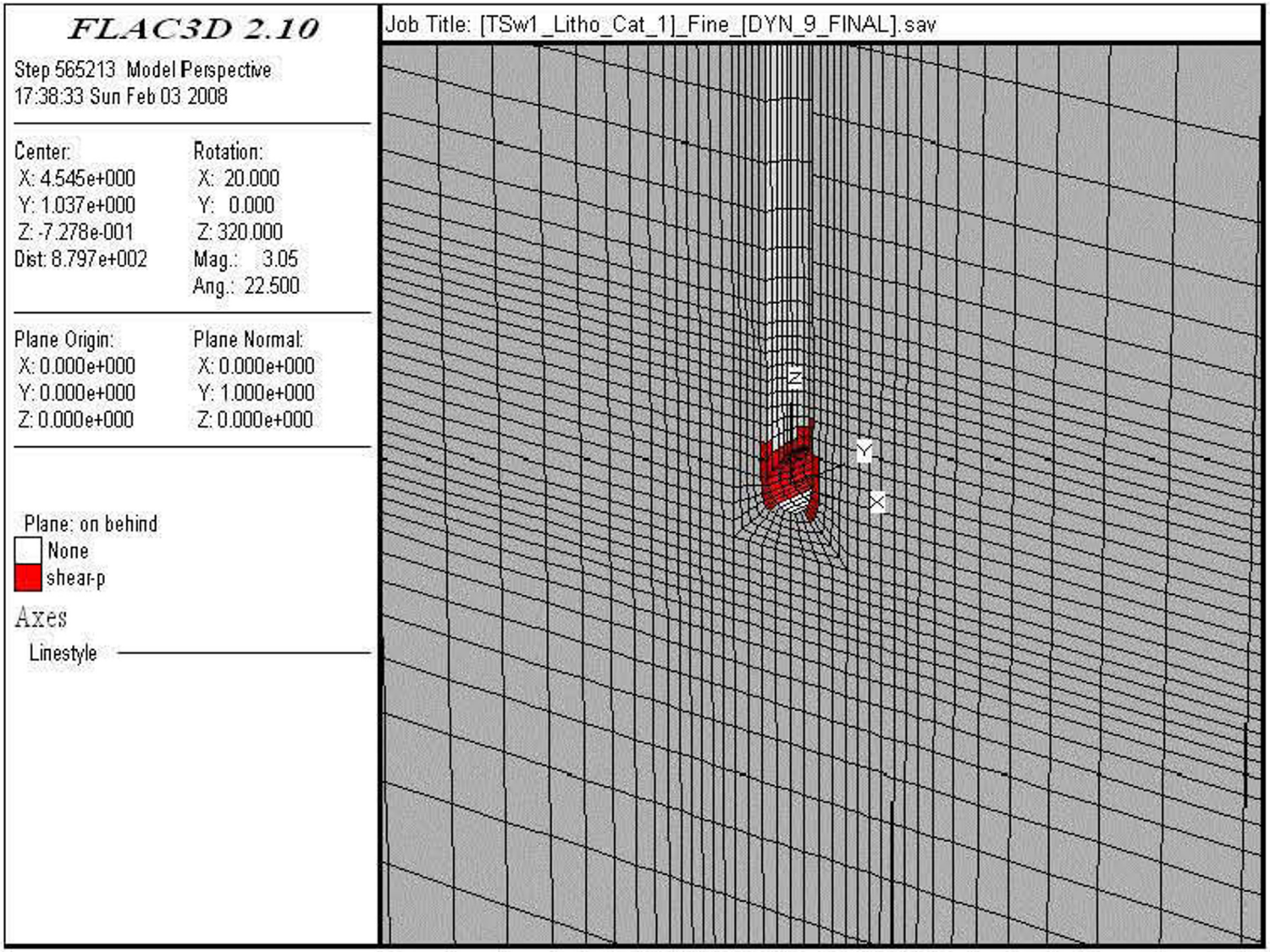

Source: MO0707THRB1E4A.000 (Reference 2.2.33)

Figure 6-34 T-type Intersection - View of Extent of the Failure Zone After Application of the Seismic Load in the “T-type” Intersection (The vertical plane cutting the model contains the axis of the shaft and is perpendicular to the axis of the drift.)

6.5.1.4.2 Results for "L-type" Intersection

Observations similar to those made for the "T-type" intersection can be made for the case of the "L" intersection. Figure 6-35 through Figure 6-38 show views of an extent of the plastic zone after excavation. The plastic zone shows in the walls of the drifts, however, no plastic zone along the shafts is evident. Figure 6-38 shows plasticity in the horizontal section through the center of the drift and the connecting tunnel. Only minor yielding can be observed at the pillar, here delineated by a corner between the drift and the shaft. In general, it does not appear that geometry of the intersection will pose any major stability problems

Contours of the vertical normal stresses plotted in the same horizontal section that is shown in Figure 6-38, are also displayed in Figure 6-39. The stress concentration visible in the pillar corner is equal to 22 MPa, approximately. However, pillar corners are usually slightly tapered, which causes dispersion of the highly concentrated stresses and improves stress distribution. In effect, this localized stress concentration should not be of great concern.

Contours of displacement magnitudes in the intersection shown in Figure 6-40 through Figure 6-42 indicate that displacements are relatively small, and even in the poorest quality rock mass considered do not exceed 0.041 m. This displacement is somewhat higher than displacements calculated for the shaft alone (Table 6-10), and the T-type shaft and horizontal drift intersection (Section 6.5.1.4.1). It should be noted, that displacements at the intersection of two horizontal drifts result in higher stress concentration factors than those around the shaft alone and at the intersection between the shaft and a horizontal drift. Consequently, the corresponding displacements are higher as well.

Figure 6-43 and Figure 6-44 show the locations of points, at which ground motion histories were acquired. Figure 6-45 and Figure 6-49 show the seismic signal velocities applied at the base of the model for both time histories of velocity components of 1×10^{-4} ground motion as presented in Figure 6-5 and Figure 6-6, respectively. The resulting ground motions recorded at various points within the model are shown in Figure 6-46 through Figure 6-48 for Rev A analysis and Figure 6-50 through Figure 6-52 for seismic data based on MO0707THRB1E4A.000 (Reference 2.2.33). The form of imposed and recorded ground velocities at various points in the intersection appears to be almost identical both in form and magnitude. Figure 6-53 through Figure 6-58 show the extent of the failure zone after the application of the both seismic loads. As in the earlier case ("T-type" intersection), here also the extent of plastic zone before and after seismic shaking remains unchanged.

The overall assessment of modeling results indicate that "L-type" intersection is considered to be stable.

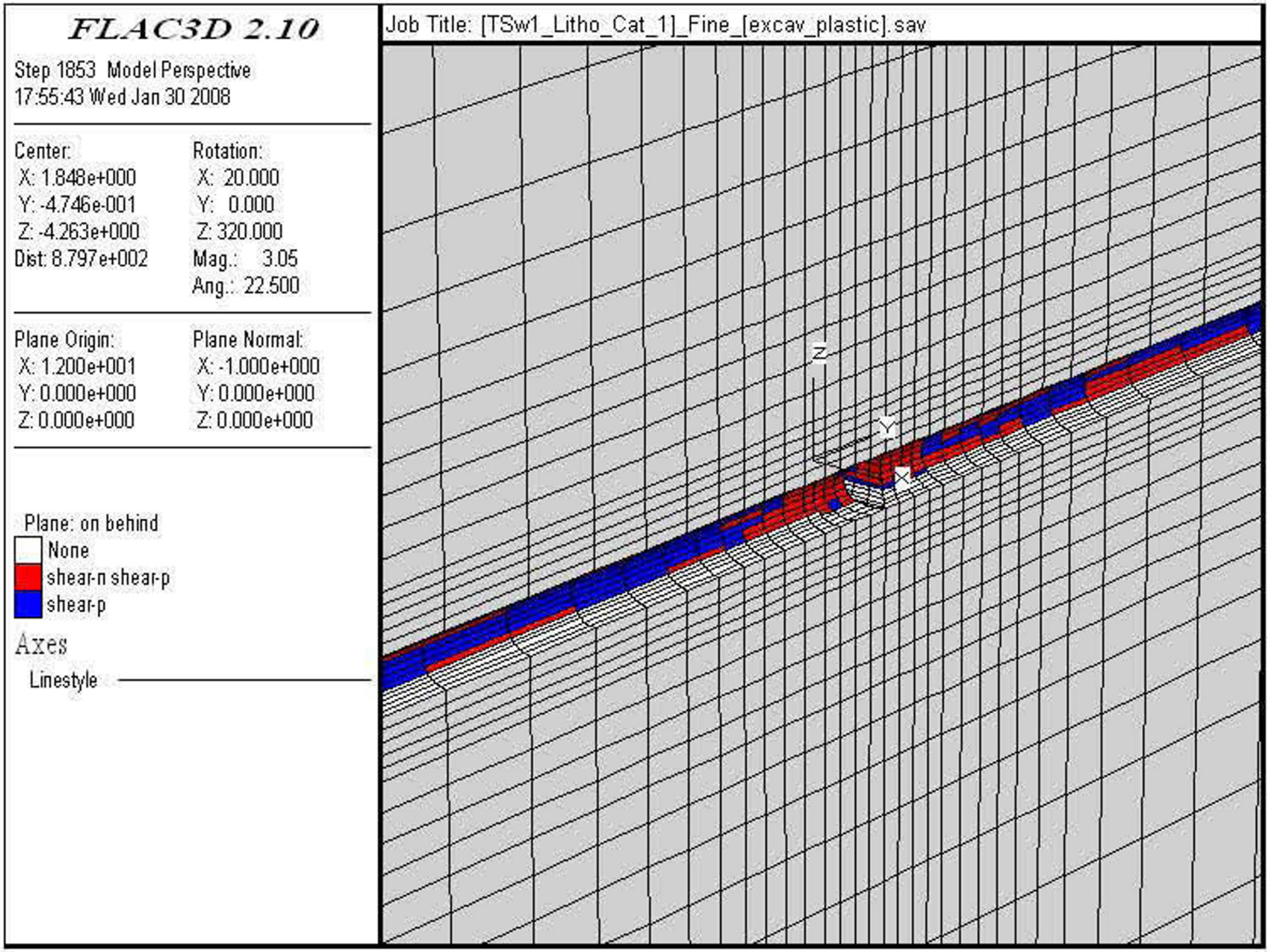

Figure 6-35 L-type Intersection - Extent of Plastic Failure After Excavation Represented on a Vertical Plane Containing the Axis of the Drift for the "L-type" Intersection

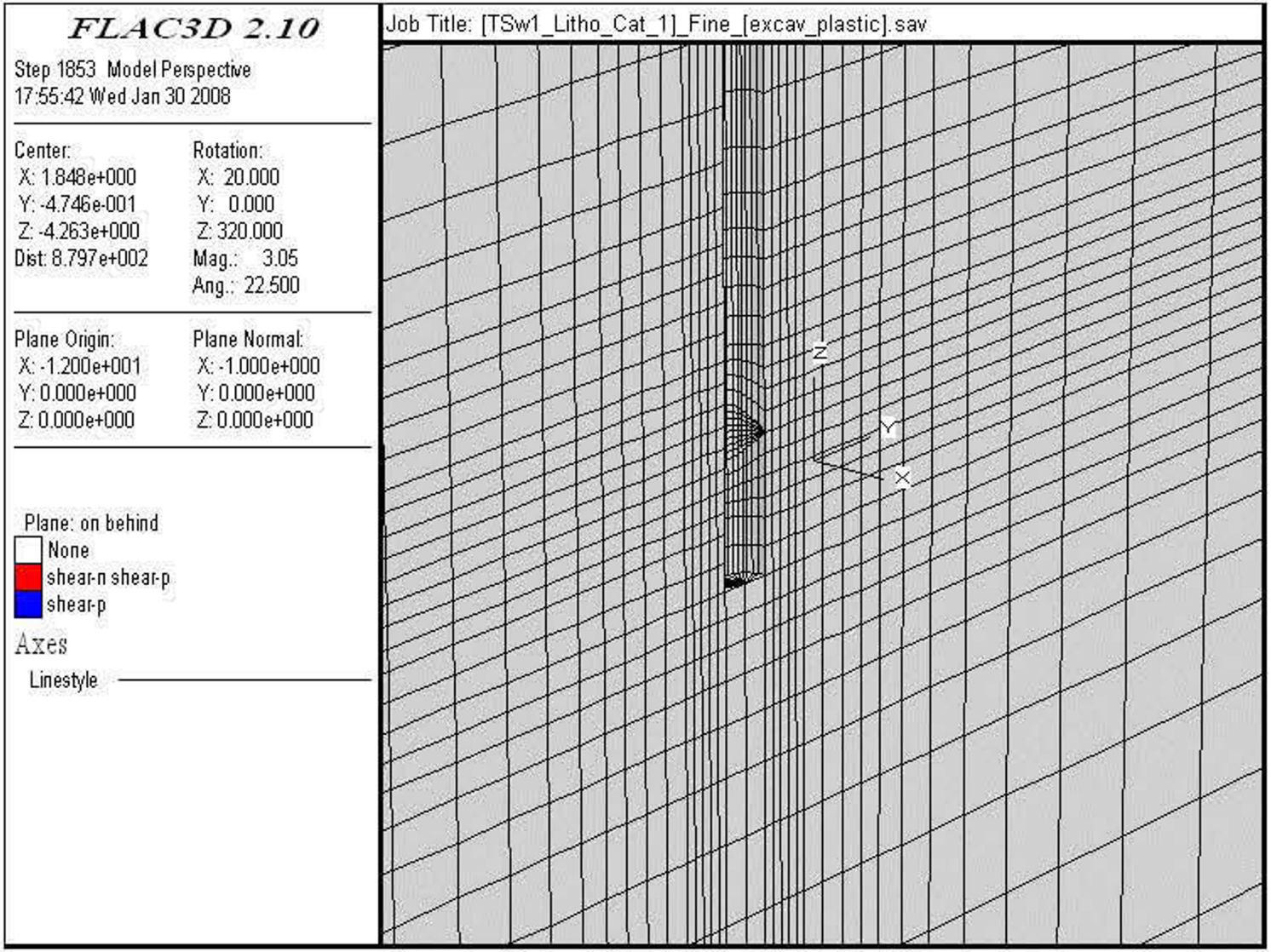

Figure 6-36 L-type Intersection - Extent of Plastic Failure After Excavation Represented on a Vertical Plane Parallel to the Axis of the Drift and Containing the Axis of the Shaft for the “L-type” Intersection

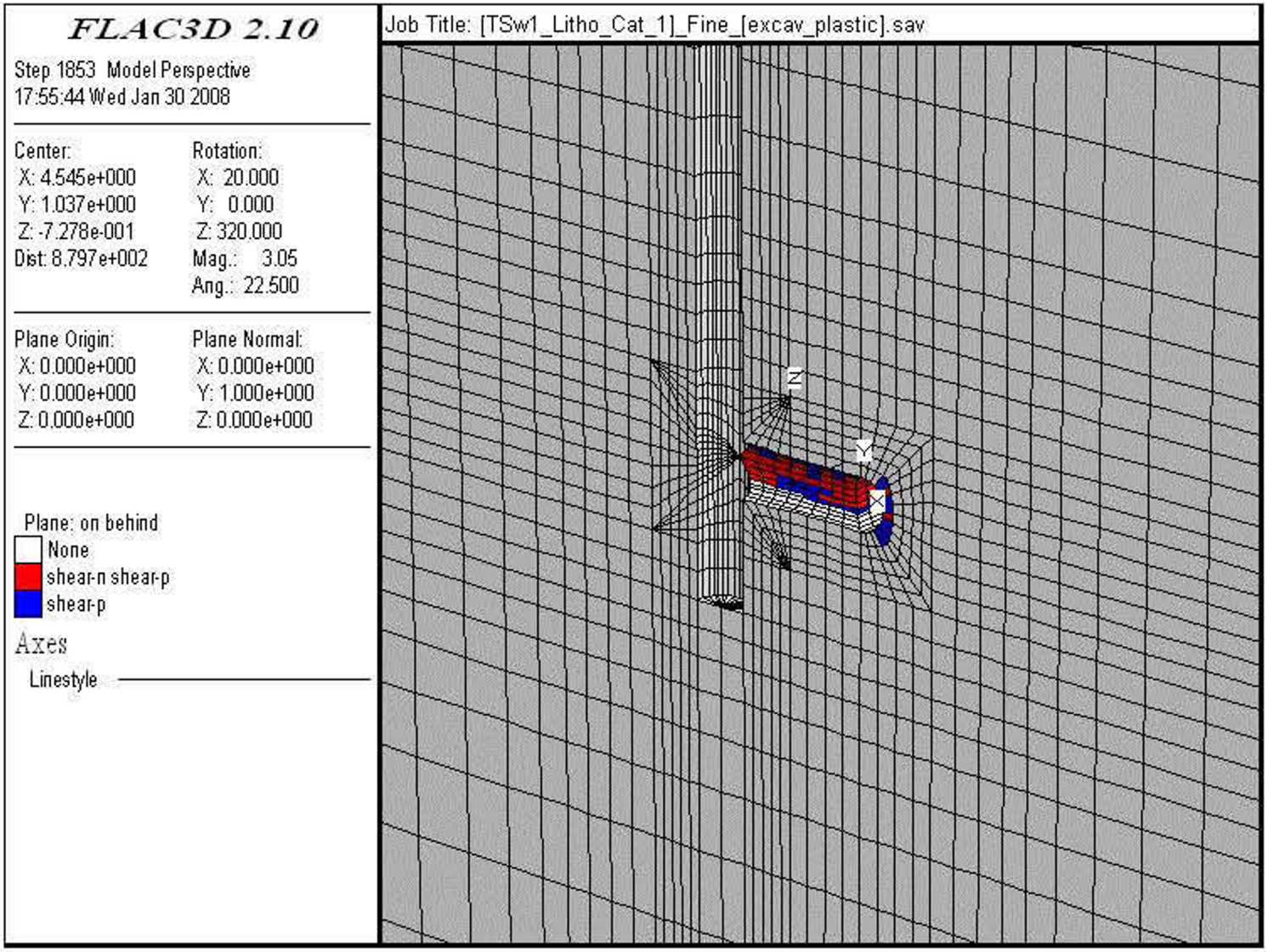

Figure 6-37 L-type Intersection - Extent of Plastic Failure After Excavation Represented on a Vertical Plane Containing the Axis of the Drift and the Connection Between Shaft and Drift

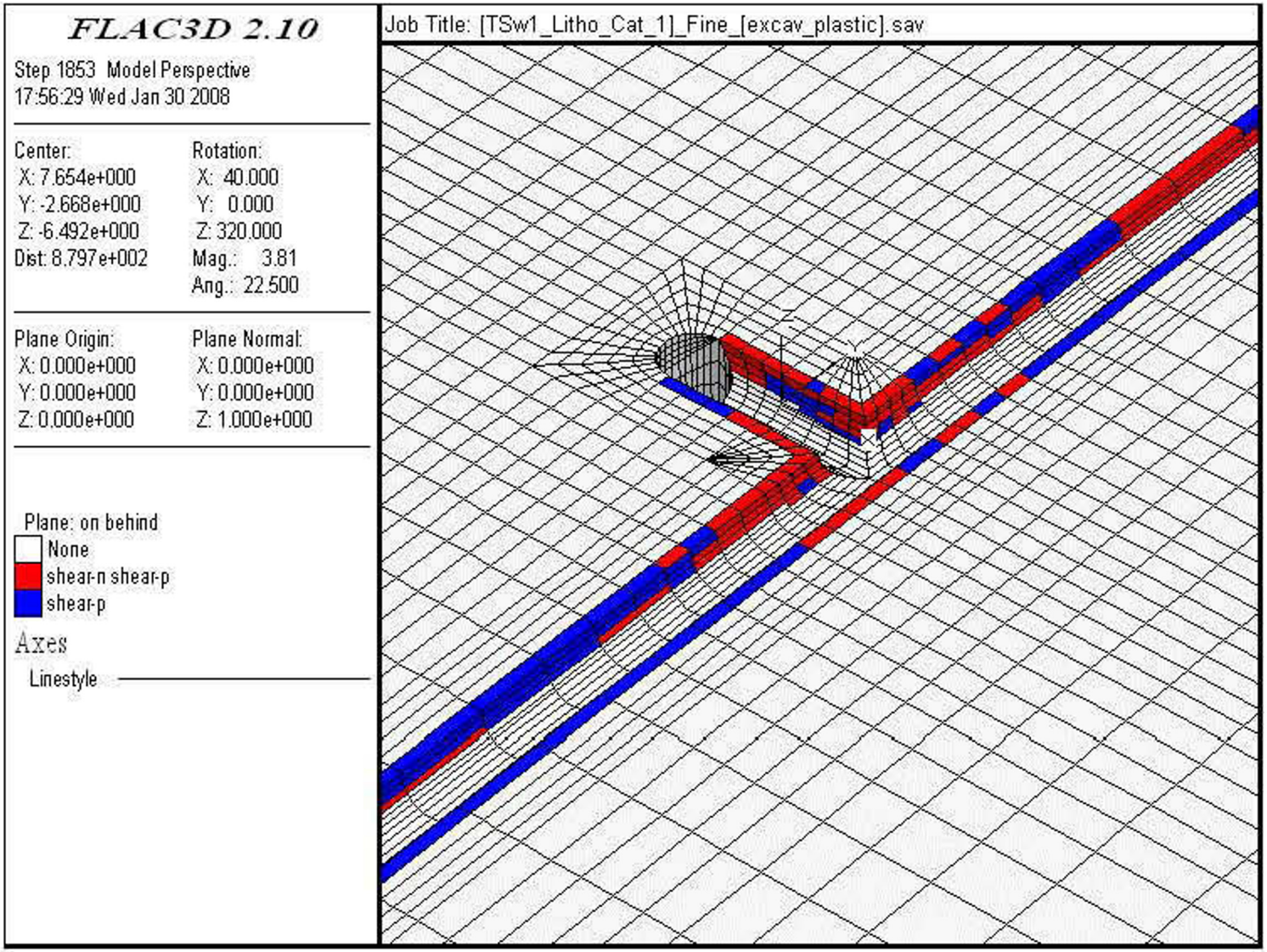

Figure 6-38 L-type Intersection - Extent of Plastic Failure After Excavation Represented on a Horizontal Plane Containing the Axis of the Drift and the Connection Between Shaft and Drift

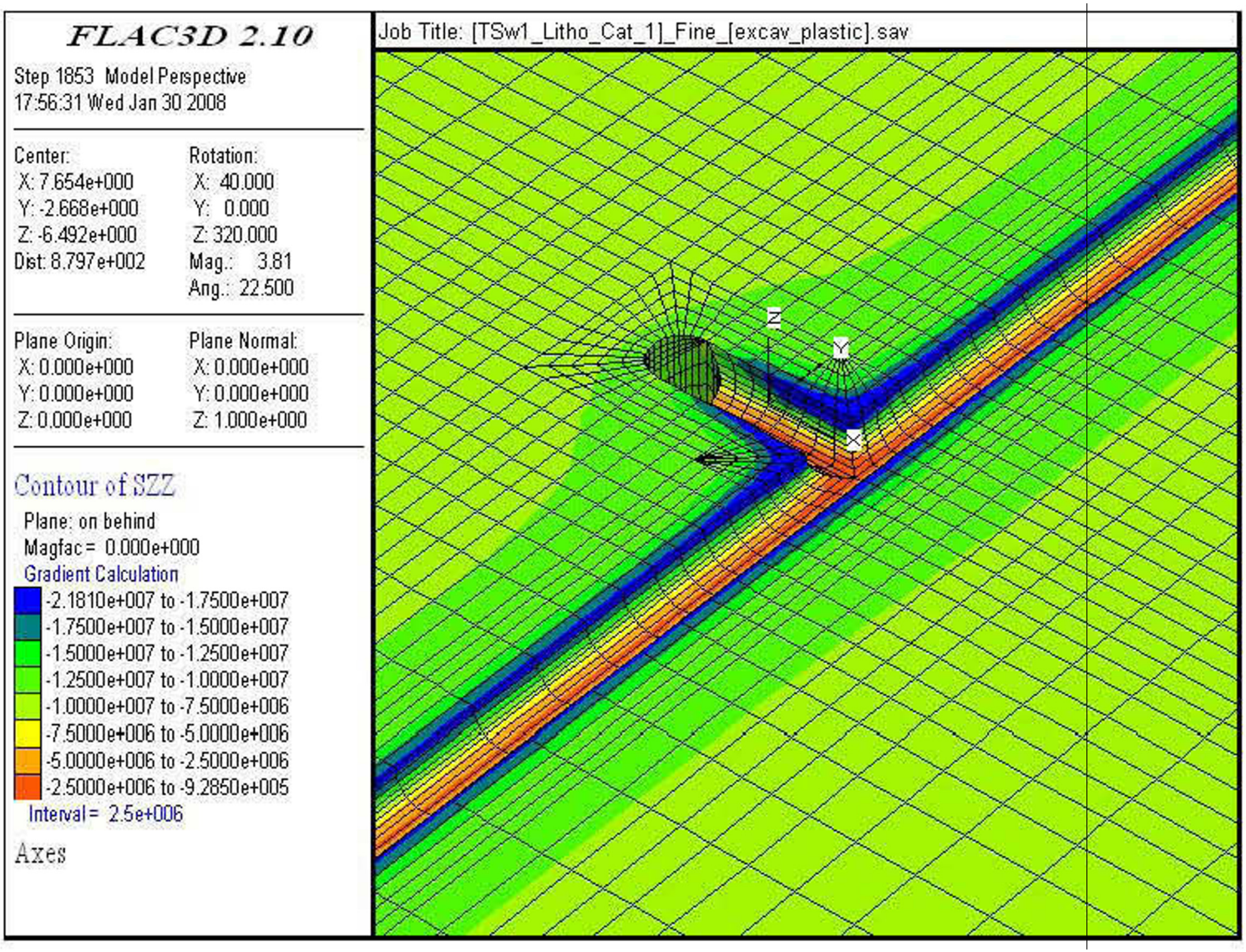

Figure 6-39 L-type Intersection - Contours of the Vertical Normal Stress (MPa) After Excavation Represented on a Horizontal Plane Containing the Axis of the Drift and the Connection Between Shaft and Drift

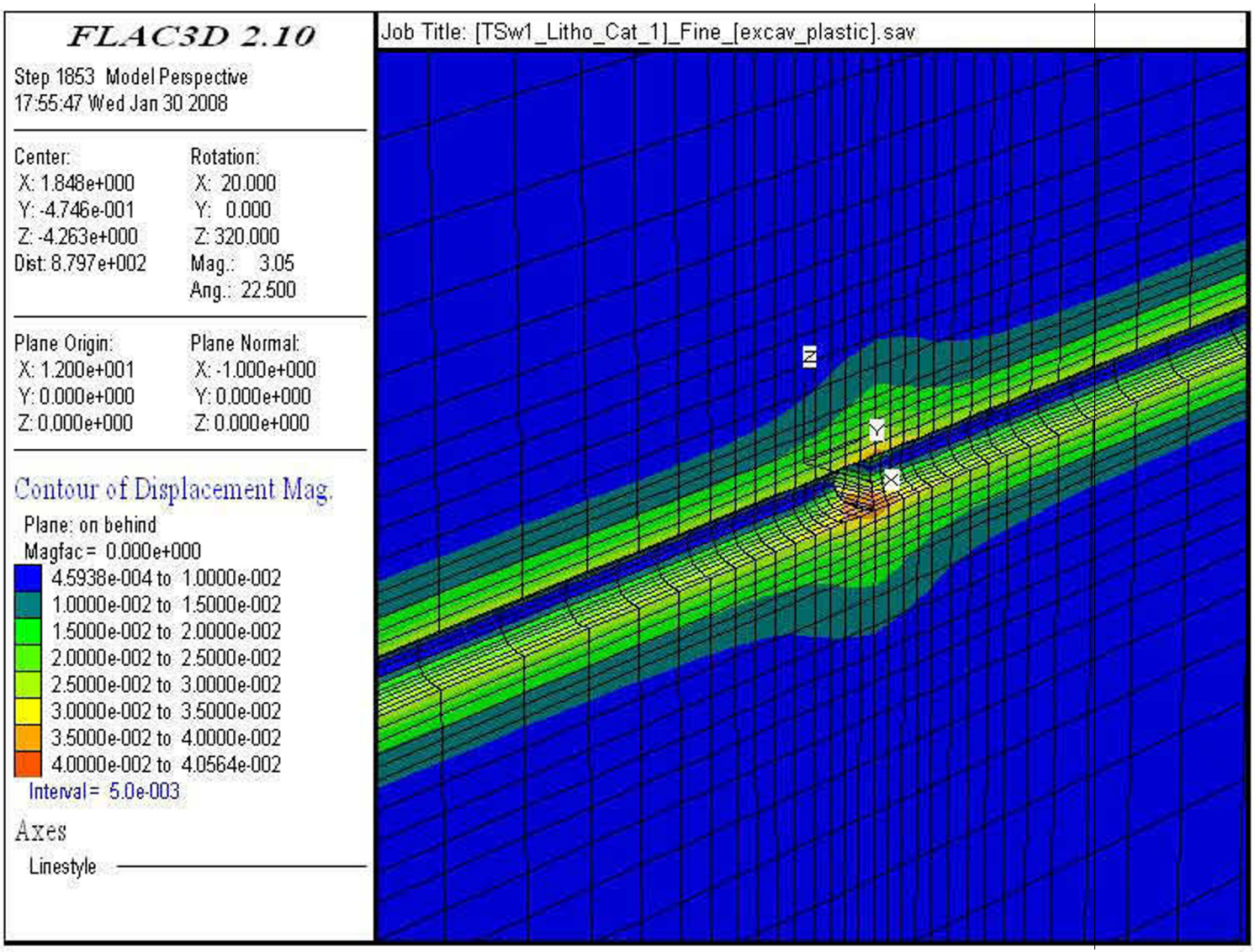

Figure 6-40 L-type Intersection - Contours of Magnitude of Displacement (m) After Excavation Represented on a Vertical Plane Containing the Axis of the Drift for the “L-type” Intersection

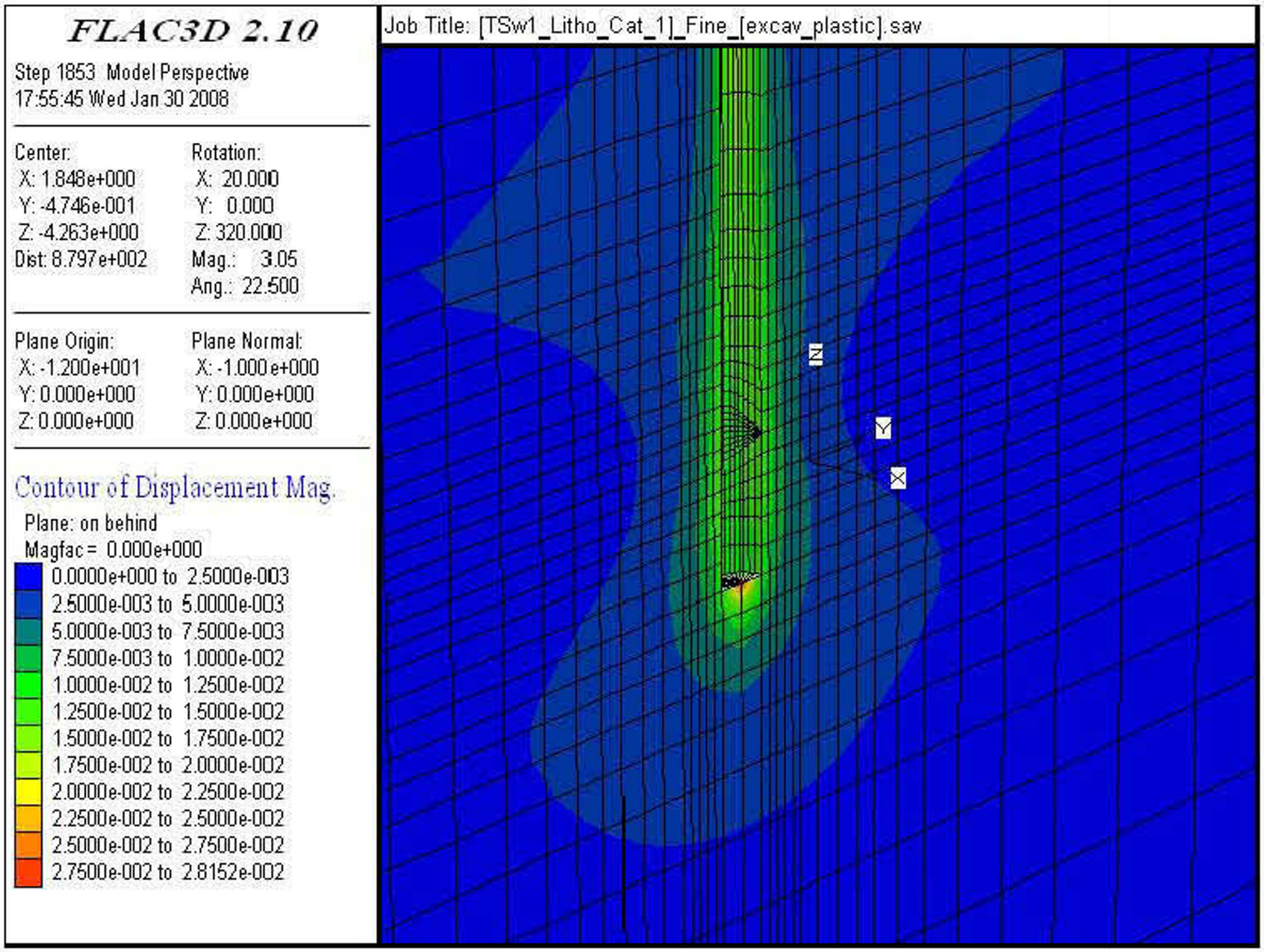

Figure 6-41 L-type Intersection - Contours of Magnitude of Displacement (m) After Excavation Represented on a Vertical Plane Parallel to the Axis of the Drift and Containing the Axis of the Shaft for the “L-type” Intersection

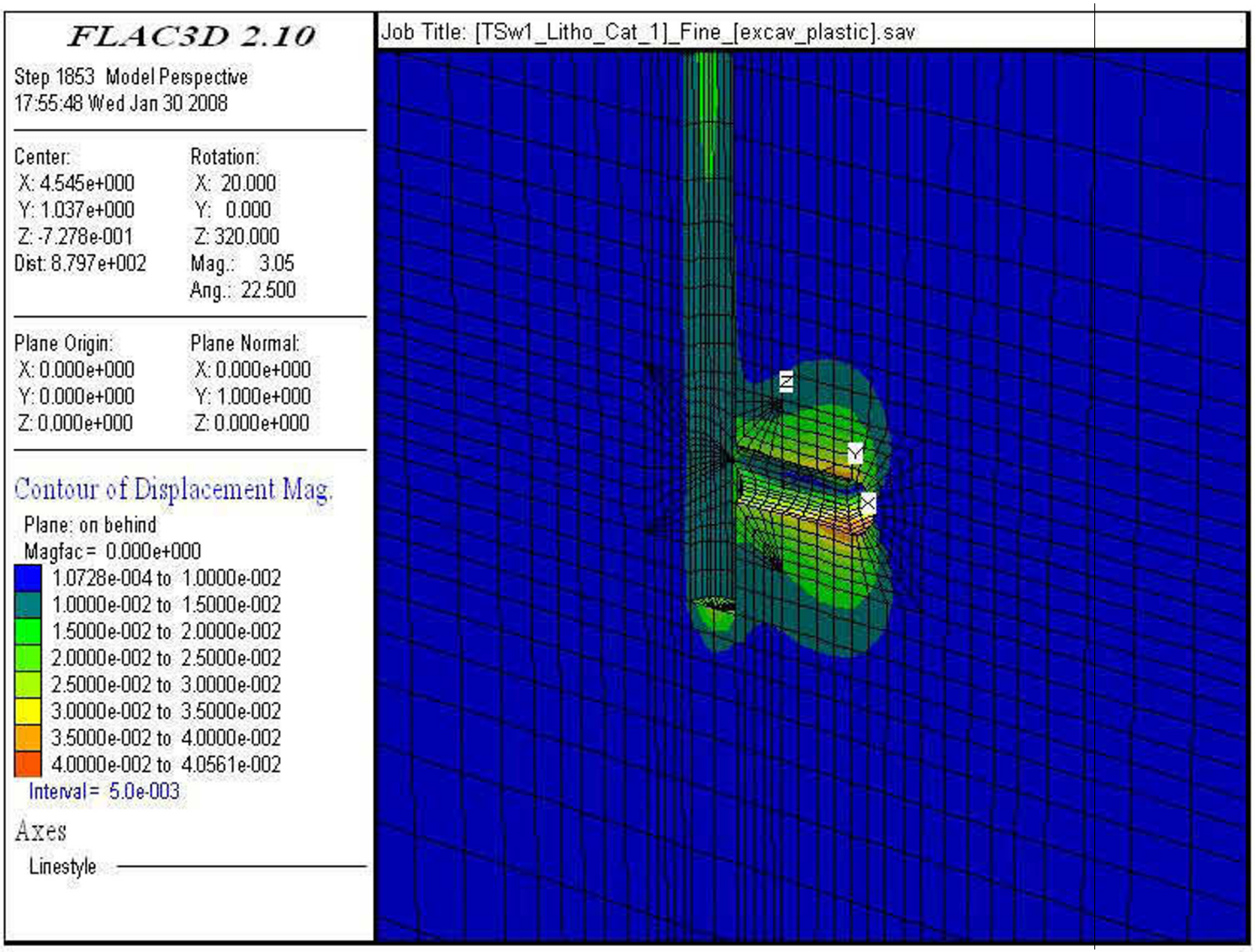

Figure 6-42 L-type Intersection - Contours of Magnitude of Displacements (m) After Excavation Represented on a Vertical Plane Containing the Axis of the Drift and the Connection Between Shaft and Drift

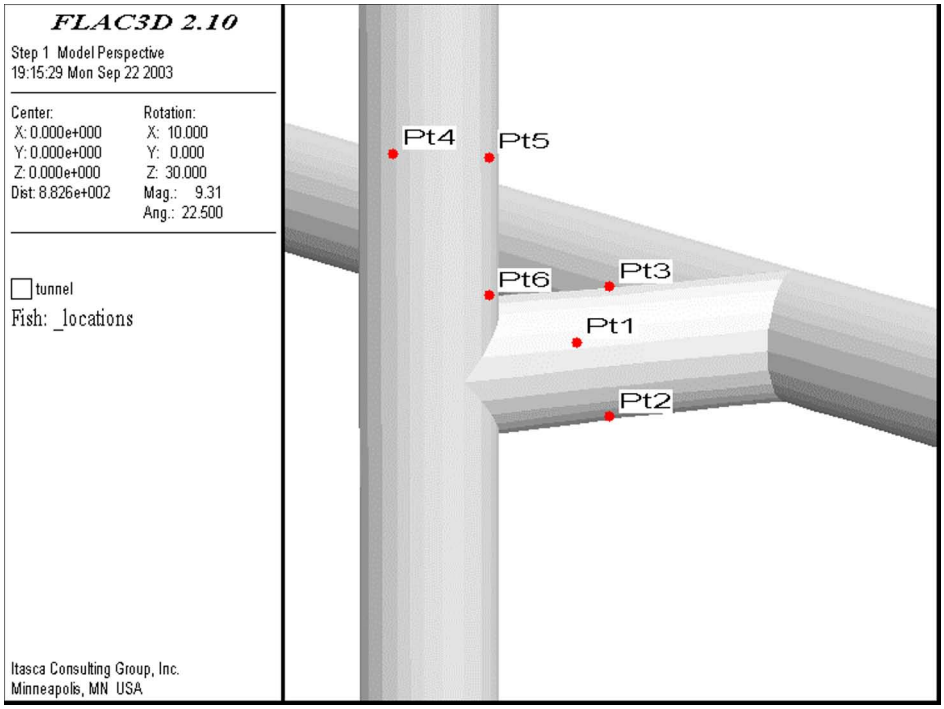

Figure 6-43 L-type Intersection – View 1 Showing Points Where Velocities Induced by Seismic Excitation Have Been Calculated and Recorded During Simulations

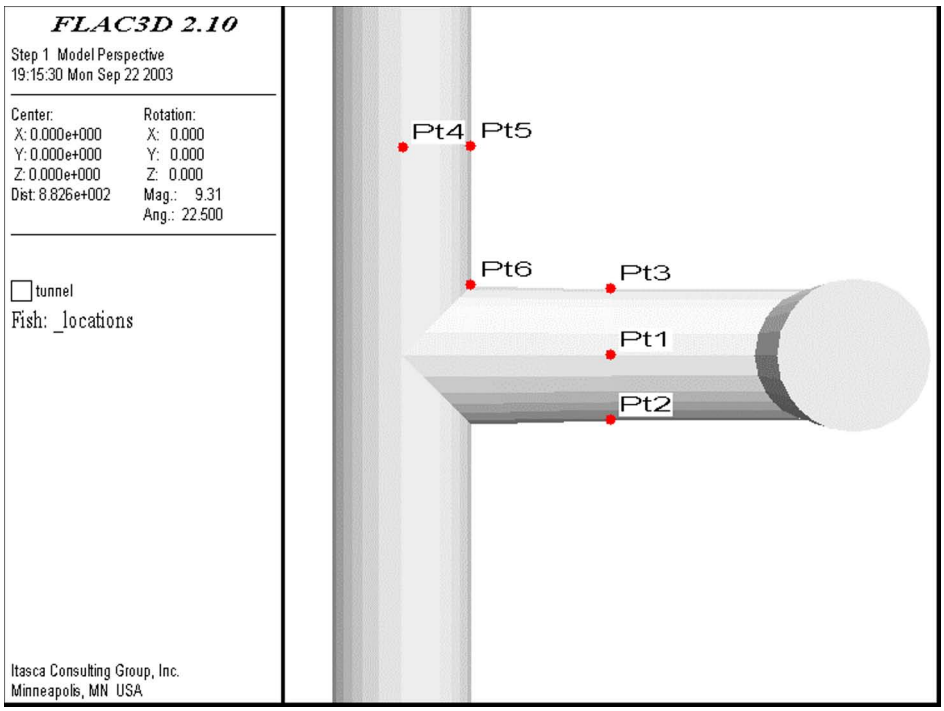

Figure 6-44 L-type Intersection – View 2 Showing Points Where Velocities Induced by Seismic Excitation Have Been Calculated and Recorded During Simulations

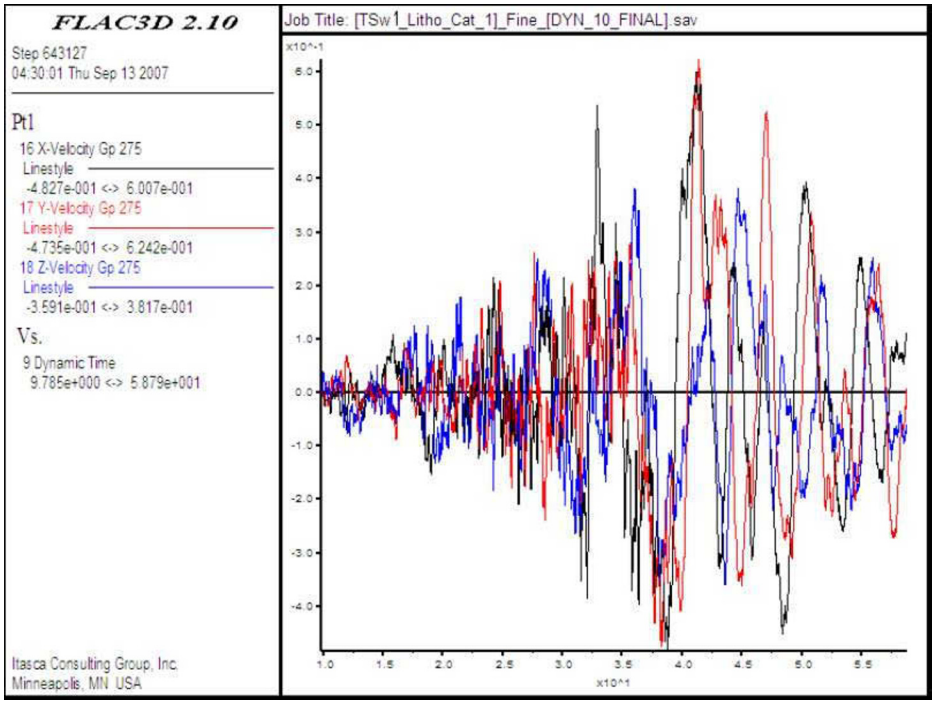

Source: Rev A (Reference 2.2.14)

Figure 6-45 L-type Intersection - Record of Input Velocities (m/s) in the X-, Y- and Z-Directions at the Base of the Model for the "L-type" Intersection (10-4 ground motion)

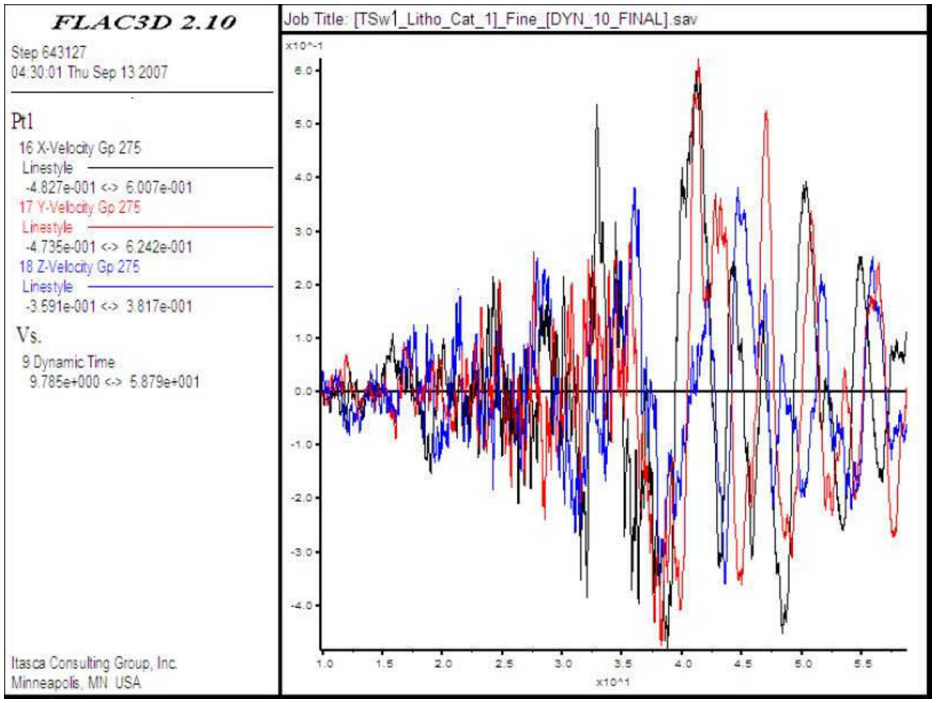

Source: Rev A (Reference 2.2.14)

Figure 6-46 L-type Intersection - Record of Velocities (m/s) at Point 1 in the "L-type" Intersection Induced by Application of Seismic Excitation

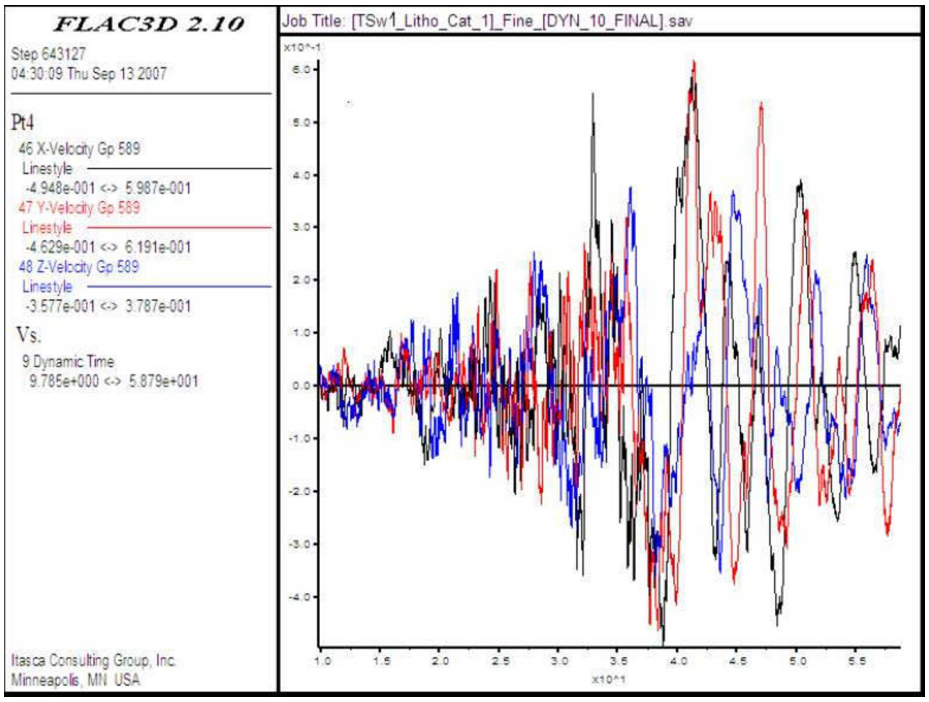

Source: Rev A (Reference 2.2.14)

Figure 6-47 L-type Intersection - Record of Velocities (m/s) at Point 4 in the "L-type" Intersection Induced by Application of Seismic Excitation.

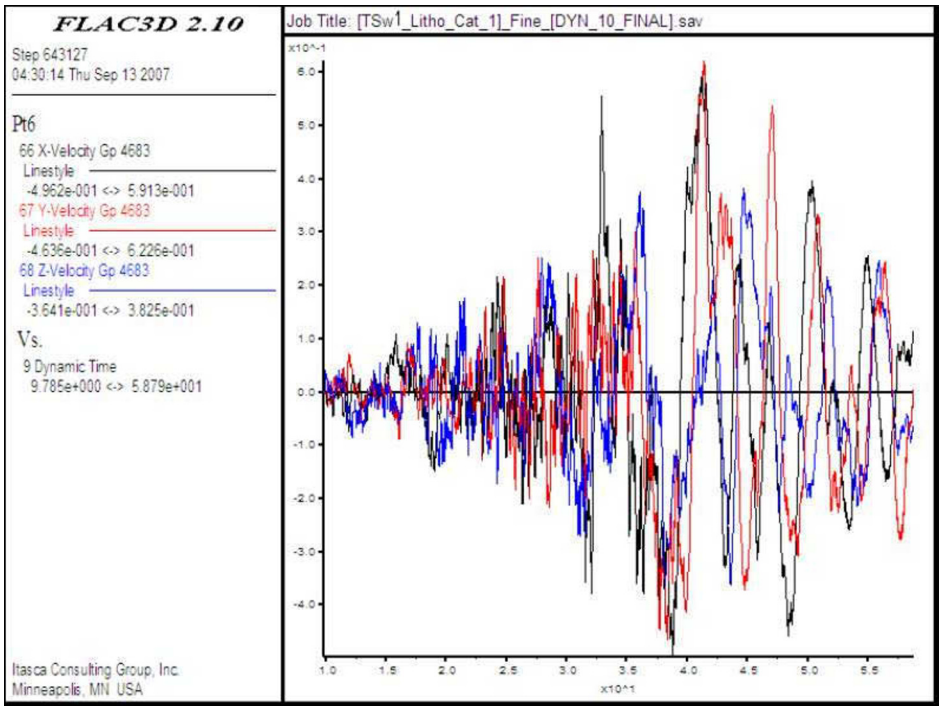

Source: Rev A (Reference 2.2.14)

Figure 6-48 L-type Intersection - Record of Velocities (m/s) at Point 6 in the "L-type" Intersection Induced by Application of Seismic Excitation.

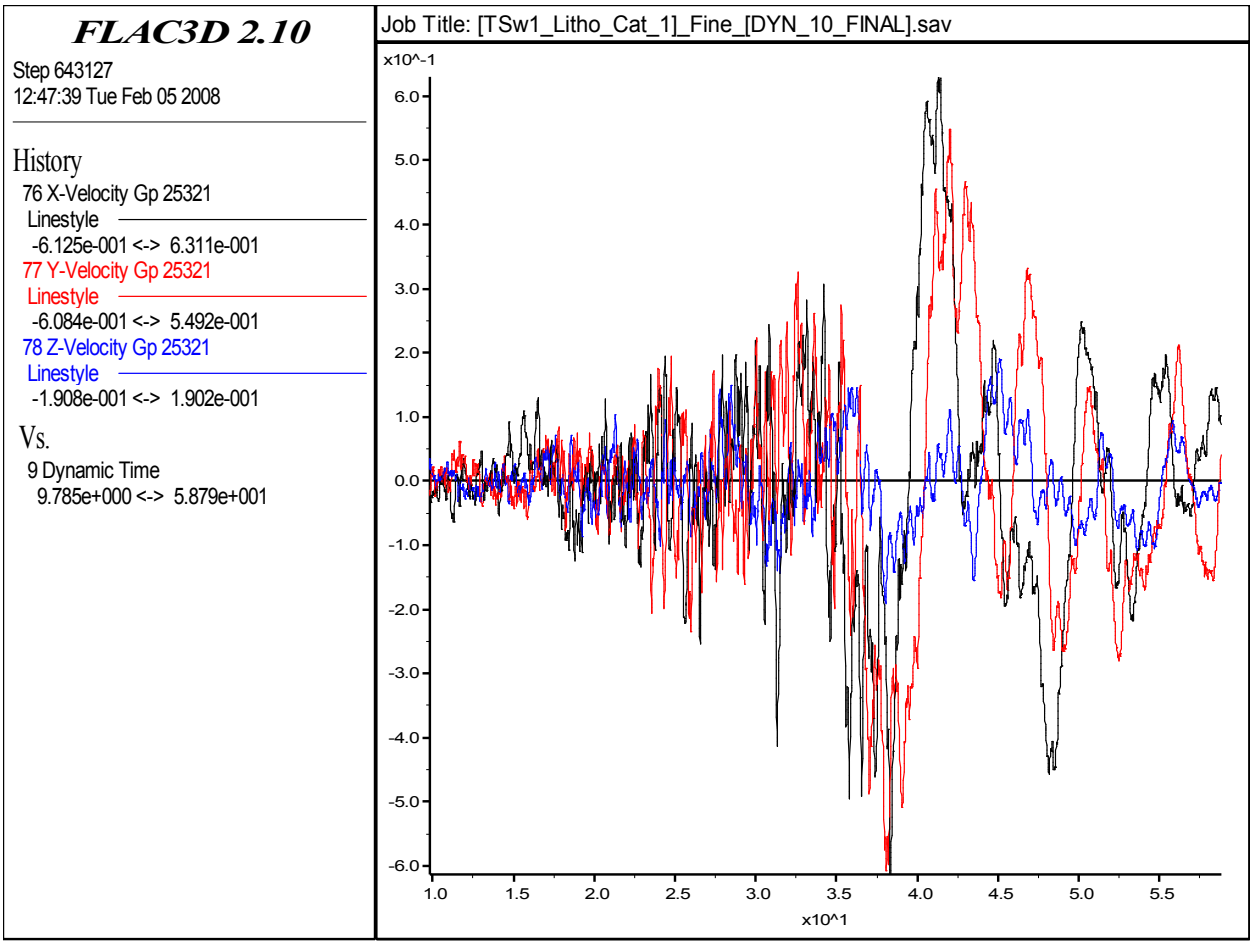

Source: MO0707THRB1E4A.000 (Reference 2.2.33)

Figure 6-49 L-type Intersection - Record of Input Velocities (m/s) in the X-, Y- and Z-Directions at the Base of the Model for the "L-type" Intersection (10-4 ground motion)

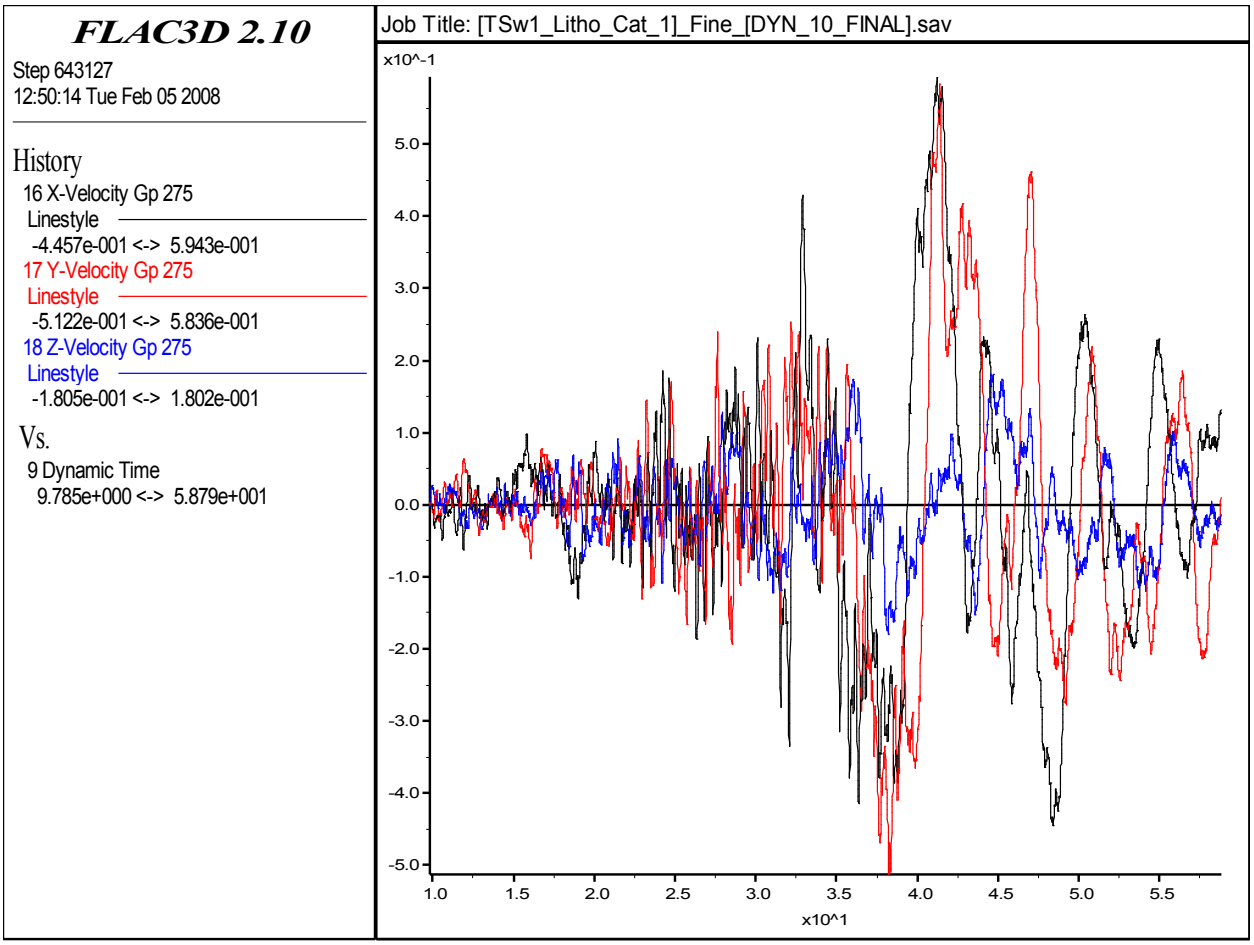

Source: MO0707THRB1E4A.000 (Reference 2.2.33)

Figure 6-50 L-type Intersection - Record of Velocities (m/s) at Point 1 in the “L-type” Intersection Induced by Application of Seismic Excitation

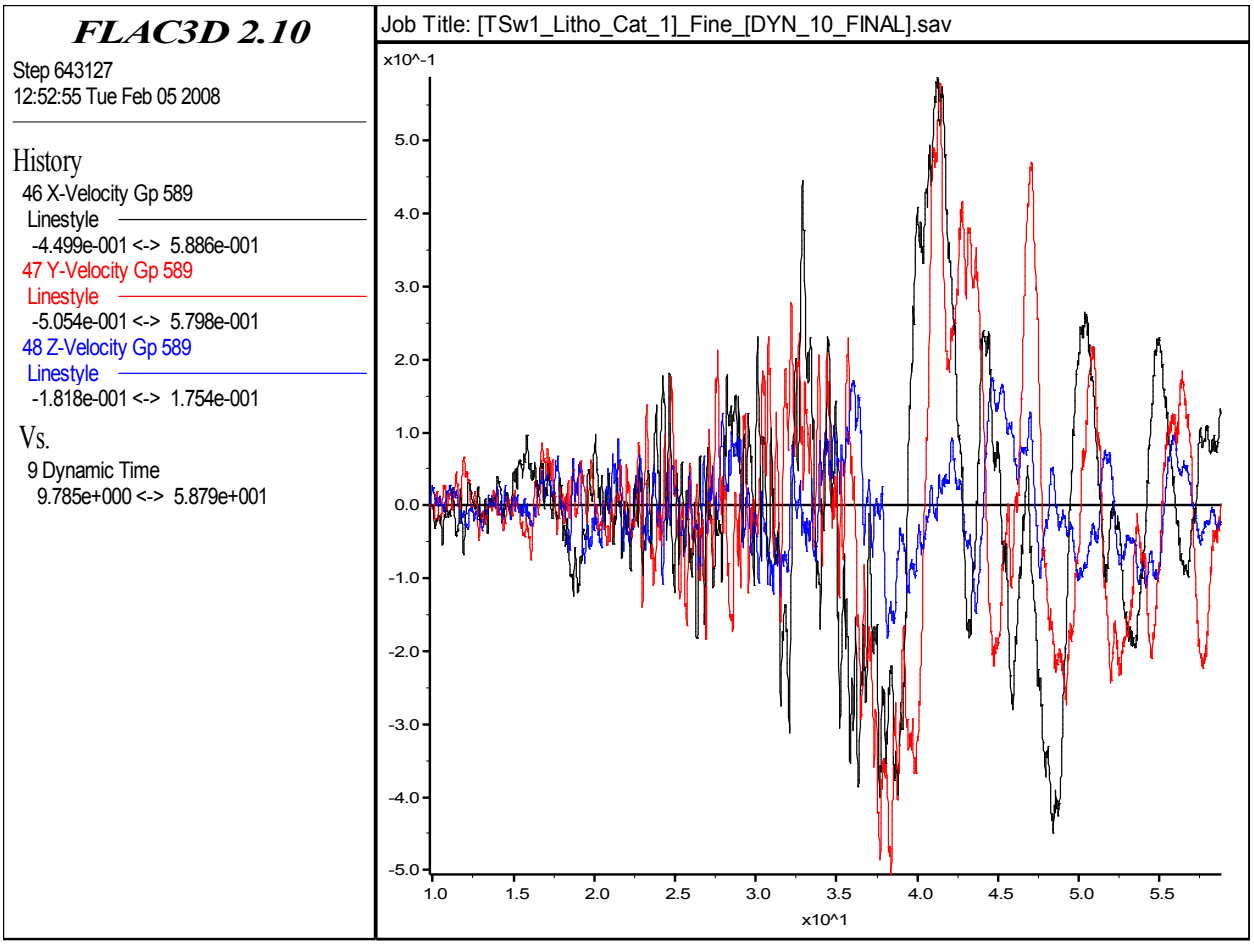

Source: MO0707THRB1E4A.000 (Reference 2.2.33)

Figure 6-51 L-type Intersection - Record of Velocities (m/s) at Point 4 in the “L-type” Intersection Induced by Application of Seismic Excitation.

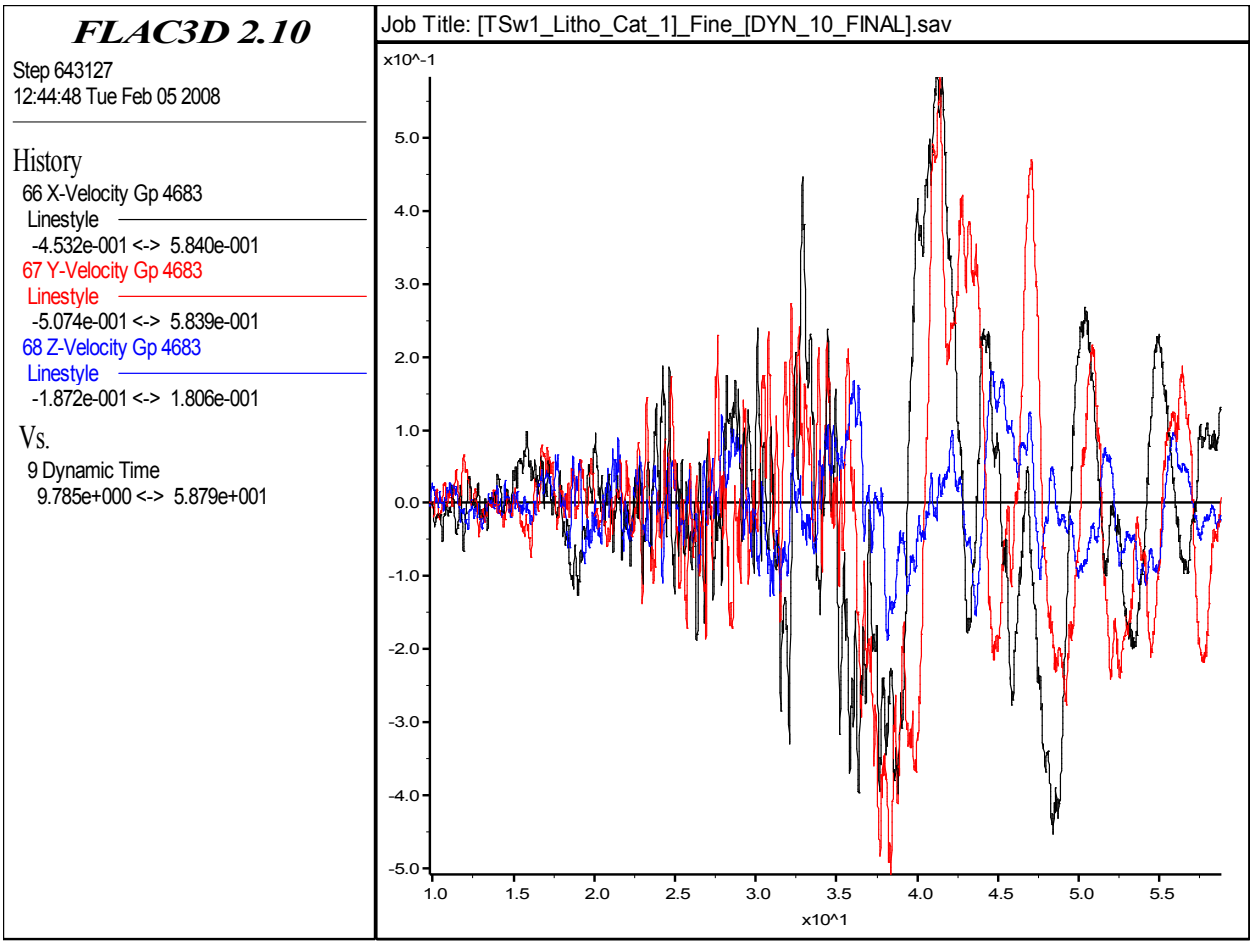

Source: MO0707THRB1E4A.000 (Reference 2.2.33)

Figure 6-52 L-type Intersection - Record of Velocities (m/s) at Point 6 in the “L-type” Intersection Induced by Application of Seismic Excitation.

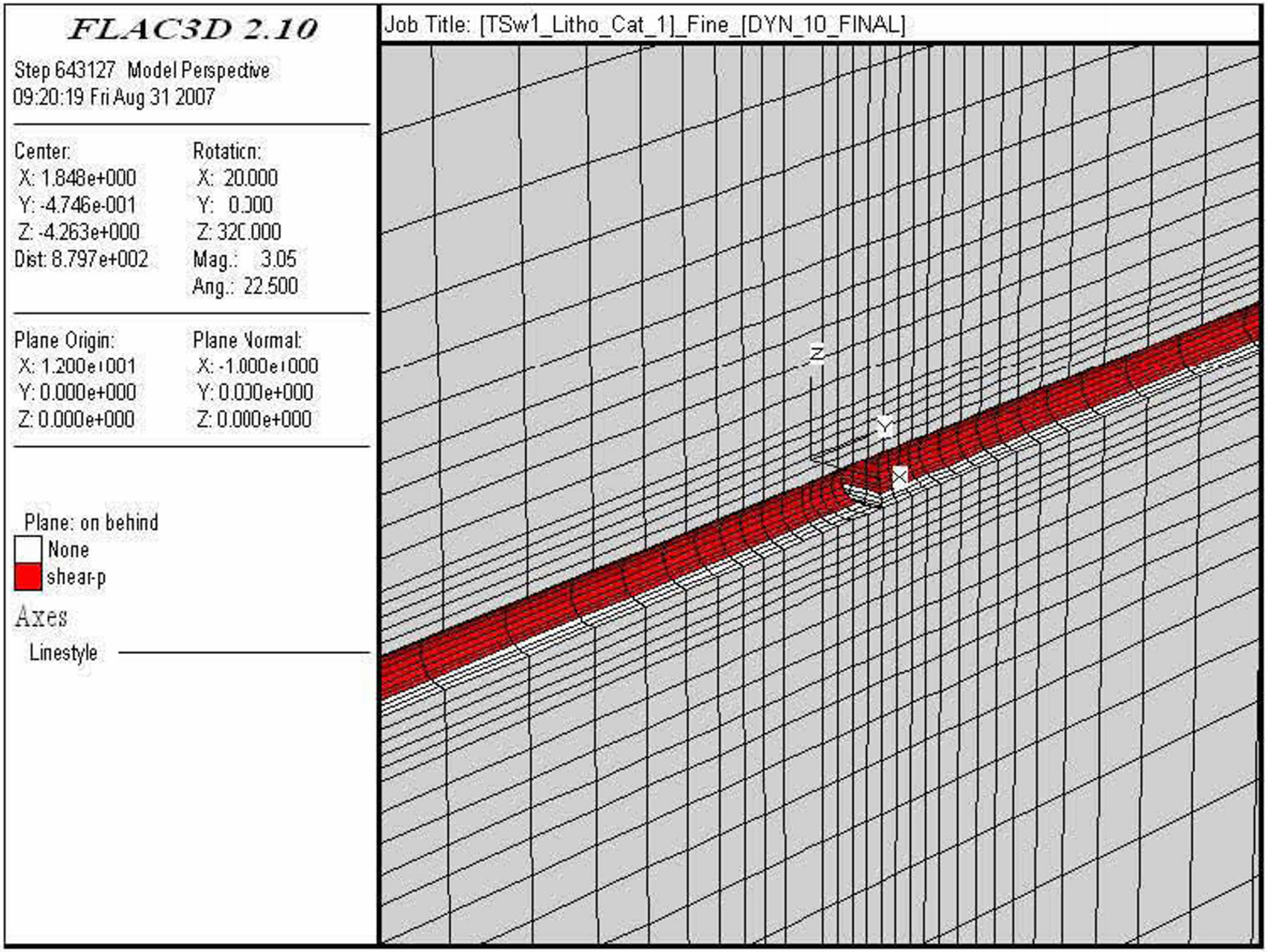

Source: Rev A (Reference 2.2.14)

Figure 6-53 L-type Intersection - View of Extent of the Failure Zone After Application of the Seismic Load in the “L-type” Intersection (The vertical plane cutting the model contains the axis of the drift).

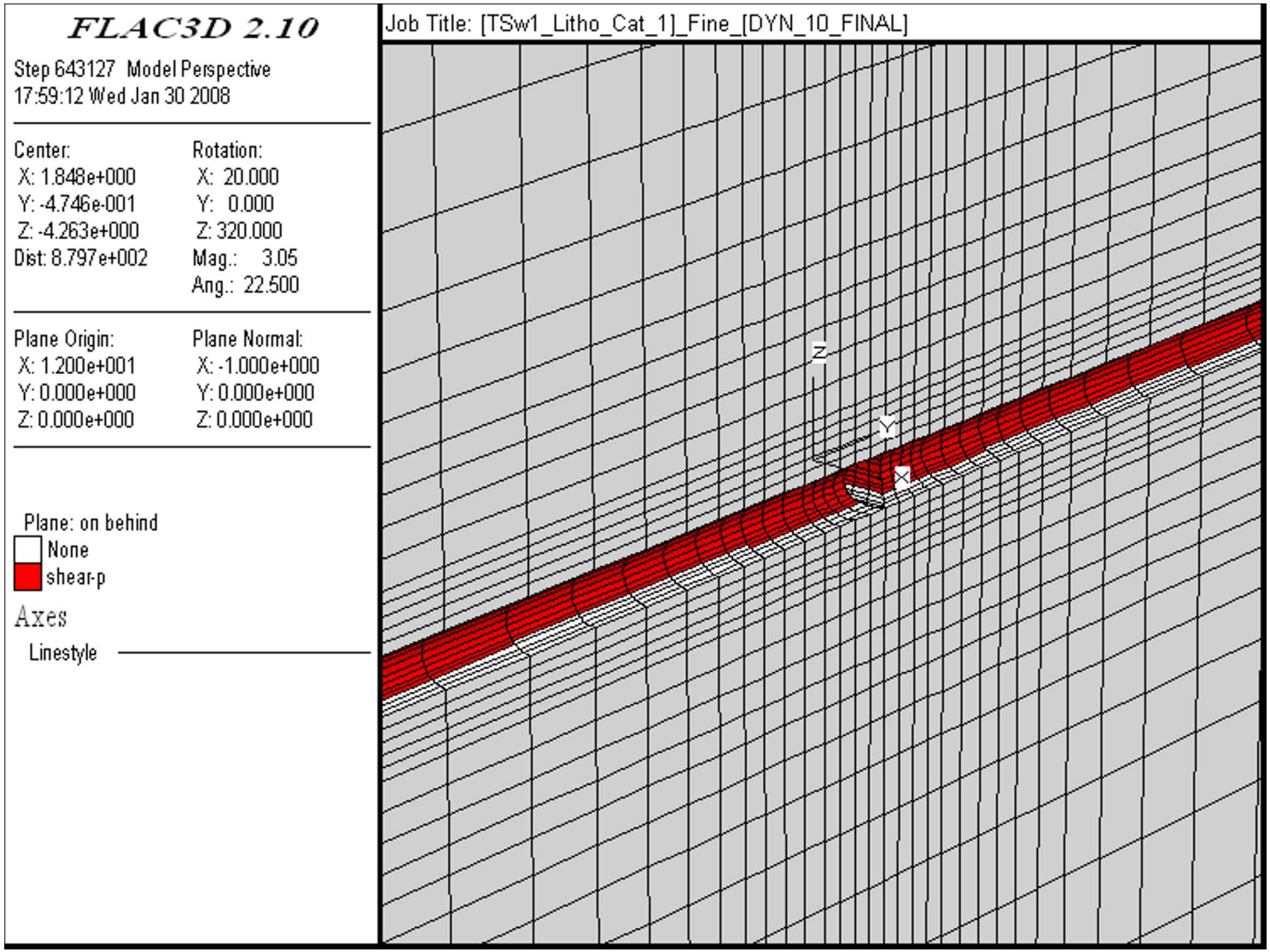

Source: MO0707THRB1E4A.000 (Reference 2.2.33)

Figure 6-54 L-type Intersection - View of Extent of the Failure Zone After Application of the Seismic Load in the “L-type” Intersection (The vertical plane cutting the model contains the axis of the drift).